DEVELOPMENT AND TESTING OF INTRICATE, AMPHIPHILIC CROSSLINKED HYPERBRANCHED FLUOROPOLYMERS WITH INTEGRATED LIQUID CRYSTALLINE PROPERTIES AS ANTI-ICING COATINGS IN AEROSPACE AND DEFENSE APPLICATIONS

A Dissertation

by

JENNIFER SUMMERHILL ZIGMOND

Submitted to the Office of Graduate and Professional Studies of
Texas A&M University
in partial fulfillment of the requirements for the degree of

DOCTOR OF PHILOSOPHY

Chair of Committee,	Karen L. Wooley
Committee Members,	James D. Batteas
	Steven E. Wheeler
	Hong Liang
Head of Department,	Simon W. North

December 2016

Major Subject: Chemistry

ABSTRACT

Atmospheric icing, the process by which supercooled water droplets freeze upon contact with a surface, has proven to be devasting when not controlled or prevented. Currently, the solution for addressing this problem is the use of deicing fluids, which are toxic and inefficient, leading to the development of intrinsically anti-icing materials to focus on prevention rather than response after manifestation. Amphiphilic polymer coatings have been of particular interest as they are capable of presenting complex nano- and microscopic heterogeneities for inhibition of ice formation, which is not a typical approach toward anti-icing technologies. We have previously synthesized crosslinked networks comprised of hyperbranched fluoropolymers (HBFP) and poly(ethylene glycol) (PEG), which demonstrated superb anti-biofouling capabilities credited to their amphiphilic morphology, nanoscopic surface topography and dynamic surface reorganization. Through the tuning of the amphiphilicity and thermo-responsive molecular ordering of this crosslinked hyperbranched network, we expand the application of these materials by exploiting their characteristics for development of robust, dynamic, anti-icing coatings for aerospace applications.

An array of films was synthesized by varying the PEG crosslinker to study the effect of hydrophilic:hydrophobic component ratios on the thermal, mechanical and surface properties. Differential scanning calorimetry (DSC) data show significant reductions in the water melting transition temperatures (-5 °C and -27 °C for free and bound water, respectively). The novel application of this system displays the expansion

and diversity of a well-established coating that demonstrates unique water confinement and sequestration behaviors with the ability to reorganize at the surface. Due to its great potential as an anti-icing coating, additional investigations and chemical manipulation of the binary system led to the integration of a thermally-dynamic molecule, a liquid crystalline (LC) moiety. A library of LC systems was developed in order to probe the effects that size, mesophase and topology would have on the water depression efficiency of these materials. An LC monomer was incorporated into the polymer during polymerization in order to enhance the dynamic reorganization of the system during changes in temperature and wetting. The results suggest that the unique LC-HBFP system is a viable option as a dynamic coating for extreme environments.

DEDICATION

To my supportive and loving husband, RJ Zigmond, my strong and determined mother, Evelyn Miller, and my late father, Edward Summerhill, who was the driving inspiration for this work.

ACKNOWLEDGEMENTS

The first person I would like to thank is my Ph.D. advisor, Dr. Karen L. Wooley, for her guidance, support, trust and advice throughout my graduate studies at Texas A&M University. I will never be able to fully express my gratitude and appreciation toward her. She is a remarkable woman in science, friend and boss. Her passion and dedication to the field of Polymer Chemistry is unfathomable, and I find myself lucky to have shared these last 5 years with someone so knowledgable. She has taught me a plethora of techniques and skills that I know has prepared me for my future as a chemist. I appreciate her compassion and support after the passing of my father, while still pushing me to move forward and allowing me the freedom to pursue this project. Without her, I would not be the chemist or person I am today and look forward to her continued mentorship and friendship.

Thank you to my committee members, Prof. James D. Batteas, Prof. Steven E. Wheeler and Prof. Hong Liang for their time, support and advice throughout the course of this research. I would like to also extend my thanks to Texas A&M University, in particular, the Department of Chemistry, Department of Materials Science & Engineering and Mays Business School. Additionally, thank you to my collaborators at The Pennsylvania State University, Dr. Michael A. Hickner and Dr. Sarah Smedley.

I would like to show my appreciation toward past and present members of the Wooley group. Dr. Adriana Pavia-Sanders provided a constant source of inspiration and entertainment inside and outside the lab. She is also a great friend and colleague who is

very supportive. I would like to thank Jeniree A. Flores for her friendship, advice and continuous motivation these last five years. Thank you to Joel D. Russell, Dr. Ashlee A. Jahnke and Dr. Rachel Letteri for their help in lab as well as their friendship. There are several Wooley members who contributed to my personal and professional development and deserve my gratitude including Dr. Jeffery E. Raymond, Dr. Guorong Sun, Dr. Marco Giles, Dr. Kevin A. Pollack, Dr. Lauren A. Link, Dr. Jingwei Fan, Simcha E. Felder, Xun He, Christopher Komatsu and Mariela Vazquez. I would also like to extend my thanks to Dr. Rita Silbernagel and Dr. Jacqueline Pope.

My undergraduate mentors, Dr. Dede Dunlavy and Dr. Dennis Johnson also deserve recognition because I would not have pursued my Ph.D. or attended Texas A&M University without their guidance and encouragement. They also contributed to my academic growth and development and were invaluable mentors.

To those who helped me maintain my sanity during my academic career, I would like to show my appreciation toward my very close friends, Mandi Garcia, Gabe Martinez, Jon Hart and Jon Sanders.

Finally, for all their unconditional love and support throughout my life, I thank and will always continue to show gratitude toward my parents, Evelyn Miller and Edward Summerhill. The qualities and lessons gained from them continue to shape who I am as a person. Thank you, Mom, for always giving me a choice and supporting my decisions, no matter how difficult. Dad, I miss you every day and know you would be proud of everything I have accomplished. Thank you for making me stronger and continuing to be an inspiration. To my furry children, Miracle and Jacoby, thank you for

your unequivocal love and bringing a smile to my face. Last, but not least, thank you to my amazing and loving husband, RJ Zigmond, who has put a lot on hold for us to follow this path. He has always been patient, supportive and had confidence in me. Thank you for motivating me when I had little left and for believing I could accomplish anything. I will always express my gratitude toward you: my best friend, biggest supporter, rock and teammate.

NOMENCLATURE

AIBN	Azobisisobutyronitrile
ATR-FTIR	Attenuated total reflectance Fourier-transform infrared spectroscopy
ATR-SCVCP	Atom transfer radical self-condensing vinyl copolymerization
ATR-SCVP	Atom transfer radical self-condensing vinyl polymerization
ATRP	Atom transfer radical polymerization
CA	Contact angle
$CDCl_3$	Deuterated chloroform
CTA	Chain transfer agent
CTM	Chain transfer monomer
DCC	*N,N'*-dicyclohexylcarbodiimide
DCM	Dichloromethane
DI	Deionized water
DIPEA	*N*,*N*-diisopropylethylamine
DMA	Dynamic mechanical analysis
DMAP	4-(dimethylamino) pyridine
DMF	*N*,*N*-dimethylformamide
DSC	Differential scanning calorimetry
E’	Young’s modulus
FAA	Federal Aviation Administration

FP	Fluoropolymer
FTIR	Fourier-transform infrared spectroscopy
GC/MS	Gas chromatography/mass spectrometry
GPC	Gel permeation chromatography
HBFP	Hyperbranched fluoropolymer
$HBFP^{(I)}$	Hyperbranched fluoropolymer 1st generation
$HBFP^{(II)}$	Hyperbranched fluoropolymer 2nd generation
$HBFP^{(III)}$	Hyperbranched fluoropolymer 3rd generation
$HBFP^{(III)}$-a	Hyperbranched fluoropolymer 3rd generation homopolymer
$HBFP^{(III)}$-b	Hyperbranched fluoropolymer 3rd generation copolymer
HRMS	High resolution mass spectrometry
Inimer	Initiating monomer
LC	Liquid crystalline
LCP	Liquid crystalline polymer
LFP	Linear fluoropolymer
MC-LCP	Main-chain liquid crystalline polymer
M_n	Number-average molecular weight
M_w	Weight-average molecular weight
NMR	Nuclear magnetic resonance
PDMS	Poly(dimethylsiloxane)
PEG	Poly(ethylene glycol)
PEGMA	Poly(ethylene glycol) methacrylate

PEO	Poly(ethylene oxide)
PFS	2,3,4,5,6-pentafluorostyrene
PHEMA	Poly(2-hydroxyethyl) methacrylate
PMDETA	*N,N,N',N'',N''*-pentamethyldiethyltriamine
POM	Polarized optical microscopy
PS	Polystyrene
R_a	Roughness
RAFT	Reversible addition-fragmentation chain-transfer polymerization
RT	Room temperature
Sa	Surface area roughness
SC-LCP	Side-chain liquid crystalline polymer
SEC	Size exclusion chromatography
T_c	Crystalline transition temperature
T_d	Decomposition transition temperature
TEA	Triethylamine
TEG	Triethylene glycol
TFS	2,3,5,6-Tetrafluorostyrene
T_g	Glass transition temperature
TGA	Thermal gravimetric analysis
THF	Tetrahydrofuran
T_m	Melting transition temperature
XRD	X-ray diffraction

TABLE OF CONTENTS

Page

Page

LIST OF FIGURES

Page

Page

Page

LIST OF SCHEMES

LIST OF TABLES

Page

CHAPTER I

INTRODUCTION AND LITERATURE REVIEW

1.1 Anti-icing and Deicing Methods

Atmospheric icing is a problem that has plagued the aviation industry since the inception of airplanes as a mode of general transportation. Aircraft icing is an accumulation of water droplets that freeze on an aircrafts' exterior surface, within the induction system and/or within the instrumentation, compromising flight safety and costing the aviation industry time and money.[1-4] These negative consequences present themselves in the form of poor aircraft performance and efficiency, extended holdover times and high unforeseen costs when not addressed.[1] As little as 0.03 inches of ice can adversely alter the shape and roughness of the aircraft, particulary the surface of the wings, which can result in a decrease in lift by 25% and an increase in drag during takeoff.[1, 5] The results of this added weight include increased fuel uptake, decreased thrust and possible accidents during takeoff.[5]

Currently, the commercial solution for combating the issue involves the application of deicing fluids, which are primarily composed of propylene glycol and ethylene glycol, through spraying the heated glycol/water fluid mixture over the entire aircraft.[6] This process, is inherently costly, time-consuming and damaging to the environment, partly due to the toxicity of the fluids and their inefficiency.[6, 7] Breaking the entire process down, the extent of detail and cost involved can be illustrated. The deicing fluids, costing *ca.* $10 per gallon, need to be heated and mixed with water prior

to use and amounts required vary depending on icing intensity and aircraft size. For a mid-size jet, this cost can range from $300 with light icing to $10,000 for moderate icing. [4, 8] Additionally, the fluid must be sprayed from a deicing truck, which can cost *ca*. $250,000.[4] Since current deicing methods can only address moderate levels of icing, based on the Federal Aviation Administration's (FAA) current icing intensity definitions (Table 1), and cannot successfully alleviate severe levels of icing, it is clear that there is a need for new technology to address this significant challenge.

Table 1.1. The Federal Subcommittee on Meteorological Services version of airframe icing reporting adopted in 1968.[8]

TRACE	Ice becomes perceptible. The rate of accumulation is slightly greater than the rate of sublimation. It is not hazardous even though deicing/anti-icing equipment is not utilized, unless encountered for an extended period of time – over 1 hour.
LIGHT	The rate of accumulation may create a problem if flight is prolonged in this environment (over 1 hour). Occasional use of deicing/anti-icing equipment removes/prevents accumulation. It does not present a problem if the deicing/anti-icing equipment is used.
MODERATE	The rate of accumulation is such that even short encounters become potentially hazardous and the use of deicing/anti-icing equipment or flight diversion is necessary.
SEVERE	The rate of accumulation is such that deicing/anti-icing equipment fails to reduce or control the hazard. Immediate flight diversion is necessary.

Recent efforts toward the generation of anti-icing systems have resulted in many different technologies for the prevention of ice manifestation and ease of removal, including superhydrophobic coatings,[9-23] liquid crystalline polymers[24-26] and while not covered within the scope of this dissertation, antifreeze(glyco) proteins.[27-29] Superhydrophobicity gained popularity from surfaces in nature such as lotus leaves[30, 31] and water strider legs.[32] This superhydrophobic property is a result of low surface

energy and a rough microscopic topography.[31] The coorelation between superhydrophobicity and ice-repellency was first observed by Saito *et al.*, where results from the development of a resin, composed of poly(tetrafluoroethylene) and poly(vinylidene) fluoride, compared water contact angle, free surface energy and ice adhesion strength.[33] Since this research, superhydrophobic surfaces have been prepared through a variety of mechanical and chemical methods, but thus far, only a few have demonstrated anti-icing character.[10, 17, 34]

Around the time Saito *el al.* related superhydrophobicity and ice-repellency, liquid crystalline polymers (LCPs) were gaining attention for their potential as protective coatings.[24] Though there are several characteristics that make LCPs desirable toward coating applications, the major setback for the success of LCP materials has been the difficulties in processing.[24] While each system offers its own merits and weaknesses, it was hypothesized that the employment of various chemistries would result in a highly complex, robust coating with varying degrees of dynamic character that would exhibit unique surface characteristics including low surface energy,[9, 12-16, 18, 19, 22, 35] wide-range of thermal stability[24-26, 36] and low adhesion,[37-39] which would inhibit the organization of water into ice crystals, thus eradicating the deicing problem by preventing ice formation.

1.2 Hyperbranched Fluoropolymers

The Wooley laboratory has a long-standing reputation for synthesizing complex, amphiphilic hyperbranched fluoropolymer poly(ethylene glycol) crosslinked networks, primarily for use as anti-biofouling materials.[40-44] While research has resulted in three

generations of hyperbranched fluoropolymers (HBFP) with different structural features and synthesized through a variety of synthetic methods, key similarities within each generation included the incorporation of a fluorinated hydrophobic component crosslinked with a hydrophilic moiety, resulting in a highly branched, amphiphilic polymer coating.[40, 45] Specifically, the third generation of HBFP ($HBFP^{(III)}$) introduced hydrophilic character with the addition of tri(ethylene glycol) (TEG) units into the polymer framework, which had resulted in significant changes on the material properties including lower glass transition (T_g) values and thermal degradation temperatures when compared to the two previous generations, $HBFP^{(I)}$ and $HBFP^{(II)}$.[45] Additionally, $HBFP^{(III)}$ was synthesized as a homopolymer, $HBFP^{(III)}$-a (Figure 1.1), and a copolymer, $HBFP^{(III)}$-b (Figure 1.2), by atom transfer radical self-condensing vinyl polymerization (ATR-SCVP) or copolymerization (ATR-SCVCP). By systematically varying the hydrophobic:hydrophilic components, an array of amphiphilic crosslinked networks were prepared for evaluation of thermal, mechanical and surface properties, specifically towards anti-biofouling assessment, which showed low barnacle cyprid settlement and high release of diatoms and sporelings.[41] Additionally, coatings with distinct topographical, compositional and morphological features were obtained through tailoring of the type and amount of crosslinker, showing increase resistance to protein adsorption than a commercially-available anti-bioufouling standard.[43]

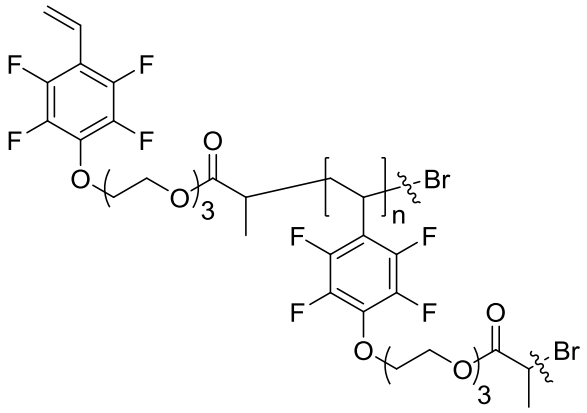

Figure 1.1. Structure of HBFP$^{(III)}$-a (homopolymer).

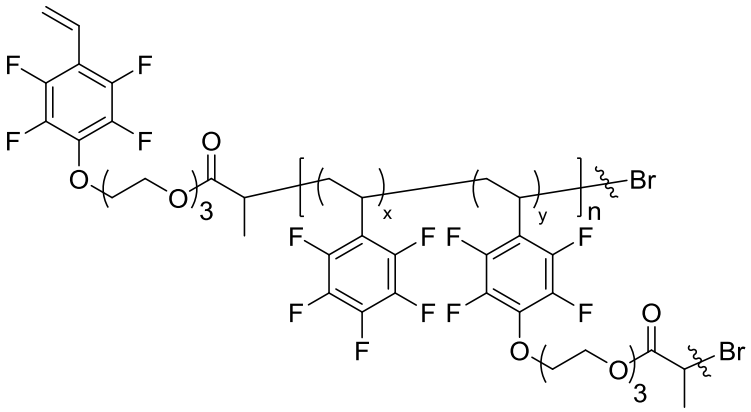

Figure 1.2. Structure of HBFP$^{(III)}$-b (copolymer).

1.3 Liquid Crystalline Polymers

Liquid cystalline polymers are macromolecular systems that dynamically order when subjected to an increase in solution concentration (lyotropic) or a decrease in temperature (thermotropic).[26] LCPs are composed of fundamental units known as mesogens that are usually attached to a flexible spacer resulting in mesogenic units. The mesogens induce structural order while the flexible spacer increases fluidity resulting in

unique polymers with unconventional properties.[26, 46] Generally, LCPs are found with two main types of architectures (Figure 1.3): main-chain (MC), where the mesogen composes the backbone of the polymer, and side-chain (SC), where the mesogen is attached to the polymer backbone by a flexible spacer. While MC-LCPs have been implemented in several technologies requiring high strength and semiconducting applications,[47-53] the difficulties in processing as well as elevated transition temperatures of these materials have steered research efforts toward SC-LCPs. The incorporation of thermotropic mesogenic units through the use of a side-chain allows for easier preparation and eliminates many difficulties in processing, such as rigidity issues responsible for poor solvent solubility at room temperature, which is required to extract LC properties from lytotropic systems.[24, 26, 46]

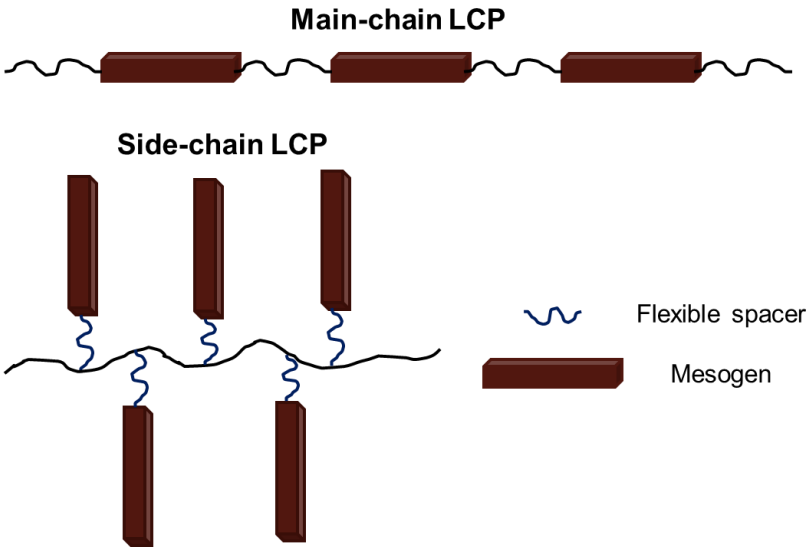

Figure 1.3. Schematic illustrations of main-chain LCP and side-chain LCP architectures.

This new generation of thermotropic LCPs as coatings was proposed partly due to the materials' ability to possess properties of each individual component and also display new features, but primarily, because LCP materials have shown remarkable coating properties including thermal resistance, environmental resistance to weathering and chemicals, low permeability and a low coefficient of linear thermal expansion.[24-26, 36, 54-56] Several research groups have demonstrated an increase in general coating properties including hardness, flexibility and adhesion with the addition of an LC moiety, over non LC-containing polymers.[25, 37-39, 57, 58] Athawale and coworkers observed comparable adhesion and shorter drying times for their LC acrylic copolymer coatings when compared to the parent acrylic copolymers.[37, 57] They notably mentioned that the LC acrylic copolymer coatings also demonstrated an increase in hardness while maintaining comparable flexibility to the non LC-containing coatings.[37, 57] Additionally, the LC acrylic copolymer coatings showed visual stability after submersion in acid, alkali and water for 24 h.[37, 57] Gähde *et al.* recognized that by using LC polyurethanes, they could effectively adhere the film to a steel substrate and hinder the penetration of water to the interface.[36] Van der Wielen and coworkers also showed suitable coating adhesion to polar substrates including metals.[39] We hypothesize that by enhancing the hydrophobicity of LCP coatings through integration into amphiphilic hyperbranched fluoropolymers, we combine all the advantageous features of superhydrophobic surfaces and LCPs into one superior coating.

1.4 Scope of Dissertation

This dissertation focuses on the design, development and investigation of dynamic, complex, amphiphilic fluoropolymer poly(ethylene glycol) crosslinked networks as materials for use in environmentally-extreme conditions, primarily as anti-icing coatings for aerospace applications. Studies began with the investigation of our well-established binary system (Chapter II). This topographically, morphologically and compositionally complex system was then expanded by the incorporation of an LC monomer, to probe the effects this thermally-dynamic component would have on the polymer and subsequent coatings (Chapter III). After obtaining an understanding of the dynamic character that the LC moiety lended to the polymer matrix, the impact of a variety of LC comonomers and polymer topology was explored in different aqueous environments (Chapter IV).

In Chapter II, we investigated a previously crosslinked network, comprised of $HBFP^{(III)}$ and poly (ethylene glycol) (PEG), that displayed noteable anti-biofouling characteristics credited to its low surface energy, amphiphilic morphology, nanoscopic surface topography and dynamic surface reorganization. It was hypothesized that these complex nano- and microscopic heterogeneitic features could be extracted to inhibit ice formation and subsequently, depress the freezing/melting temperature of water. Through the tuning of the amphiphilicity, low surface energy and thermo-responsive molecular ordering, we studied the effect on thermal, mechanical and surface properties. Differential scanning calorimetry (DSC) studies revealed two melting transition temperatures attributed to the bound water within the $HBFP^{(III)}$-PEG matrix and the free

water on the surface of the coating. Data from DSC and Fourier transform infrared (FTIR) spectroscopy, provided insight into the behavior of the crosslinked networks and a further understanding of the interaction between water and the binary system. Additionally, through modification of the drop-casting solvent, a lower T_m was obtained, which was accredited to the higher mobility and greater reactivity the solvent provided to the system. Overall, the depression of the freezing/melting temperature of water extended the utility for these crosslinked networks as potential anti-icing materials.

With the success of the binary system, in Chapter III, the polymer was expanded to integrate a thermally-dynamic molecule, a mesogenic unit, for the purpose of lending liquid crystalline properties to the crosslinked network. A series of amphiphilic networks was synthesized through the variation of the polymer molecular weights and the hydrophilic:hydrophobic component ratios. These innovative materials showed a remarkable reduction in the free water melting transition temperature, measured by DSC, and an increase in water contact angle for dry and water-swollen systems resulting in a more hydrophobic surface. As the water contact angle increased, the water uptake % also increased. These results were attributed to the added ordering parameter from the incorporation of the LC comonomer. The high degree of ordering also generated a unique coating topography visualized *via* polarized optical microscopy (POM) and 3D optical microscopy, while maintaining an overall macroscopic homogeneity. The ability for the polymer matrix to retain key features, such as the sequestration and confinement of water molecules, impart an additional dynamic character during temperature change,

and enhance the depression of waters' freezing point supports our claim to use these materials as protective coatings in extreme environments.

With an understanding of how liquid crystalline properties affected our amphiphilic crosslinked networks, Chapter IV explored the influence of different LC comonomers and polymer architecture on the overall performance and efficiency of the coatings. Through variation of the LC comonomers and hydrophilic:hydrophobic component ratios, several arrays were synthesized and underwent a variety of analyses to investigate differences in melting transition temperatures, water absorption, gross wettability and solution stability in an assortment of aqueous media. These materials demonstrated an unprecendented reduction in the free water melting transition temperature across the hyperbranched and linear versions. All polymer networks displayed a remarkable % water uptake, while retaining an overall hydrophobic surface. Additionally, LC characteristics were preserved in the hyperbranched polymer networks as seen by POM, and showed great promise in salt-water aqueous environments and cold-weather conditions.

CHAPTER II

INVESTIGATION OF INTRICATE, AMPHIPHILIC CROSSLINKED HYPERBRANCHED FLUOROPOLYMERS AS ANTI-ICING COATINGS FOR EXTREME ENVIRONMENTS[1]

2.1 Overview

Atmospheric icing, the process where supercooled water droplets freeze upon contact with a surface, has proven to be devastating when not controlled or prevented. Examples that endanger human safety include power line outages,[59, 60] malfunctioning of wind turbines,[61, 62] and crashes on roads and runways.[2, 3] Aside from compromising flight safety, icing is costly to remove and time consuming for the aviation industry.[1, 25] The primary reason for this cost is aircraft icing that can accumulate in aircraft induction systems and instrumentation, which negatively impacts performance and efficiency, and adds consequential factors, such as extended holdover times and unforeseen costs when not addressed.[1] The current reactive approach for addressing aircraft icing is the use of deicing fluids, which are toxic and inefficient.[7] The commercial deicing process involves the use of these fluids (primarily propylene glycol or ethylene glycol) that must first be heated, prior to their use, in conjunction with water.[6] Several laboratories have responded to these issues with materials that have a foundation in prevention and,

[1]Reprinted (adapted) with permission from "Investigation of intricate, amphiphilic crosslinked hyperbranched fluoropolymers as anti-icing coatings for extreme environments" by Jennifer S. Zigmond, Kevin A. Pollack, Sarah Smedley, Jeffery E. Raymond, Lauren A. Link, Adriana Pavía-Sanders, Michael A. Hickner and Karen L. Wooley, *J. Polym. Sci. A Polym. Chem.* **2016**, 54 (2), 238-244. Copyright 2015 by John Wiley and Sons.

therefore, present a proactive approach to address icing before manifestation through the use of intrinsically anti-icing materials. Materials that are currently being investigated as anti-icing coatings include superhydrophobic surfaces[9, 12, 18, 21-23] and antifreeze proteins.[29] Superhydrophobic surfaces have been generated through a variety of methods: mechanical and chemical etching followed by the application of a thin film that is typically fluoropolymer-based,[9, 12, 15, 16] or by utilizing unmodified surfaces that are cast with a polymer coating.[11, 17, 21, 23] Of the superhydrophobic surfaces synthesized thus far, anti-icing character has only been demonstrated in a few of these systems.[17, 23] Though superhydrophobic surfaces display great potential as anti-wetting agents, they suffer from high cost, extensive preparation procedures and long times when using surface etching to pre-treat surfaces and ease of damage (since they are typically monolayers). Additionally, Farhadi and coworkers observed an increase in ice adhesion strength when superhydrophobic samples were maintained in air for periods of time at temperatures *ca.* 0 °C, concluding that these systems are limited to low humidity atmospheres because they lose their anti-icing efficiency with increased condensation rates.[12]

In contrast to the generation of superhydrophobic surfaces,[9, 11, 12, 15-17, 21, 23, 34] which avoid wetting and limit water and ice adhesion to substrates, as a typical approach toward anti-icing coatings technologies, we have investigated amphiphilic polymer coatings that present complex nano- and microscopic heterogeneities for inhibition of ice formation in extreme environments. Previously, crosslinked networks comprised of hyperbranched fluoropolymers (HBFP) and poly(ethylene glycol) (PEG) were designed,

synthesized, and shown to exhibit superb anti-biofouling capabilities against marine organisms, credited to their low surface energy, combination of fluoropolymer and PEG compositions, amphiphilic morphology, nanoscopic surface topography and dynamic surface reorganization.[41] As an extension to the anti-biofouling behavior, it was hypothesized that the PEG-water interactions that lead to the organization of water molecules and contribute to resistance of protein adsorption[63-67] could be used as a water-sorbed phase within and on the surface of HBFP-PEG bulk samples to prevent icing.[68, 69] In the current work, surface phenomena and water melting point depression and hydrogen bonding variation resulting from water confinement were further evaluated toward the development of HBFP-PEG-based anti-icing materials for marine, aerospace and other extreme environment applications.

Through the tuning of the amphiphilicity, low surface energy and thermo-responsive molecular ordering of this crosslinked hyperbranched network, the application of these materials was expanded by exploiting their characteristics for the development of robust, dynamic, anti-icing coatings. These materials were produced with the purpose of inhibiting the crystalline organization of water molecules, and subsequently, preventing the formation of ice by increasing the complexity of the amphiphilic surface topography and advancing the molecular ordering of the heterogeneous assemblies, with focus on the molecular interactions that occur between water and the polymer materials at the surface and within the bulk. Initial differential scanning calorimetry (DSC) data showed that these materials exhibit inhibition of ice formation, as determined from reductions in the water melting transition temperatures

(freezing point depressions). Therefore, an array of films was synthesized varying the PEG crosslinker content to study the effect of PEG-to-HBFP ratio on the thermal, mechanical and surface properties, as well as the overall anti-icing efficiency of these materials. The advances of these materials are discussed in terms of the formulations, the structure-function relationships driving the empirically-derived water melting transition temperatures, and the final effects on the water phases at the surfaces.

2.2 Experimental Section

2.2.1 Materials

Reagents and starting materials were purchased from Sigma-Aldrich, Acros and VWR and used as received unless otherwise noted. 2,3,4,5,6-Pentafluorostyrene (PFS) was purchased from Apollo Scientific (U.K.) and purified by passing through a neutral alumina column to remove the inhibitor prior to use.

2.2.2 Instrumentation

Nuclear magnetic resonance spectroscopy. ^{1}H, ^{13}C and ^{19}F nuclear magnetic resonance (NMR) spectroscopies were recorded on a Varian Inova 300 spectrometer. Spectra were analyzed using the solvent signal as an internal reference.

Gel permeation chromatography. The polymer molecular weight and molecular weight distribution were determined by gel permeation chromatography (GPC) performed on a Waters 1515 HPLC pump (Waters Chomatography, Inc.) equipped with a 2414 differential refractometer (Waters, Inc.), a PD2020 dual-angle (15° and 90°) light scattering detector (Precision Detectors, Inc.) and a four-column series of

PL gel columns (Polymer Laboratories, Inc.): 5 μm Guard (50 x 7.5 mm), 5 μm Mixed C (300 x 7.5 mm), 5 μm 10^4 Å (300 x 7.5 mm) and 5 μm 500 Å (300 x 7.5 mm). Polymer solutions were prepared at a known concentration (3-6 mg/mL) and an injection volume of 200 μL was used. The system was equilibrated at 40 °C in THF, which served as the polymer solvent and eluent (flow rate set to 1.00 mL min^{-1}). The differential refractometer was calibrated with Polymer Laboratories, Inc. polystyrene standards (300 to 467 000 Da). Data collection and analysis were performed using the Breeze (version 3.30, Waters, Inc.) software.

Water uptake studies. Water uptake studies were performed on prepared films that underwent two soakings in deionized water. The first was to remove excess residual PEG and was followed by drying under N_2. Dried films were weighed and then submerged in deionized water for 24 h. The wet films were removed and lightly patted with a Kimwipe to remove any free surface water and subsequently weighed.

Fourier-transform infrared spectroscopy. Infrared spectra were obtained on a Shimadzu IR Prestige attenuated total reflectance Fourier-transform infrared spectrometer (ATR-FTIR). Spectra were analyzed using IRsolution software.

Elemental analysis. Elemental analysis was performed at Midwest Microlab, LLC (Indianapolis, IN).

Thermal analysis. Differential scanning calorimetry (DSC) studies were performed on a Mettler Toledo DSC822 (Mettler Toledo, Inc.) with a heating rate of 5 °C/min. Traces were analyzed using STAR^e Evaluation software (version 10.00d,

Mettler Toledo, Inc.) and the T_m was taken at the onset threshold upon the average of the second and third heating scans.

Dynamic mechanical analysis. Mechanical analysis was performed on a Mettler Toledo TT-DMA. All measurements were taken in compression with a frequency of 1.0 Hz, a dynamic force of 1 N, and a static-dynamic force ratio of 1.5. The temperature scans were performed at a ramp rate of 3 °C/min with a 10s sampling interval.

Static surface contact angle. Water contact angles were measured as static contact angles using the sessile drop technique with an Attension Theta optical tensiometer (Biolin Scientific). Drops were fitted with a Young-Laplace formula to calculate the static contact angle in the Theta software (Biolin Scientific).

Confocal microscopy. Confocal microscopy images were taken on a full spectral Olympus FV-1000 laser scanning confocal microscope operating with a 405/488 nm diode laser and fluorescence collection selected by a wide band monochromator from 435 to 535 nm.

2.2.3 Synthesis

4-[Oxy(tri(ethylene glycol))]-2,3,5,6-tetra-fluorostyrene (1). To a 1000 mL three-neck round bottom flask equipped with a magnetic stir bar and addition funnel suspended in an ice bath, sodium hydride (60 wt % dispersion in mineral oil, 4.94 g, 124 mmol) was added followed by dropwise addition of THF (230 mL). A solution of triethylene glycol (42.0 mL, 309 mmol) and THF (43.0 mL) was added dropwise to the stirring solution. Upon completion, a solution of 2,3,4,5,6-pentafluorostyrene (PFS)

(14.2 mL, 20.0 g, 103 mmol) and THF (15.0 mL) was added dropwise. The solution was allowed to warm to room temperature and stir under N_2 for 16 hours. The reaction was concentrated, and the crude product was washed three times against deionized water. The organic phase was dried over sodium sulfate, filtered and concentrated *in vacuo* to afford a pale yellow oil. Further purification by silica gel flash chromatography using a gradient of hexanes to ethyl acetate as eluent afforded **1** as a clear, colorless oil in 67% yield (22.0 g). ^{1}H NMR (300 MHz, $CDCl_3$, ppm): δ 6.60 (dd, *J* = 18 Hz and 12 Hz, 1H, H_2C=C***H***-R), 6.00 (d, *J* = 18 Hz, 1H, ***H***(H)C=CH-R (*trans*)), 5.61 (d, *J* = 12 Hz, 1H, H(***H***)C=CH-R (*cis*)), 4.36 (t, *J* = 4.5 Hz, 2H, TFS-O-C***H***$_2$-CH_2-OR), 3.82 (t, *J* = 4.5 Hz, 2H, R'-O-CH_2-C***H***$_2$-OH), and 3.75-3.55 (m, 8H, TFS-O-CH_2-C***H***$_2$-O-C***H***$_2$-C***H***$_2$-O-C***H***$_2$-CH_2-OH). ^{13}C NMR (75 MHz, $CDCl_3$, ppm): δ 146.6, 143.3, 142.8, 139.4, 136.3, 122.2, 122.0, 110.8, 74.1, 70.8, 70.7, 70.2, 68.8 and 64.9. ^{19}F NMR (282 MHz, $CDCl_3$, ppm): δ -145 (m, 2F, ***ortho-F*** to -CH=CH_2) and -158 (m, 2F, ***meta-F*** to –CH=CH_2). IR: 3600 – 3200, 3050 – 2750, 1680 – 1590, 1550 – 1390, 1360, 1290, 1250, 1200 – 1000, 960, 940, 880, 850 cm^{-1}. HRMS m/z calculated for $C_{14}H_{16}O_4F_4$ $[M+H]^+$ 325.11 Da, found 325.1063.

4-[Oxy(tri(ethylene glycol))bromoisopropionyl] -2,3,5,6-tetrafluorostyrene (2). To a 1000 mL two-neck round bottom flask equipped with a magnetic stir bar and addition funnel suspended in an ice bath, a solution of **1** (10.0 g, 30.8 mmol), triethylamine (16.0 mL, 111 mmol) and THF (235 mL) was added. A solution of 2-bromopropionyl bromide (3.90 mL, 37.0 mmol) and THF (20.0 mL) was added dropwise. The solution was allowed to warm to room temperature and stir under N_2 for

14 hours. The reaction was concentrated, and crude product was washed three times against brine. The organic phase was dried over sodium sulfate, filtered and concentrated *in vacuo* to afford a pale yellow oil. Further purification by silica gel flash chromatography using a gradient of hexanes to ethyl acetate as eluent afforded **2** as a clear, pale yellow oil in 59% yield (8.40 g). ^{1}H NMR (300 MHz, $CDCl_3$, ppm): δ 6.61 (dd, *J* = 18 Hz and 12 Hz, 1H, H_2C=C***H***-R), 6.02 (d, *J* = 18 Hz, 1H, ***H***(H)C=CH-R (*trans*)), 5.62 (d, *J* = 12 Hz, 1H, H(***H***)C=CH-R (*cis*)), 4.39 (q, *J* = 6.9 Hz, 1H, R-C(***H***)(Br)CH_3), 4.37 (t, *J* = 4.8 Hz, 2H, TFS-O-C***H***$_2$-CH_2-OR), 4.31 (t, *J* = 4.8 Hz, 2H, R-O-CH_2-C***H***$_2$-O(O)C-R'), 3.83 (t, *J* = 4.8 Hz, 2H, TFS-O-CH_2-C***H***$_2$-OR), 3.75-3.60 (m, 6H, R-O-C***H***$_2$-C***H***$_2$-O-C***H***$_2$-CH_2-O(O)C-R') and 1.81 (d, *J* = 6.9 Hz, 3H, R-C(H)(Br)C***H***$_3$). ^{13}C NMR (75 MHz, $CDCl_3$, ppm): δ 170.9, 146.6, 143.3, 142.8, 139.3, 136.3, 122.2, 122.0, 110.8, 74.1, 70.8, 70.6, 70.1, 68.8, 64.6, 55.6 and 30.5. ^{19}F NMR (282 MHz, $CDCl_3$, ppm): δ -145 (m, 2F, ***ortho-F*** to –CH=CH_2) and -158 (m, 2F, ***meta-F*** to –CH=CH_2). IR: 3070 – 2750, 1740, 1640, 1550 – 1310, 1220, 1190 – 1000, 965, 935, 855, 760, 675 cm^{-1}. HRMS m/z calculated for $C_{17}H_{19}O_5F_4Br$ $[M+H]^+$ 459.02 Da, found 459.0430.

Hyperbranched fluoropolymer (HBFP$^{(III)}$, w/67 mol% PFS) (3). To a flame-dried 10 mL schlenk flash equipped with a magnetic stir bar, a solution of **2** (2.00 g, 4.36 mmol), PFS (1.20 mL, 1.70 g, 8.71 mmol), 2,2'-bipyridine (150 mg, 0.96 mmol) and anisole (5 mL) was added. The solution was deoxygenated *via* freeze-pump-thaw (x3) upon adding CuBr (62.5 mg, 0.44 mmol). An additional two deoxygenation cycles were performed, and the vessel was backfilled with N_2 then placed in a preheated oil bath (65

°C) and allowed to proceed for 16 hours. The polymerization was quenched by opening the flask to air and submerging the flask in liquid nitrogen. Copper was removed by elution through an aluminum oxide plug, and the polymer was obtained after three precipitations in cold hexanes to afford a white powder of **3** in quantitative yield (2.79 g). M_n^{GPC} = 46900 Da, M_w/M_n = 1.66. T_g = 60 °C. T_d: 361 – 433 °C, 57% mass loss at 500 °C. ^{1}H NMR (300 MHz, $CDCl_3$, ppm): δ 4.45 – 4.20 (br, m, TFS-O-C***H***$_2$-CH_2-OR and R-O-CH_2-C***H***$_2$-O(O)C-R'), 3.90 – 3.60 (br, m, TFS-O-CH_2-C***H***$_2$-O-C***H***$_2$-C***H***$_2$-O-C***H***$_2$-OR), 2.80 – 1.50 (br, m, C***H***$_2$-C***H***(R)- backbone), 1.30 – 0.85 (br, m, C-C***H***$_3$). ^{13}C NMR (75 MHz, $CDCl_3$, ppm): δ 176.6, 144.7, 140.7, 137.6, 122.2, 114.7, 74.3, 70.8-70.0, 68.8, 63.6, 41.7-32.1, 30.7-29.7, 24.7. ^{19}F NMR (282 MHz, $CDCl_3$, ppm): δ -143 (br, m, ***ortho-F*** (PFS) and ***ortho-F*** (TFS)), -156 (br, m, ***para-F*** (PFS) and ***meta-F*** (TFS)), -161 (br, m, ***meta-F*** (PFS)). IR: 3050 – 2790, 1740, 1645, 1575 – 1400, 1360, 1320 – 1190, 1185 – 1010, 955, 860, 785 – 710 cm^{-1}. Anal. calcd. for $C_{1874}H_{1132}F_{946}Br_{34}$: C, 48.03; H, 2.43; F, 38.35; Br, 5.80%. Found: C, 48.22; H, 3.01; F, 30.68; Br, 10.10%.

General procedure for the preparation of HBFP$^{(III)}$-PEG crosslinked networks. To a scintillation vial, bis(3-aminopropyl) terminated PEG (30.0 mg, 0.02 mmol) and THF (0.75 mL) were added and stirred until homogeneous *ca*. 10 min. To the solution, **3** (30.0 mg, 0.006 mmol) and *N*,*N*-diisopropylethylamine (DIPEA) (21.0 μL) were added and allowed to stir for 30 min. The solution was drop cast onto pre-cut aluminum squares or 40 μL aluminum DSC pans. A period of *ca.* 1 hour allowed for the excess solvent to evaporate and afford a pre-gel that was cured at 110 °C for 45 min

under N_2 atmosphere. IR: 3030 – 2750, 1730, 1650, 1545 – 1400, 1320 – 1010, 980, 955, 900 – 780 and 730 cm^{-1}. T_g = -53 °C. T_m = 30 °C. T_d: 246 – 434 °C, 64% mass loss at 500 °C. Subsequent films were prepared in the same manner by varying the wt% PEG, calculated as w/w% of the total mass to afford a total of 9 formulations.

2.3 Results and Discussion

The amphiphilic HBFP$^{(III)}$-PEG networks were composed of a hydrophobic, low surface energy third generation hyperbranched fluorocopolymer,[40] crosslinked with diamino poly(ethylene glycol), a hydrophilic, water soluble moiety, and were fully hydrated in liquid water. The amphiphilic networks were prepared and characterized as previously described[40] through nucleophilic substitution between the amino chain ends of bis(3-aminopropyl) terminated PEG (M_n = 1500 Da) and the benzylic bromide and bromoacetyl functionalities of the hyperbranched fluorocopolymer, HBFP$^{(III)}$-b, (M_n = 47 kDa) upon casting from tetrahydrofuran (THF) solution into 40 μL aluminum DSC pans or pre-cut, aluminum squares (Scheme 2.1). The coated pans and squares were cured at 110 °C for 45 minutes under an inert atmosphere. The stoichiometries of the HBFP$^{(III)}$ and PEG were varied to produce an array of coatings for evaluation of compositional effects on the thermal, mechanical and surface properties. To take advantage of the

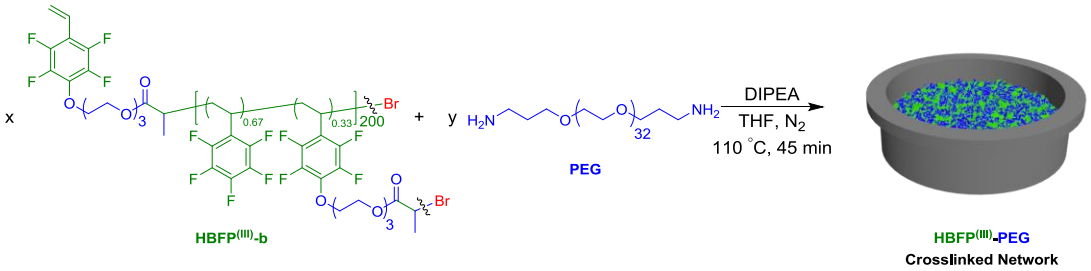

Scheme 2.1. Preparation of HBFP$^{(III)}$-PEG crosslinked networks, where the mass ratios of HBFP$^{(III)}$-b:diamino PEG were 5:2, 2:1, 3:2, 1:1, 2:3, 1:2, and 2:5, corresponding to molar ratios x:y of 1:12, 1:18, 1:22, 1:35, 1:47, 1:63, and 1:78.

complex surface topography, the films were fully hydrated in liquid water to experience the dynamic reorganization. Water uptake studies were performed to determine the amount of water required to fully hydrate each film, which ranged from 6.6 to 73.7 wt % water for the lowest to highest PEG wt % within the networks (Table 2.1).

Table 2.1. Wt % H_2O uptake of HBFP$^{(III)}$–PEG coatings.

	Mass ratio HBFP$^{(III)}$-b to PEG (wt %)								
	HBFP$^{(III)}$	5:2	2:1	3:2	1:1	2:3	1:2	2:5	PEG
Wt % H_2O	6.6	16.9	27.9	29.1	42.5	17.5	42.5	67.0	73.7

For the DSC studies of anti-icing performance, 200 wt % water was added to each sample, so the films would be fully hydrated in the presence of excess free water. The calorimetric properties of the seven HBFP$^{(III)}$-PEG networks and two control samples of neat HBFP$^{(III)}$ and PEG were investigated from (-50 °C to 20 °C) over three cycles, in both heating and cooling modes. The freezing point measurements upon cooling exhibited high degrees of variability (Table 2.2) and, therefore, were considered

unreliable. In contrast, the heating cycles provided consistent water melting temperature measurements within a given sample composition. DSC data showed two melting transition temperatures, one in the *ca.* -25 °C range, and another at *ca.* 0 °C for the hybid HBFP$^{(III)}$-PEG systems, whereas each neat polymer sample exhibited only a single T_m transition. The lower temperature transition is attributed to the T_m of the bound water within the HBFP$^{(III)}$-PEG matrix and the transition around 0 °C is the melting of the free

Table 2.2. Average onset crystalline temperature (T_c) for the array of HBFP$^{(III)}$–PEG coatings and HBFP$^{(III)}$ and PEG control samples, each with 200 wt % water.

	Mass ratio HBFP$^{(III)}$-b to PEG (wt %)								
	HBFP$^{(III)}$	5:2	2:1	3:2	1:1	2:3	1:2	2:5	PEG
Avg. T_c Onset (°C)	-22.2 ± 1.4	-17.4 ± 1.2	-18.4 ± 1.5	-19.3 ± 0.8	-16.8 ± 0.8	-18.4 ± 0.7	-19.5 ± 0.0	-18.0 ± 1.2	-17.9 ± 1.0

water on the surface.[70] Although melting transition temperature measurements provide for an observation of a maximum temperature as an upper limit of anti-icing behavior, the results from both the bound- and free-water melting transitions clearly indicate that the binary system depresses the freezing point of water (Table 2.3). From the data, some relationships can be drawn between both types of melting curves and the ratio of PEG. As the wt % PEG increased, the T_m of bound water increased, suggesting that the water molecules became less confined and more bulk-like. In contrast, the T_m of free water decreased and approached the T_m observed in the presence of neat PEG, suggesting a higher proportion of surface-active PEG with increasing PEG wt %. This indirect relationship between the bound water T_m and free water T_m suggests that by tuning one

melting transition, the other will alter in a predictable manner, and the optimized coincident anti-icing behavior can be tuned at an intermediate stoichiometry.

Table 2.3. Average onset melting temperatures (T_m) for the array of HBFP$^{(III)}$–PEG coatings and HBFP$^{(III)}$ and PEG control samples, each with 200 wt % water.

Mass ratio HBFP$^{(III)}$-b to PEG (wt %)									
HBFP$^{(III)}$		5:2	2:1	3:2	1:1	2:3	1:2	2:5	PEG
Avg. H_2O T_m onset (°C)									
Bound	-3.1 ± 0.0	-1.6 ± 0.0	-25.5 ± 0.1	-27.0 ± 0.0	-26.5 ± 0.1	-25.8 ± 0.0	-25.7 ± 0.0	-25.5 ± 0.0	-10.4 ± 1.3
Free			-1.5 ± 0.1	-1.6 ± 0.1	-2.9 ± 0.1	-3.5 ± 0.0	-4.4 ± 0.0	-4.6 ± 0.0	

The interaction between water and the binary system was explored further using Fourier transform infrared (FTIR) spectroscopy. The shifts of the water OD stretch absorbance signals for two samples were studied, relative to the absorbance for neat deuterated water; one with relatively high PEG content (2:5) and one with relatively low content (5:2). The relative humidity was adjusted by flowing a 5 mol % D_2O in H_2O (to form predominantly HOD in H_2O) solution through the FTIR flow cell.[71] The samples experienced a blue shift in comparison to bulk water (2509 cm^{-1}) as a function of hydration. The hypothesis is that this shift is due to water molecules being confined by the polymer matrix, *e.g.* the hydrophilic PEG domains are sequestering water as previously observed.[41, 68] The OD peak was deconvoluted to extract the populations of water in the two different microenvironments, free and bound, using a method that has been discussed previously (Figure 2.1).[72] The percentages correspond with the DSC

measurements, as the amount of PEG in the sample increased, so did the amount of free water. The 5:2 sample contained 12.3% free water while the 2:5 sample contained 30.5% bulk-like water.

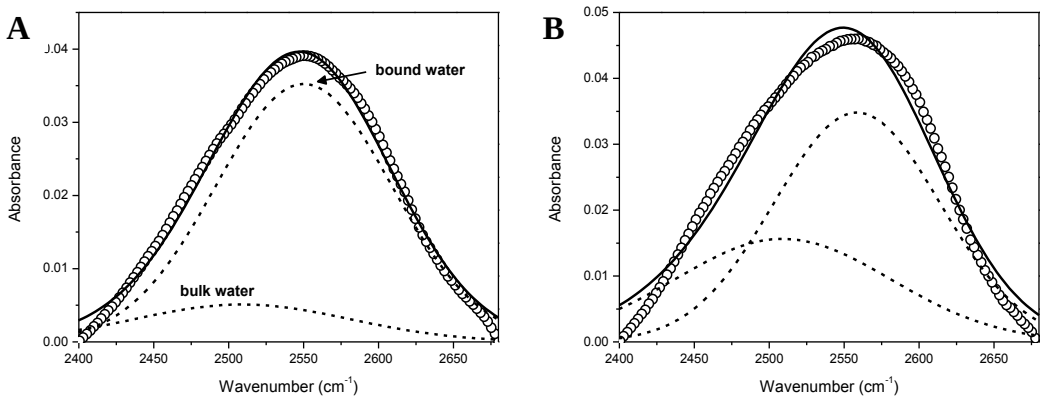

Figure 2.1. Deconvolution of OD peak stretch vibration of (A) 5:2 HBFP$^{(III)}$-PEG and (B) 2:5 HBFP$^{(III)}$-PEG used to extract percentages of water in either the free or the bound state.

The same two formulations (2:5 and 5:2) and the sample with the lowest variation in T_m based on DSC (2:3) in the dry state were subjected to dynamic mechanical analysis (DMA) under compression to observe their viscoelastic behaviors as a function of temperature (Figure 2.2). At low temperatures, where the semi-crystalline PEG domains are expected to act as reinforcing fillers, the formulations with higher PEG content (2:3 and 2:5) exhibited greater storage modulus values compared to the formulation in which PEG was the minority phase (5:2). The 2:3 and 2:5 formulations also expressed a rapid drop in modulus at *ca.* -40 °C corresponding to the glass transition of the PEG domains. All three formulations expressed a drop in modulus

between 20 and 60 °C corresponding to the glass transition of the HBFP$^{(III)}$. At high temperatures, where PEG is expected to act as long flexible chains, decrease the crosslink density, and soften the network, the modulus was lower for formulations with higher PEG wt %. The storage moduli of formulations above 60 °C remained constant or slightly increased, which is characteristic of crosslinked networks, where this rubbery modulus plateau is proportional to the crosslink density of the network. As expected, the crosslink density decreased as the weight fraction of PEG in the network increased.

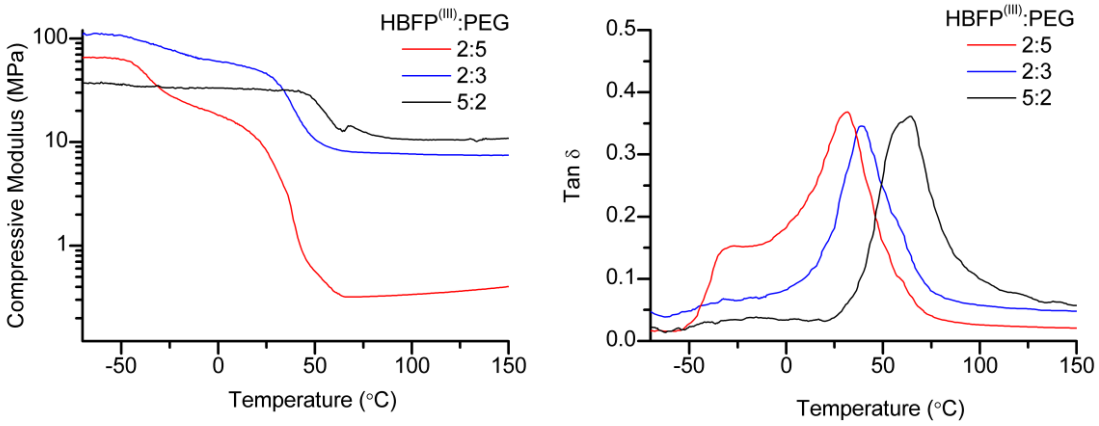

Figure 2.2. Dynamic mechanical analysis results, compressive storage modulus (left) and tan δ (right) as a function of temperature. See Table 2.4 for detailed values at various temperatures.

Similar to the behavior observed in previously reported HBFP-PEG networks, when PEG was in its semi-crystalline phase, increasing the PEG content enhanced the mechanical properties of the network, but when PEG was in its rubbery phase, due to increased temperature or water content, increasing the PEG content reduced the

mechanical performance of the network.[40, 69] The tan δ behavior was used to investigate the phase transitions and homogeneity of the three formulations. The tan δ_{max} (maximum tan δ values) of the 2:5, 2:3, and 5:2 formulations were observed at 31, 38, and 67 °C, respectively, and correspond to glass transitions of the networks. The 2:5 formulation, containing the highest weight fraction of PEG, also expressed a second minor tan δ peak at -26 °C, which can be attributed to the glass transition of a second PEG-rich phase within the 2:5 formulation (Table 2.4).

Table 2.4. Temperatures at which tan δ peak values occur and storage modulus at various temperatures. [a]Corresponds to the minor tan δ peak.

$HBFP^{(III)}$:PEG	Tan δ_{max} (°C)	E' at -50 °C (MPa)	E' at -10 °C (MPa)	E' at 25 °C (MPa)	E' at 100 °C (MPa)
2:5	-26[a], 31	62	21	8.0	0.34
2:3	38	107	64	46	7.6
5:2	67	36	33	32	11

To investigate the mechanical performance in an environment close to that would be experienced in the field, the 2:3 formulation was subjected to *in situ* submersion DMA in deionized water at 10 °C and the storage modulus was measured over 18 h (Figure 2.3). There was an initial rapid increase in modulus from 16 to 50 MPa within the first 30 min, an effect of the sudden decrease in temperature from room temperature to 10 °C. The modulus continued to increase by 13 MPa over the following 17 h, in response to the water, resulting in a net response to submersion of $\Delta E' = 47$ MPa. As the network became fully saturated, the PEG domains absorbed water and caused the

amorphous HBFP-rich domains to rigidify, increasing the overall stiffness of the material.

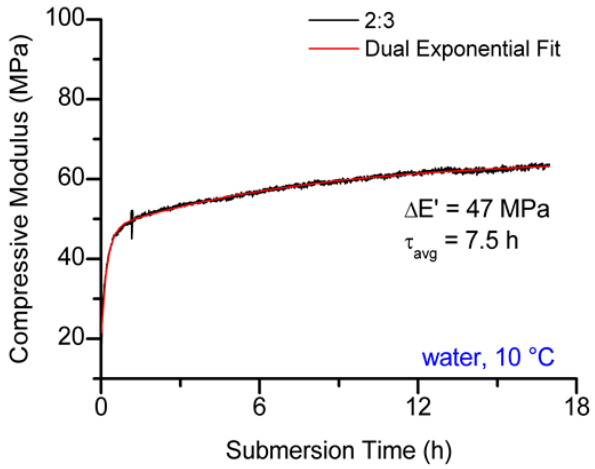

Figure 2.3. Compressive storage modulus of the 2:3 formulation as a function of submersion time in deionized water at 10 °C. Data was fit to a dual-exponential decay function (R_2 = 0.994), total change in modulus was +47 Mpa, calculated average lifetime based on exponential fit was 7.5 h.

To determine whether film morphology could be altered to induce greater water T_m depression, the solvent used during the crosslinking step, tetrahydrofuran, was changed to a comparable, aprotic solvent, methylene chloride (DCM); for testing of this premise, the 2:3 HBFP$^{(III)}$-PEG network was chosen for consistency. Films were prepared in the same manner as previously described with a modification of addition of various amounts of DCM with THF for casting to produce a second array of films. Overall, the T_m's of free and bound water were lower, and lower concentrations of THF corresponded with a lower water T_m (Table 2.5). In other words, the T_m values for the

bound and free water within the 100 volume % DCM sample were lower than the T_m values of the 100 volume % THF film (Figure 2.4).

Table 2.5. Average onset melting temperature (T_m) for solvent array of HBFP$^{(III)}$–PEG coatings with 200 wt % water.

Avg. T_m onset (°C)	Volume percentage of THF						
	100%	75%	50%	40%	25%	20%	0%
Bound	-25.8 ± 0.0	-26.9 ± 0.0	-26.9 ± 0.1	-26.9 ± 0.0	-26.8 ± 0.0	-27.0 ± 0.0	-27.1 ± 0.0
Free	-3.5 ± 0.0	-3.3 ± 0.1	-4.1 ± 0.1	-3.6 ± 0.1	-3.9 ± 0.1	-4.5 ± 0.1	-4.5 ± 0.1

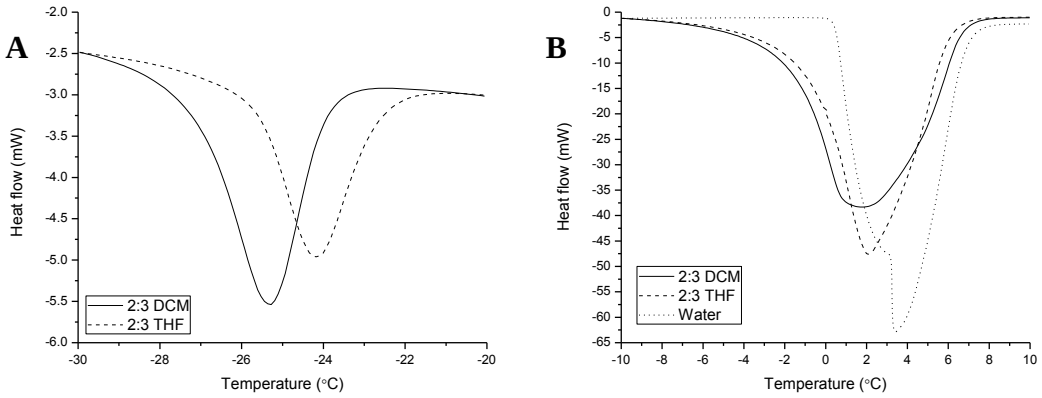

Figure 2.4. DSC heating traces of 2:3 HBFP$^{(III)}$-PEG film dropcasted from 100 vol % DCM (solid) and 100 vol % THF (dash), over the temperature ranges of the (A) bound water and (B) free water melting transitions with neat water (dot) as a reference.

This trend was explored further with the use of FTIR to study the different evaporation rates of the two solvents (Figure 2.5). A 2:3 HBFP$^{(III)}$-PEG formulation composed of equivalent volumetric amounts of THF and DCM was directly cast onto the

FTIR crystal and monitored every 15 seconds for 1 minute. From the CH_2 alkyl stretch (2970 cm^{-1}) and C-O ether stretch (1060 cm^{-1}) of THF, it was observed that THF was no longer present within the film after 30 seconds following casting. However, the C-Cl stretch (730 cm^{-1}) of DCM was still apparent at 60 seconds, suggesting that DCM is the predominant solvent present during the annealing of the films. Additionally, the $HBFP^{(III)}$ and PEG were visually more soluble in DCM than THF, suggesting there is higher mobility and greater reactivity within the system with DCM as the solvent.

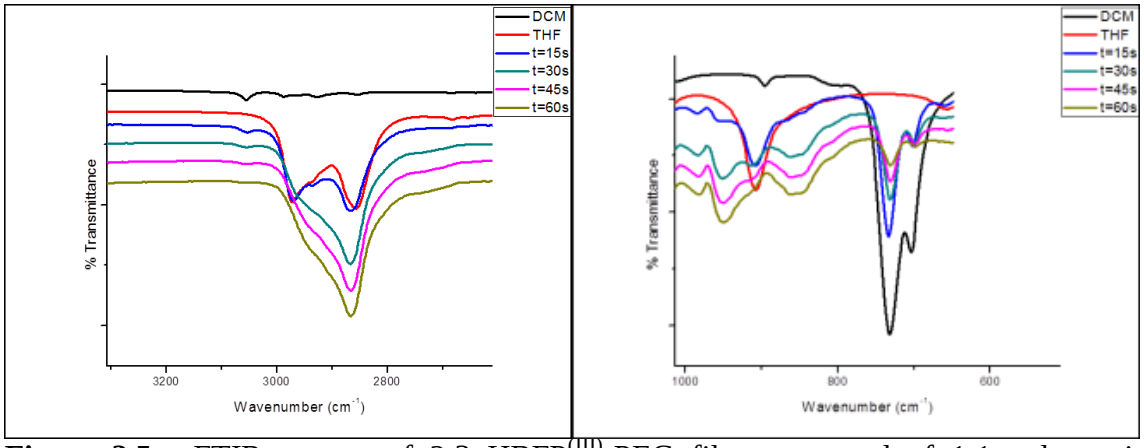

Figure 2.5. FTIR spectra of 2:3 $HBFP^{(III)}$-PEG film composed of 1:1 volumetric amounts of DCM and THF.

To assess the gross wettability of this array of samples, water contact angle measurements were performed on the dry films at different time intervals. The general measurement procedure involved placing a film on the stage and dropping one- 1.0 µL sessile drop on the film. Measurements were taken at 0, 10, 30 and 60 seconds for each film (Table 2.6). The reduction of contact angle over time indicates a strong effect by

the hydrophilic PEG, driving molecular reorganization events as water is sorbed into the films. A more interesting result was observed at 0 seconds, with a decrease in the water contact angle as the concentration of THF decreased. This effect can also be observed in Table 2.1 with the 0 volume % THF formulation exhibiting the lowest free water T_m. Due to the fact that these are dry films, the lower initial contact angle suggests a higher proportion of PEG-rich surface composition and/or a shorter surface reorganization time for the DCM dominant films. To explore these PEG and HFBP domains further,

Table 2.6. Summary of static water contact angle measurements of dry binary systems cast from varying amounts of DCM and THF.

	t = 0 s	t = 10 s	t = 30 s	t = 60 s
100 vol % THF	63° ± 4	45° ± 5	40° ± 6	38° ± 4
75 vol % THF	63° ± 3	51° ± 8	46° ± 7	43° ± 6
50 vol % THF	63 ° ± 2	54° ± 4	45° ± 6	37° ± 5
40 vol % THF	65° ± 5	49° ± 11	48° ± 9	45° ± 9
25 vol % THF	61° ± 7	49° ± 11	40° ± 7	33° ± 5
20 vol % THF	58° ± 2	42° ± 2	35° ± 3	32° ± 1
0 vol % THF	52° ± 4	37° ± 2	36° ± 7	35° ± 4

confocal microscopy measurements were performed utilizing the autofluorescence of the HBFP$^{(III)}$. Using two films, 2:3 annealed from THF and 2:3 annealed from DCM, large differences in domain sizes were observed (Figure 2.6). For the DCM film, large PEG-rich domains can be observed surrounded by smaller, nonuniform PEG-rich domains. However, in the THF film, the PEG-rich domains are more evenly distributed throughout the film. These measurements aid in understanding the difference in water contact angle measurements between the two systems, annealed in DCM or THF. There

is initially higher water adsorption/absorption in the DCM films due to the large PEG domains present, leading to observation of lower water contact angles. In contrast, in the THF-produced films, the water is more evenly dispersed throughout the film, leading to the initially higher contact angle. Over time, the water fully equilibrates throughout the materials resulting in the minor difference in contact angle measurements at 60 seconds.

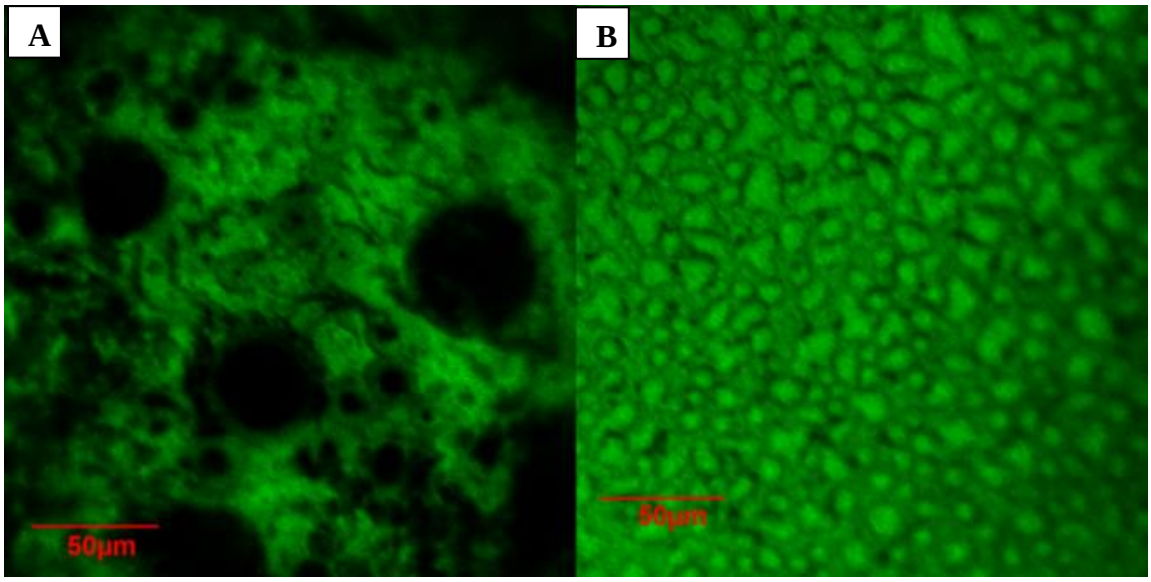

Figure 2.6. Confocal microscopy image of 2:3 HBFP$^{(III)}$-PEG film cast from (A) 100 vol % DCM and (B) 100 vol % THF.

2.4 Conclusions

In summary, we have demonstrated unique anti-icing characteristics for an established HBFP$^{(III)}$-PEG crosslinked network, which expands the utility for these materials and extends anti-icing materials concepts to include complex, heterogeneous amphiphilic materials. Through DSC studies, the binary system has shown great

potential as an anti-icing coating due to the film's ability to depress the freezing/melting temperature of water. Additionally, by tuning the weight percentage of PEG and the drop casting solvent, greater effects on the organization of water and potential anti-icing ability can be achieved. All of the studies performed have demonstrated common behaviors of this system including confinement of water molecules by the polymer matrix, sequestration of water by the hydrophilic PEG domains and dynamic surface reorganization upon full hydration. DMA analyses alluded to the mechanical performance of the films in the dry state, where the PEG domains behave as crystallites, and the wet state, where PEG domains are soft and water-absorbing, making them prime candidates for engineering materials in anti-icing applications. An interesting result that presented itself is the difference in maximum hydration achieved through direct and indirect contact with water, which should be further explored due to the presence of humidity in most regions.

2.5 Acknowledgements

Financial support from the Office of Naval Research (Grant N00014-14-1-0082 and N00014-15-1-2280 to K.L.W and N00014-10-1-0875 to M.A.H) and W.T. Doherty – Welch Chair in Chemistry (A-0001) are gratefully acknowledged. We thank Joseph Fornefeld from Midwest Microlab LLC for elemental analysis and the Laboratory of Biological Mass Spectrometry.

CHAPTER III

DYNAMIC ANTI-ICING COATINGS: COMPLEX, AMPHIPHILIC HYPERBRANCHED FLUOROPOLYMER POLY(ETHYLENE GLYCOL) CROSSLINKED NETWORKS WITH AN INTEGRATED LIQUID CRYSTALLINE COMONOMER[2]

3.1 Overview

The discovery of liquid crystals occurred over a century ago; however, the development of liquid crystalline polymers (LCPs) from such molecules has only been investigated over the past few decades. Advancements in the field of LCPs have resulted in materials with unique properties that possess not only the characteristics of each individual component, but also display completely new features that make them applicable in a variety of technologies.[46-48, 73-77] In general, main-chain LCPs are commonly used in semiconducting applications[47, 48] or for materials requiring high strength, such as Kevlar®, whereas side-chain LCPs are often employed for electro-optical devices[46] or light-driven applications.[76, 77] However, due to the challenges in processing main-chain LCPs and their elevated transition temperatures, research efforts have mostly focused on side-chain LCPs. New applications have been discovered, as scientists have begun self-assembling these unique materials as side-chains within a

[2]Reprinted (adapted) with permission from "Dynamic Anti-icing Coatings: Complex, amphiphilic hyperbranched fluoropolymer poly(ethylene glycol) cross-linked networks with an integrated liquid crystalline comonomer" by Jennifer S. Zigmond, Adriana Pavía-Sanders, Joel D. Russell and Karen L. Wooley, *Chem. Mater.* **2016**. Copyright 2016 by American Chemical Society.

variety of polymers, through non-covalent[78-85] and covalent interactions.[86, 87] Non-covalent interactions have been extensively studied recently; for instance, Kato *et al*.[81, 82, 88] have investigated the incorporation of LCPs through hydrogen bonding interactions for the production of biopolymers, which allow these dynamic structures to respond to external stimuli. Nevertheless, although the non-covalent systems are of high interest, covalent incorporation of LC mesogens has the greatest potential for long-term retention of the LC components under challenging conditions.

The question of whether thermotropic LCPs could be integrated into the field of coatings was first proposed near the turn of the 21st century, due to their thermal resistance, environmental resistance to weathering and chemicals, and a low coefficient of linear thermal expansion.[24, 26, 36] Recent research and development advances have focused on general coating properties, such as adhesion, hardness and flexibility.[25, 37-39, 57] For instance, Athawale and coworkers observed comparable adhesion and flexibility between LC acrylic copolymers and conventional acrylic copolymers; moreover, they also observed an improvement in pencil hardness for the copolymers containing an LC moiety.[37] Additionally, Yoshida *et al*. recognized an enhancemnet in impact resistance and elongation without compromising material hardness, among polymers with LC side groups when compared to those without LC monomers.[38] Guerriero and coworkers studied the use of thermotropic main-chain LCPs against commercially-available LCPs as protective coatings for aerospace applications and showed increased adhesion as well as an increase in wear and impact resistance.[25] Overall, thermotropic LCPs have demonstrated a great potential in coatings applications and should be further explored as

there has been little activity in the area over the last decade. Herein, we present a crosslinked network as a protective coating that is designed for anti-icing applications by incorporating an LC moiety in our binary, amphiphilic hyperbranched polymer system.[40]

The success of the binary HBFP$^{(III)}$-PEG system, initially as a compositionally-, topographically- and morphologically-complex coating that exhibited anti-biofouling properties[41] and more recently its unique anti-icing characteristics,[89] has led to additional investigations and chemical manipulations with the goal of enhancing the dynamic complexity of these materials. These previously-synthesized networks exhibit low surface energy, a nanoscopic surface topography, and dynamic surface reorganization when water-swollen, leading to unique properties that have been shown to reduce fouling by marine organisms and depress the freezing/melting point of water.[41, 89] Since the binary system presents complex nano and microscopic heterogeneities, it was important to investigate the addition of a thermally-dynamic molecule, such as a LC comonomer to create a multi-step environmentally stimuli-responsive material. The expanded amphiphilic HBFP$^{(III)}$-PEG incorporates a mesogenic unit into the polymer system for the purpose of adding a dynamic ordering effect that is typically found in liquid crystalline polymers.[46] It was hypothesized that the incorporated mesogenic unit would have a favorable effect on the properties of the polymer by adding LC motions, triggered by a change in temperature, that enhance ice formation resistance and dynamic surface reorganization versatility, thereby expanding the venue of applications for this system, without discarding the key features of the original binary HBFP$^{(III)}$-PEG system.

3.2 Experimental Section

3.2.1 Materials

Reagents and starting materials were purchased from Sigma-Aldrich, Acros and VWR and used as received unless otherwise noted. 2,3,4,5,6-Pentafluorostyrene (PFS) was purchased from Apollo Scientific (U.K.). Monomers were purified by passing through a neutral alumina column to remove the inhibitor prior to use.

3.2.2 Instrumentation

Nuclear magnetic resonance spectroscopy and mass spectrometry. Small molecules, monomers and polymers were characterized by ^{1}H and ^{13}C nuclear magnetic resonance (NMR) spectroscopies using a Varian Inova 300 spectrometer. Fluorinated compounds were also characterized by ^{19}F NMR spectroscopy using a Varian Inova 300 spectrometer. Spectra were analyzed using the solvent signal as an internal reference. High resolution mass spectrometry (HRMS) for the small molecules was conducted on an Applied Biosystems PE SCIEX QSTAR.

Size exclusion chromatography. The polymer molecular weight and molecular weight distribution were determined by size exclusion chromatography (SEC) performed on a Waters 1515 HPLC pump (Waters Chomatography, Inc.) equipped with a 2414 differential refractometer (Waters, Inc.), a PD2020 dual-angle (15° and 90°) light scattering detector (Precision Detectors, Inc.) and a four-column series of PL gel columns (Polymer Laboratories, Inc.): 5 μm Guard (50 x 7.5 mm), 5 μm Mixed C (300 x 7.5 mm), 5 μm 10^4 Å (300 x 7.5 mm) and 5 μm 500 Å (300 x 7.5 mm). Polymer solutions were prepared at a known concentration (3-6 mg/mL) and an injection volume

of 200 μL was used. The system was equilibrated at 40 °C in THF, which served as the polymer solvent and eluent (flow rate set to 1.00 mL min^{-1}). The differential refractometer was calibrated with Polymer Laboratories, Inc. polystyrene standards (300 to 467,000 Da). Data collection and analysis were performed using Breeze (version 3.30, Waters, Inc.) software.

Fourier-transform infrared spectroscopy. Infrared spectra were obtained on a Shimadzu IR Prestige attenuated total reflectance Fourier-transform infrared spectrometer (ATR-FTIR). Spectra were analyzed using IRsolution software.

Elemental analysis. Elemental analysis of the polymers was performed at Midwest Microlab, LLC (Indianapolis, IN).

Thermal analysis. Differential scanning calorimetry (DSC) studies were performed on a Mettler Toledo DSC822 (Mettler Toledo, Inc.) with a heating rate of 5 °C/min and a cooling rate of 2 °C/min. Traces were analyzed using STAR^e Evaluation software (version 10.00d, Mettler Toledo, Inc.) and the T_m was taken at the onset threshold upon the average of the second and third heating scans. Thermogravimetric analysis was performed under Ar atmosphere using a Mettler-Toledo model TGA/DSC 1 STAR^e system, with a heating rate of 10 °C/min. Measurements were analyzed using STAR^e Evaluation software (version 10.00d, Mettler Toledo, Inc.).

Static surface contact angle. Water contact angles were measured as static contact angles using the sessile drop technique with an Attension Theta optical tensiometer (Biolin Scientific). Drops were fitted with a Young-Laplace formula to calculate the static contact angle in the Theta software (Biolin Scientific).

Water uptake studies. Water uptake studies were performed on prepared films that underwent two soakings in deionized water. The first was to remove excess residual PEG and was followed by drying under vacuum at 35 °C for 16 h. Dried films were weighed and then submerged in deionized water for 24 h. The wet films were removed and lightly patted with a Kimwipe to remove any free surface water and subsequently weighed.

X-ray diffraction. X-ray diffraction (XRD) patterns were obtained on a Bruker D8 Advanced Power X-ray diffractometer with Cu-K_α incident radiation (λ = 1.5418 Å). Scans were taken in increments of 0.05 between 2Θ of 3 and 40 at a scan speed of 1 s^{-1}. The temperature rate was 0.08 °C/s.

Polarized optical microscopy. Polarized optical micrographs were collected using an Olympus BX60 optical microscope and cross polarizers at 20x or 50x magnification in conjunction with a Mettler FP80 Hot Stage. The heating rate was 5 °C/min and the cooling rate was 2 °C/min.

Infrared microscopy. A Thermo Scientific Nicolet iN10 Infrared Microscope was used to collect 300 x 200 micrometer surface scans. The system was operated in cooled reflection mode with a 20 x 20 micrometer aperture and 64 scans. The background was taken of the glass substrate the films were cast onto in order to remove the rotational and vibrational frequency signals associated with the glass.

3D optical microscopy. 3D optical micrographs were collected using a Bruker Contour GT-K Optical Profiler at 20x magnification.

3.2.3 Synthesis

6-(1,1'-biphenyl]-4-yloxy)hexan-1-ol (1). To a flame dried 100 mL Schlenk flask equipped with a magnetic stir bar, potassium carbonate (12.2 g, 88.1 mmol) and a trace amount of potassium iodide (198 mg, 1.22 mmol) were dried under reduced pressure for 1.5 h. A solution of 4-phenylphenol (5.06 g, 29.4 mmol) in dry DMF (41.0 mL) was added and allowed to stir at room temperature for 1 h. A solution of 6-chloro-1-hexanol (4.00 mL, 29.4 mmol) was added dropwise and the reaction was placed in a preheated oil bath (70 °C) for 16 h. Unreacted solid was filtered off and the remaining solution was washed against deionized water, sodium bicarbonate solution and brine. The organic phase was dried over sodium sulfate, filtered and concentrated *in vacuo* to afford an off-white powder. The crude product was purified by recrystallization using a 1:1 hexanes:ethyl acetate solution to afford the mesogen as a translucent solid in 72% yield (5.69 g). T_m = 80 and 97 °C. TGA in Ar: 278 - 361 °C, 99% mass loss; 0.7% mass remaining at 500 °C. ^{1}H NMR (300 MHz, $CDCl_3$, ppm): δ 7.54 (m, 4H, ***meta-H*** to –O-CH_2-R and ***2'-H*** to Ar-O-CH_2-R), 7.42 (m, 2H, ***3'-H*** to Ar-O-CH_2-R), 7.30 (m, 1H, ***4'-H*** to Ar-O-CH_2-R), 6.97 (m, 2H, ***ortho-H*** to -O-CH_2-R), 4.01 (t, J = 6.5 Hz, 2H, Ar-O-C***H$_2$***-R), 3.68 (t, J = 6 Hz, 2H, R-C***H$_2$***-OH), 1.83 (quintet, J = 6.8 Hz, 2H, Ar-O-CH_2-C***H$_2$***-R), 1.69-1.39 (m, 6H, R-C***H$_2$***-C***H$_2$***-C***H$_2$***-CH_2-OH) and 1.34 (s, 1H, R-O***H***). ^{13}C NMR (75 MHz, $CDCl_3$, ppm): δ 158.7, 140.9, 133.6, 128.7, 128.1, 126.7, 126.6, 114.8, 67.9, 62.9, 32.7, 29.3, 26.0 and 25.6. GC/MS m/z calculated for $C_{18}H_{22}O_2$ [M+TMS] 342.36 Da, found 342.10 Da. FTIR (ATR): 3310, 3080 - 3010, 2180 - 1665,

1605, 1520, 1475, 1400, 1245, 1190, 1120, 1070, 1035, 995, 915, 835, 755, 715, 685 cm^{-1}.

6-([1,1'-biphenyl]-4-yloxy)hexyl acrylate (2). To a flame dried 200 mL Schlenk flask equipped with a magnetic stir bar and suspended in an ice bath, a solution of **1** (4.00 g, 14.8 mmol) and triethylamine (2.50 mL, 17.8 mmol) in dry THF (82.0 mL) was added. A solution of acryloyl chloride (1.80 mL, 22.2 mmol) in dry THF (6.00 mL) was added dropwise and the reaction was allowed to stir at 0 °C for 2 h and then at room temperature for an additional 12 h. The reaction mixture was concentrated, dissolved in chloroform and washed against deionized water, sodium bicarbonate solution and brine. The organic phase was dried over sodium sulfate, filtered and concentrated *in vacuo* to afford a white solid in 86% yield (4.11 g). T_m = 41°C. TGA in Ar: 353 - 432 °C, 94% mass loss; 5% mass remaining at 500 °C. ^{1}H NMR (300 MHz, $CDCl_3$, ppm): δ 7.53 (m, 4H, ***meta-H*** to -O-CH_2-R and ***2'-H*** to Ar-O-CH_2-R), 7.41 (m, 2H, ***3'-H*** to Ar-O-CH_2-R), 7.32 (m, 1H, ***4'-H*** to Ar-O-CH_2-R), 6.98 (m, 2H, ***ortho-H*** to -O-CH_2-R), 6.40 (d, *J* = 17 Hz, 1H, ***H***(H)C=CH-R (*trans*)), 6.12 (dd, *J* = 17 Hz and 10 Hz, 1H, H_2C=C***H***-R), 5.82 (d, *J* = 10 Hz, 1H, H(***H***)C=CH-R (*cis*)), 4.18 (t, *J* = 6 Hz, 2H, R-C***H$_2$***-O(O)C-R'), 4.00 (t, *J* = 6.5 Hz- 2H, Ar-O-C***H$_2$***-R) and 1.89 - 1.41 (m, 8H, R-C***H$_2$***-C***H$_2$***-C***H$_2$***-C***H$_2$***-CH_2-O(O)C-R'). ^{13}C NMR (75 MHz, $CDCl_3$, ppm): δ 166.3, 158.6, 140.9, 133.6, 130.6, 128.7, 128.6, 128.1, 126.7, 126.6, 114.8, 67.9, 64.6, 29.2, 28.6 and 25.8. GC/MS m/z calculated for $C_{21}H_{24}O_3$ [M] 324.17 Da, found 324.11 Da. FTIR (ATR): 3105 – 3005, 2190 – 1845, 1710, 1605, 1520, 1485, 1405, 1295, 1195, 995, 825, 760, 695 cm^{-1}.

4-[Oxy(tri(ethylene glycol))bromoisopropionyl]-2,3,5,6-tetrafluorostyrene (3). Compound **3** was prepared according to a previously reported method.[89] Briefly, to a 1000 mL two-neck round bottom flask equipped with a magnetic stir bar and addition funnel suspended in an ice bath, a solution of 4-[oxy(tri(ethylene glycol))]-2,3,5,6-tetrafluorostyrene (10.0 g, 30.8 mmol), triethylamine (16.0 mL, 111 mmol) in THF (235 mL) was added. A solution of 2-bromopropionyl bromide (3.90 mL, 37.0 mmol) in THF (20.0 mL) was added dropwise. The solution was allowed to warm to room temperature and stir under N_2 for 14 h. The reaction was concentrated, and crude product was washed three times against brine. The organic phase was dried over sodium sulfate, filtered, and concentrated *in vacuo* to afford a pale yellow oil. Further purification by silica gel flash chromatography using a gradient of hexanes:ethyl acetate as eluent afforded **3** as a clear, pale yellow oil in 59% yield (8.40 g). TGA in Ar: 248 - 327 °C, 20% mass loss, 327 – 430 °C, 58% mass loss; 19% mass remaining at 500 °C. ^{1}H NMR (300 MHz, $CDCl_3$, ppm): δ 6.61 (dd, *J* = 18 Hz and 12 Hz, 1H, H_2C=C***H***-R), 6.02 (d, *J* = 18 Hz, 1H, ***H***(H)C=CH-R (*trans*)), 5.62 (d, *J* = 12 Hz, 1H, H(***H***)C=CH-R (*cis*)), 4.39 (q, *J* = 6.9 Hz, 1H, R-C(***H***)(Br)CH_3), 4.37 (t, *J* = 4.8 Hz, 2H, TFS-O-C***H*****$_2$**-CH_2-OR), 4.31 (t, *J* = 4.8 Hz, 2H, R-O-CH_2-C***H*****$_2$**-O(O)C-R'), 3.83 (t, *J* = 4.8 Hz, 2H, TFS-O-CH_2-C***H*****$_2$**-OR), 3.75-3.60 (m, 6H, R-O-C***H*****$_2$**-C***H*****$_2$**-O-C***H*****$_2$**-CH_2-O(O)C-R') and 1.81 (d, *J* = 6.9 Hz, 3H, R-C(H)(Br)C***H*****$_3$**). ^{13}C NMR (75 MHz, $CDCl_3$, ppm): δ 170.9, 146.6, 143.3, 142.8, 139.3, 136.3, 122.2, 122.0, 110.8, 74.1, 70.8, 70.6, 70.1, 68.8, 64.6, 55.6 and 30.5. ^{19}F NMR (282 MHz, $CDCl_3$, ppm): δ -145 (m, 2F, ***ortho-F*** to -CH=CH_2) and -158 (m, 2F, ***meta-F*** to -CH=CH_2). ESIHRMS m/z calculated for $C_{17}H_{19}O_5F_4Br$ $[M+H]^+$ 459.02

Da, found 459.0430. FTIR (ATR): 3070 - 2750, 1740, 1640, 1485, 1450, 1405, 1335, 1225, 1120, 1080, 965, 935, 855, 760, 675 cm^{-1}.

4-[Oxy(tri(ethylene glycol))azidoisopropionyl] -2,3,5,6-tetrafluorostyrene (4). To a flame dried 10 mL Schlenk flask equipped with a magnetic stir bar, sodium azide (212 mg, 3.27 mmol) was added and dried under reduced pressure for 10 min. A solution of **3** (1.02 g, 2.18 mmol) in dry DMF (2.50 mL) was added and the solution was allowed to stir at room temperature for 48 h. The reaction was concentrated, dissolved in DCM and washed two times against deionized water and two times with brine. The organic phase was dried over sodium sulfate, filtered and concentrated *in vacuo* to afford a dark yellow oil in 74% yield (675 mg). TGA in Ar: 161 - 310 °C, 14% mass loss, 310 – 405 °C, 45% mass loss; 34% mass remaining at 500 °C. ^{1}H NMR (300 MHz, $CDCl_3$, ppm): δ 6.62 (dd, *J* = 18 Hz and 12 Hz, 1H, H_2C=C***H***-R), 6.03 (d, *J* = 18 Hz, 1H, ***H***(H)C=CH-R (*trans*)), 5.64 (d, *J* = 12 Hz, 1H, H(***H***)C=CH-R (*cis*)), 4.36 (t, *J* = 4.5 Hz, 2H, TFS-O-C***H*****$_2$**-CH_2-OR), 4.32 (t, *J* = 4.8 Hz, 2H, R-O-CH_2-C***H*****$_2$**-O(O)C-R'), 3.97 (q, *J* = 6.9 Hz, 1H, R-C(***H***)(N_3)CH_3), 3.82 (t, *J* = 4.5 Hz, 2H, TFS-O-CH_2-C***H*****$_2$**-OR), 3.75-3.61 (m, 6H, R-O-C***H*****$_2$**-C***H*****$_2$**-O-C***H*****$_2$**-CH_2-O(O)C-R') and 1.47 (d, *J* = 6.9 Hz, 3H, R-C(H)(N_3)C***H*****$_3$**). ^{13}C NMR (75 MHz, $CDCl_3$, ppm): δ 170.9, 146.6, 143.3, 142.8, 139.3, 136.3, 122.2, 122.0, 110.8, 74.1, 70.8, 70.6, 70.1, 68.8, 64.6, 57.2 and 16.8. ^{19}F NMR (282 MHz, $CDCl_3$, ppm): δ -145 (m, 2F, ***ortho-F*** to –CH=CH_2) and -158 (m, 2F, ***meta-F*** to -CH=CH_2). ESIHRMS m/z calculated for $C_{17}H_{19}O_5F_4N_3$ $[M+H]^+$ 422.34 Da, found 422.1238 Da. FTIR (ATR): 3050 – 2755, 2110, 1745, 1645, 1500, 1485, 1450, 1425, 1405, 1380, 1350, 1250, 1190, 1115, 1075, 1030, 965, 935, 855 cm^{-1}.

Prop-2-yn-1-yl 2-(dodecylthiocarbonothioyl thio)-2-methylpropanoic acid (5). To a flame dried 10 mL Schlenk flask equipped with a magnetic stir bar, 2-(dodecylthiocarbonothioylthio)-2-methylpropionic acid (1.00 g, 2.74 mmol) and 4-(dimethylamino)pyridine (69.0 mg, 0.55 mmol) were added and dried under reduced pressure for 30 mins. A solution of *N,N'* – dicyclohexylcarbodiimide (0.68 g, 3.29 mmol) in dry DCM (8.50 mL) was added. A solution of propargyl alcohol (0.56 mL, 9.60 mmol) in dry DCM (8.50 mL) was added dropwise and the reaction was allowed to stir overnight at room temperature. The solid was filtered off and the organic phase was washed three times against a sodium bisulfate solution and a sodium bicarbonate solution. The organic phase was dried over sodium sulfate, filtered and concentrated *in vacuo* to afford a dark yellow solid in 58% yield (641 mg). T_m = 11 and 20 °C. TGA in Ar: 196 - 254 °C, 31% mass loss, 254 – 331 °C, 55% mass loss; 8% mass remaining at 500 °C. ^{1}H NMR (300 MHz, $CDCl_3$, ppm): δ 4.70 (d, *J* = 2.4 Hz, 2H, HC≡C***H₂***-OR), 3.27 (t, *J* = 7.5 Hz, 2H, R-S(S)S-C***H₂***-R'), 2.46 (t, *J* = 2.4 Hz, 1H, ***H***C≡CH_2-OR), 1.71 (s, 6H, R-O(O)C-C(C***H₃***)(C***H₃***)-S(S)S-R'), 1.69 – 1.60 (m, 2H, R-S(S)S-CH_2-C***H₂***-R'), 1.34 – 1.22 (m, 18H, R-S(S)S-CH_2-CH_2-C***H₂***-C***H₂***-C***H₂***-C***H₂***-C***H₂***-C***H₂***-C***H₂***-C***H₂***-C***H₂***-CH_3) and 0.88 (t, *J* = 6.9 Hz, 3H, R-C***H₃***). ^{13}C NMR (75 MHz, $CDCl_3$, ppm): δ 221.1, 172.3, 77.3, 75.1, 55.6, 53.3, 37.0, 31.9, 29.6, 29.5, 29.4, 29.3, 29.1, 28.9, 27.8, 25.2, 22.7 and 14.1. ESIHRMS m/z calculated for $C_{20}H_{34}O_2S_3$ $[M+H]^+$ 403.17 Da, found 403.1797 Da. FTIR (ATR): 3300, 3030 - 2765, 2125, 1740, 1465, 1385, 1365, 1245, 1150, 1120, 1065, 1010, 990, 815, 745, 715, 670, 630 cm^{-1}.

Macro 'click' chain transfer monomer (6). To a flame dried 10 mL Schlenk flask equipped with a magnetic stir bar, a solution of **4** (565 mg, 1.34 mmol), **5** (479 mg, 1.19 mmol) and *N,N,N'N'',N''*-pentamethyldiethylenetriamine (50.0 mg, 0.29 mmol) in dry DMF (8.00 mL) was added. A solution of Cu(I)Br (58.0 mg, 0.41 mmol) dissolved in dry DMF (0.50 mL) was added and the reaction was allowed to stir for 30 h at room temperature. Copper was removed by elution through an aluminum oxide plug and the product was obtained after drying *in vacuo* to afford a dark brown oil in 94% yield (924 mg). T_g = 34 °C. TGA in Ar: 229 - 280 °C, 18% mass loss, 280 – 394 °C, 62% mass loss; 16% mass remaining at 500 °C. ^{1}H NMR (300 MHz, $CDCl_3$, ppm): δ 7.77 (s, 1H, R-C(H)(CH_3)-N_3C_2***H***-R'), 6.62 (dd, *J* = 18 Hz and 12 Hz, 1H, H_2C=C***H***-R), 6.02 (d, *J* = 18 Hz, 1H, ***H***(H)C=CH-R (*trans*)), 5.66 (d, *J* = 12 Hz, 1H, H(***H***)C=CH-R (*cis*)), 5.48 (q, *J* = 7.5 Hz, 1H, R-C(***H***)(CH_3)-N_3C_2H-R'), 5.26 (d, *J* = 5.4 Hz, 2H, R-N_3C_2H-C***H₂***-O(O)C-R'), 4.37 (t, *J* = 4.5 Hz, 2H, TFS-O-C***H₂***-CH_2-OR), 4.32 (t, *J* = 4.8 Hz, 2H, R-O-CH_2-C***H₂***-O(O)C—C(H)(CH_3)-N_3C_2H-R'), 3.82 (t, *J* = 4.5 Hz, 2H, TFS-O-CH_2-C***H₂***-OR), 3.72 – 3.58 (m, 6H, R-O-C***H₂***-C***H₂***-O-C***H₂***-CH_2-O(O)C—C(H)(CH_3)-N_3C_2H-R'), 3.22, (t, *J* = 7.5 Hz, 2H, R-S(S)S-C***H₂***-R'), 1.84 (d, *J* = 7.5 Hz, 3H, R-C(H)(C***H₃***)-N_3C_2H-R') 1.70 – 1.56 (m, 8H, R-O(O)C-C(C***H₃***)(C***H₃***)-S(S)S-CH_2-C***H₂***-R'), 1.31 – 1.23 (m, 18H, R-S(S)S-CH_2-CH_2-C***H₂***-C***H₂***-C***H₂***-C***H₂***-C***H₂***-C***H₂***-C***H₂***-C***H₂***-C***H₂***-CH_3) and 0.87 (t, *J* = 6.6 Hz, 3H, R-C***H₃***). ^{13}C (75 MHz, $CDCl_3$, ppm): δ 221.1, 172.9, 169.1, 146.6, 143.3, 142.8, 142.6, 139.3, 136.3, 123.4, 122.2, 122.0, 110.8, 74.2, 70.9, 70.6, 70.3, 68.7, 65.2, 59.1, 58.2, 55.9, 37.0, 31.9, 29.6, 29.5, 29.4, 29.3, 29.1, 28.9, 27.8, 25.2, 22.7, 18.3 and 14.1. ^{19}F NMR (282 MHz, $CDCl_3$, ppm): δ 145 (m, 2F, ***ortho-F*** to

–CH=CH_2) and -158 (m, 2F ***meta-F*** to -CH=CH_2). ESIHRMS m/z calculated for $C_{36}H_{63}O_7F_4N_3S_3$ $[M+H]^+$ 825.02 Da, found 825.3180 Da. FTIR (ATR): 3050 - 2700, 1740, 1680, 1485, 1385, 1250, 1150, 1120, 1075, 965, 940, 865, 815, 720, 655 cm^{-1}.

Liquid crystalline hyperbranched fluoropolymer (LC_{20}-$HBFP_{30}$), (7). To a flame dried 10 mL Schlenk flask equipped with a magnetic stir bar, a solution of **2** (885 mg, 2.74 mmol), **3** (1.26 g, 2.74 mmol), **6** (74.0 mg, 0.09 mmol) and azobisisobutyronitrile (3.00 mg, 0.02 mmol) in dry DMF (8.00 mL) was added. The solution was deoxygenated *via* freeze-pump-thaw (x3) then placed in a preheated oil bath (70 °C) and allowed to react for 27 h. The polymerization was quenched by opening the flask to air and submerging the flask in liquid nitrogen. Polymer was obtained after two precipitations in cold diethyl ether to afford a yellow viscous oil in 38% yield (721 mg). M_n^{GPC} = 19 kDa, M_w/M_n.= 1.44. T_g = 85 °C. TGA in Ar: 283 - 359 °C, 31% mass loss, 359 - 446 °C, 43% mass loss; 22% mass remaining at 500 °C. ^{1}H NMR (300 MHz, $CDCl_3$, ppm): δ 7.58 – 7.29 (br, m, ***meta-H*** to –O-CH_2-R and ***2'-H***, ***3'-H*** and ***4'-H*** to Ar-O-CH_2-R), 7.00 – 6.85 (br, m, ***ortho-H*** to –O-CH_2-R), 4.47 – 4.14 (br, m, Ar-R-C***H₂***-O(O)C-R' and TFS-O-C***H₂***-CH_2-O-CH_2-CH_2-O-CH_2-C***H₂***-O(O)C-R'), 4.03 - 3.88 (br, m, Ar-O-C***H₂***-R), 3.85 - 3.55 (br, m, TFS-O-CH_2-C***H₂***-O-C***H₂***-C***H₂***-O-C***H₂***-CH_2-O(O)C-R'), 2.85 – 2.62 (br, m, C***H₂***-C***H***(R)- backbone), 2.10 – 1.05 (br, m, R-C***H₂***-C***H₂***-C***H₂***-C***H₂***-CH_2-O(O)C-R' and C-C***H₃***). ^{13}C NMR (75 MHz, $CDCl_3$, ppm): δ 170.2, 160.0, 158.2, 146.7, 142.5, 140.7, 139.1, 136.0, 133.5, 128.7, 128.0, 126.7, 114.7, 74.3, 70.7, 69.9, 68.7, 68.1, 67.8, 65.0, 64.4, 40.0, 34.7, 30.3, 29.1, 28.3, 25.7, 21.6, 16.9 and 14.3. ^{19}F NMR (282 MHz, $CDCl_3$, ppm): δ -143 (br, m,

ortho-F (TFS)) and -157 (br, m, ***meta-F*** (TFS)). Elem. Anal. Calcd. for $C_{862}H_{1028}S_3N_3F_{124}Br_{30}$: C, 53.09; H, 5.31; S, 0.49; N, 0.22; F, 12.08; Br, 12.29%. Found: C, 55.17; H, 4.94; S, 0.78; N, 0.21; F, 11.12; Br, 7.63%. FTIR (ATR): 3030 – 2800, 1730, 1650, 1610, 1490, 1460, 1365, 1245, 1120, 960, 830, 765, 695 cm^{-1}.

Liquid crystalline hyperbranched fluoropolymer (LC_{10}-$HBFP_{15}$), (8). To a flame dried 10 mL Schlenk flask equipped with a magnetic stir bar, a solution of **2** (445 mg, 1.37 mmol), **3** (696 mg, 1.37 mmol), **6** (70.0 mg, 0.09 mmol) and azobisisobutyronitrile (3.00 mg, 0.02 mmol) in dry DMF (5.00 mL) was added. The solution was deoxygenated *via* freeze-pump-thaw (x3) then placed in a preheated oil bath (70 °C) and allowed to react for 25 h. The polymerization was quenched by opening the flask to air and submerging the flask in liquid nitrogen. Polymer was obtained after two precipitations in cold diethyl ether to afford a yellow viscous oil in 71% yield (745 mg). M_n^{GPC} = 15 kDa, M_w/M_n.= 1.44. T_g = 80 and 124 °C. TGA in Ar: 255 - 354 °C, 37% mass loss, 354 – 415 °C, 23% mass loss, 415 – 437 °C, 11% mass loss; 25% mass remaining at 500 °C. ^{1}H NMR (300 MHz, $CDCl_3$, ppm): δ 7.58 – 7.29 (br, m, ***meta-H*** to –O-CH_2-R and ***2'-H***, ***3'-H*** and ***4'-H*** to Ar-O-CH_2-R), 7.00 – 6.85 (br, m, ***ortho-H*** to –O-CH_2-R), 4.47 - 4.14 (br, m, Ar-R-C***H₂***-O(O)C-R' and TFS-O-C***H₂***-CH_2-O-CH_2-CH_2-O-CH_2-C***H₂***-O(O)C-R'), 4.03 – 3.88 (br, m, Ar-O-C***H₂***-R), 3.85 – 3.55 (br, m, TFS-O-CH_2-C***H₂***-O-C***H₂***-C***H₂***-O-C***H₂***-CH_2-O(O)C-R'), 2.85 – 2.62 (br, m, C***H₂***-C***H***(R)- backbone), 2.10 - 1.05 (br, m, R-C***H₂***-C***H₂***-C***H₂***-C***H₂***-CH_2-O(O)C-R' and C-C***H₃***). ^{13}C NMR (75 MHz, $CDCl_3$, ppm): δ 170.2, 160.0, 158.2, 146.7, 142.5, 140.7, 139.1, 136.0, 133.5, 128.7, 128.0, 126.7, 114.7, 74.3, 70.7, 69.9, 68.7, 68.1, 67.8, 65.0,

64.4, 40.0, 34.7, 30.3, 29.1, 28.3, 25.7, 21.6, 16.9 and 14.3. ^{19}F NMR (282 MHz, $CDCl_3$, ppm): δ -143 (br, m, ***ortho-F*** (TFS)) and -157 (br, m, ***meta-F*** (TFS)). Elem. Anal. Calcd. for $C_{502}H_{608}S_3N_3F_{64}Br_{15}$: C, 54.81; H, 5.57; S, 0.87; N, 0.38; F, 11.05; Br, 10.09%. Found: C, 54.91; H, 5.35; S, 0.96; N, 0.65; F, 11.21; Br, 10.74%. FTIR (ATR): 3030 – 2800, 1730, 1650, 1610, 1490, 1460, 1365, 1245, 1120, 960, 830, 765, 695 cm^{-1}.

Liquid crystalline hyperbranched fluoropolymer (LC_3-$HBFP_5$), (9). To a flame dried 10 mL Schlenk flask equipped with a magnetic stir bar, a solution of **2** (248 mg, 0.76 mmol), **3** (362 mg, 0.76 mmol), **6** (125 mg, 0.15 mmol) and azobisisobutyronitrile (5.50 mg, 0.03 mmol) in dry DMF (5.20 mL) was added. The solution was deoxygenated *via* freeze-pump-thaw (x3) then placed in a preheated oil bath (70 °C) and allowed to react for 23 h. The polymerization was quenched by opening the flask to air and submerging the flask in liquid nitrogen. Polymer was obtained after two precipitations in cold diethyl ether to afford a yellow viscous oil in 53% yield (347 mg). M_n^{GPC} = 5.2 kDa, M_w/M_n.= 1.54. T_g = 91 and 124 °C. TGA in Ar: 258 - 366 °C, 26% mass loss, 366 – 434 °C, 21% mass loss; 53% mass remaining at 500 °C. ^{1}H NMR (300 MHz, $CDCl_3$, ppm): δ 7.58 – 7.29 (br, m, ***meta-H*** to –O-CH_2-R and ***2'-H***, ***3'-H*** and ***4'-H*** to Ar-O-CH_2-R), 7.00 – 6.85 (br, m, ***ortho-H*** to –O-CH_2-R), 4.47 - 4.14 (br, m, Ar-R-C***H$_2$***-O(O)C-R' and TFS-O-C***H$_2$***-CH_2-O-CH_2-CH_2-O-CH_2-C***H$_2$***-O(O)C-R'), 4.03 – 3.88 (br, m, Ar-O-C***H$_2$***-R), 3.85 – 3.55 (br, m, TFS-O-CH_2-C***H$_2$***-O-C***H$_2$***-C***H$_2$***-O-C***H$_2$***-CH_2-O(O)C-R'), 2.85 – 2.62 (br, m, C***H$_2$***-C***H***(R)- backbone), 2.10 - 1.05 (br, m, R-C***H$_2$***-C***H$_2$***-C***H$_2$***-C***H$_2$***-CH_2-O(O)C-R' and C-C***H$_3$***). ^{13}C NMR (75

MHz, $CDCl_3$, ppm): δ 170.2, 160.0, 158.2, 146.7, 142.5, 140.7, 139.1, 136.0, 133.5, 128.7, 128.0, 126.7, 114.7, 74.3, 70.7, 69.9, 68.7, 68.1, 67.8, 65.0, 64.4, 40.0, 34.7, 30.3, 29.1, 28.3, 25.7, 21.6, 16.9 and 14.3. ^{19}F NMR (282 MHz, $CDCl_3$, ppm): δ -143 (br, m, ***ortho-F*** (TFS)) and -157 (br, m, ***meta-F*** (TFS)). Elem. Anal. Calcd. for $C_{206}H_{244}S_3N_3F_{24}Br_5$: C, 55.76; H, 5.54; S, 2.17; N, 0.95; F, 10.28; Br, 9.00%. found: C, 59.76; H, 6.16; S, 1.70 N, 1.19; F, 7.79; Br, 5.00%. FTIR (ATR): 3030 – 2800, 1730, 1650, 1610, 1490, 1460, 1365, 1245, 1120, 960, 830, 765, 695 cm^{-1}.

General procedure for the preparation of LC-HBFP-PEG crosslinked networks. To a scintillation vial, bis(3-aminopropyl) terminated PEG (20.0 mg, 0.013 mmol) and THF (0.50 mL) were added and stirred until homogeneous (~10 min). To the solution, **7** (20.0 mg, 0.001 mmol) and *N*,*N*-diisopropylethylamine (DIPEA) (9.50 μL) were added and allowed to stir for 30 min. The solution was drop cast onto circular glass microscope cover slips or 40 μL aluminum DSC pans. A period of about 1 h allowed for the excess solvent to evaporate and afford a pre-gel that was cured at 110 °C for 45 min under N_2 atmosphere. T_g = 5 °C. T_m = 27 and 36 °C. TGA in Ar: 252 - 350 °C, 20% mass loss, 350 – 433 °C, 43% mass loss; 33% mass remaining at 500 °C. FTIR (ATR): 3690 – 3225, 1730, 1650, 1610, 1490, 1450, 1350, 1245, 1095, 955, 835, 765, 695 cm^{-1}. Subsequent films were prepared in the same manner by varying the wt % PEG , calculated as w/w % of the total mass to afford a total of eight formulations within the series. The same procedure was followed for the preparation of films from **8** and **9** to afford two additional series with a total of 16 formulations.

3.3 Results and Discussion

For comparison purposes, it was important to design the new LC-HBFP polymer to resemble the original third generation HBFP in topology, notably, a hyperbranched network with the ability to undergo crosslinking after polymerization. This requirement led to the development of a unique chain transfer monomer (CTM) *via* click chemistry from which the chosen LC monomer, as well as the initiating monomer, or inimer, which was previously used in the preparation of $HBFP^{(III)}$-b, would undergo polymerization. The LC monomer selected for incorporation into the HBFP system is well-known, and has been synthesized and characterized by other laboratories.[90-92] Briefly, the LC monomer (Scheme 3.1) was achieved from a two-step reaction starting with the synthesis of the mesogenic unit **1** through a nucleophilic substitution of 4-phenylphenol with 6-chloro-1-hexanol, in the presence of an excess of potassium carbonate. The subsequent step involved the esterification of the remaining alcohol group by reaction with acryloyl chloride to afford **2**. The starting materials used for the synthesis of the CTM were an azide-functionalized monomer, which was achieved by reacting **3** (Scheme 3.2) with sodium azide, and a modified chain-transfer agent (CTA) **5**, prepared from the esterification of 2-(dodecylthiocarbonothioylthio)-2-methylpropionic acid with propargyl alcohol. The final CTM **6** was generated through an azide-alkyne Huisgen cycloaddition between **4** and **5** in the presence of Cu(I)Br. To probe the effect of polymer size, three LC-HBFP polymers **7-9**, varying in molecular weight, were synthesized through reversible-addition fragmentation chain-transfer (RAFT)

copolymerization of the LC monomer and inimer from the unique macro 'click' CTM (Scheme 3.3).

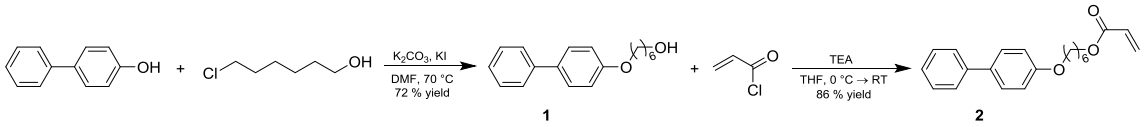

Scheme 3.1. Synthesis of mesogenic unit **1** and LC monomer **2**.

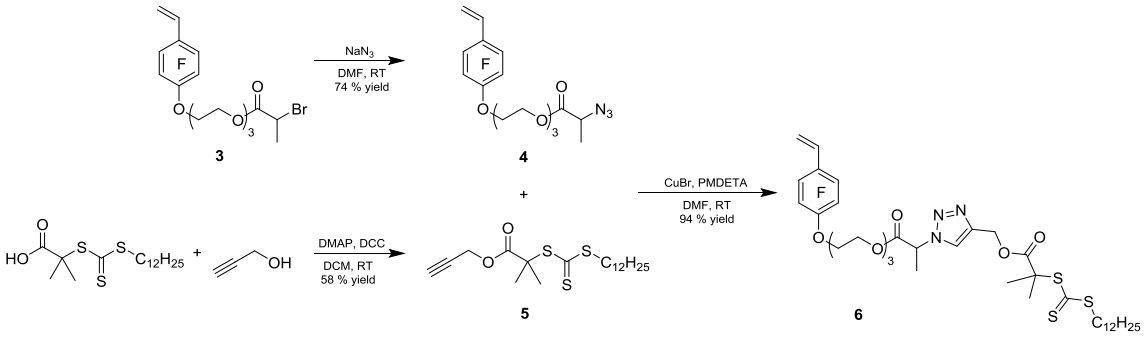

Scheme 3.2. Synthesis of the azide-functionalized monomer **4**, the alkyne-functionalized CTA **5**, and the macro 'click' chain transfer monomer **6**.

Amphiphilic networks were prepared using a previously described method[40] through nucleophilic substitution between the amino chain ends of bis(3-aminopropyl) terminated PEG (M_n = 1500 Da) and the bromoacetyl functionality of the hyperbranched LC fluorocopolymer, upon casting from tetrahydrofuran (THF) solution into 40 μL aluminum DSC pans or onto glass microscope cover slips, followed by a thermal cure at 110 °C for 45 min under inert atmosphere.

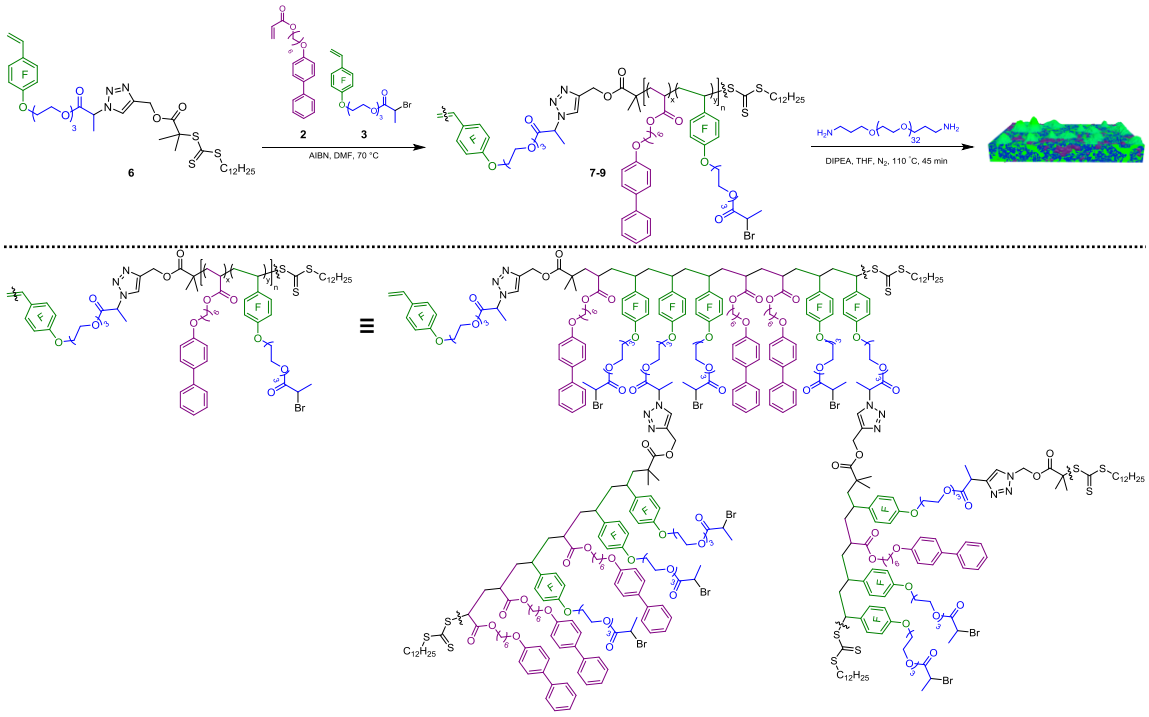

Scheme 3.3. Synthesis of LC-HBFP polymer and preparation of LC-HBFP crosslinked networks where the molar ratios x:y correspond to 3:5, 10:15, and 20:30.

To impart liquid crystalline character to the polymer matrix, a mesogenic unit was incorporated in the form of a comonomer during polymerization. In order to determine the types of mesophases and the temperatures at which these mesophases formed, a combination of differential scanning calorimetry (DSC),[58, 90, 91, 93-102] polarized optical microscopy (POM) and x-ray diffraction (XRD) were used to characterize and identify the types of liquid crystalline phases of the mesogenic unit and its corresponding monomer. From DSC, two melting transitions were observed for the mesogenic unit upon heating, at 84 °C and 100 °C (Figure 3.1). Using POM, several mesophases were observed, including crystalline, smectic and isotropic. Interestingly, while the enthalpy

change at 84 °C was quite noticeable in the DSC trace, no visible phase change was observed through POM until 94 °C. Jaglowski and coworkers observed a similar trend with their poly[((6-(4-phenylphenoxy)hexyl)oxy)-(trifluoroethoxy)phos-phazene] where DSC recorded two endotherms (*i.e.* 103 °C and 133 °C) and birefringence was not observed by POM until a higher temperature (*i.e.* 114 °C).[98] In the XRD data, sharp, structured peaks were observed at room temperature, indicating an ordered, crystalline

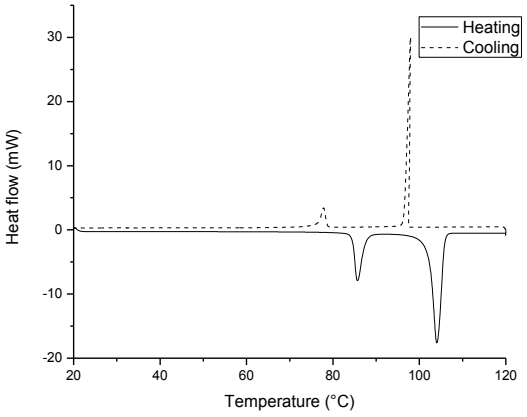

Figure 3.1. Differential scanning calorimetry trace of mesogenic unit **1** during 2nd heating (solid) and cooling (dash) cycles.

structure. As the sample was heated, there was a shift to lower angle at 70 °C, suggesting the formation of a smectic phase. We observed a decrease in intensity of the peaks, as well as broadening beginning at 80 °C, indicating a loss of order, which continued until a complete amorphous halo was observed at 110 °C (Figure 3.2). From

POM, these phase changes could be identified and attributed to crystalline-smectic-isotropic transitions (Figure 3.3).

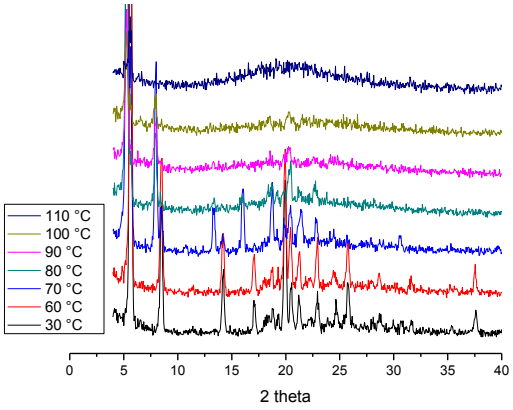

Figure 3.2. X-ray diffractogram of mesogenic unit **1** at different temperatures during heating.

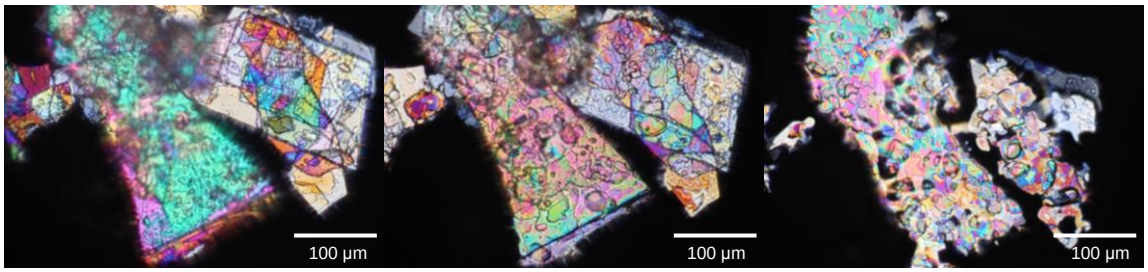

Figure 3.3. Polarized optical microscopy images of mesogenic unit **1** at 94 °C, 103 °C and 104 °C (left to right), each collected during heating.

The monomer displayed similar phase changes, but at much lower temperatures. From DSC, only one monomeric melting transition was observed, at 41 °C (Figure 3.4).

With the use of POM, greater insight was provided showing a change from a crystalline-to-smectic phase occurring around 52 °C, followed shortly by a smectic-to-isotropic phase change at 55 °C (Figure 3.5). The diffractogram from XRD, again, showed an

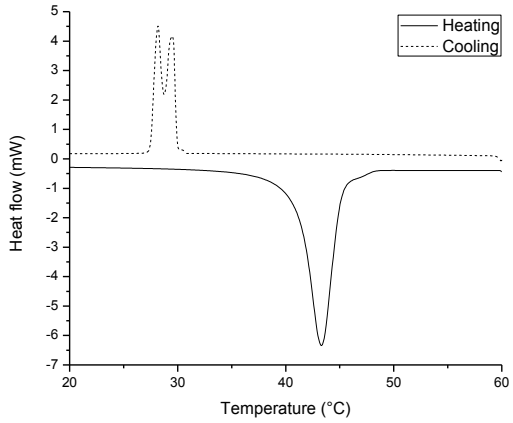

Figure 3.4. Differential scanning calorimetry trace of LC monomer **2** during 2nd heating (solid) and cooling (dash) cycles.

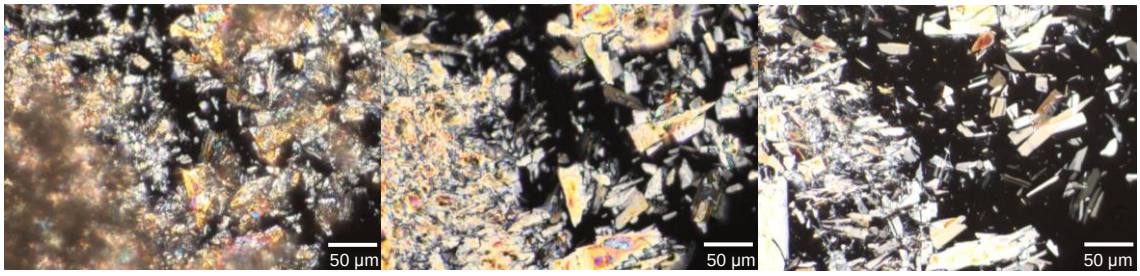

Figure 3.5. Polarized optical microscopy images of LC monomer **2** at 52 °C, 54 °C and 55 °C (left to right), each collected during heating.

ordered, crystalline structure at room temperature with increasing disorder as the temperature increased until only a prominent amorphous halo was observed at 60 °C

(Figure 3.6). After polymerization, the characteristics of the LC moiety were still observed in optical microscopy from the distributed microscopic areas of birefringence (Figure 3.7). Phase transitions were observed in crosslinked films as well, but due to the lower limitations of the heating stage, POM images were only taken while heating above 30 °C, where only one transition was observed. However from DSC experiments, it is known that the crosslinked films undergo a melting transition just below 30 °C.

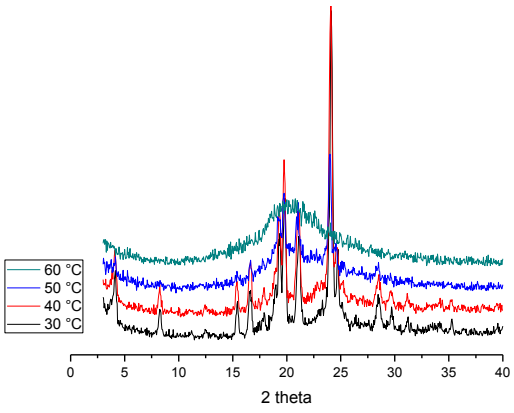

Figure 3.6. X-ray diffractogram of LC monomer **2** at different temperatures during heating.

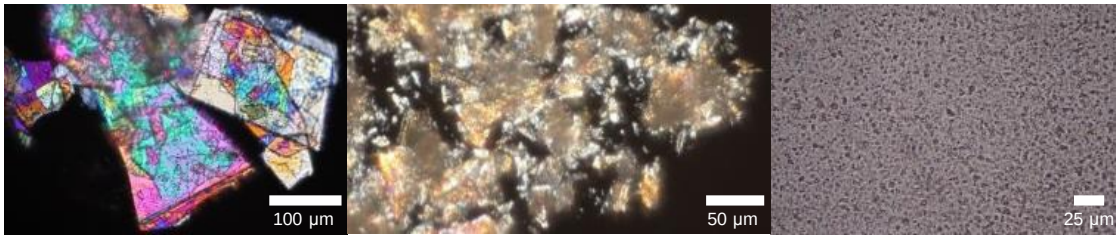

Figure 3.7. Polarized optical microscopy images of mesogenic unit (left), LC monomer (middle) and neat LC-HBFP (right) at 30 °C.

The stoichiometries of the LC-HBFP and PEG were varied to produce an array of coatings for evaluation of compositional effects on the thermal, surface, and wettability properties. As shown previously in our laboratory, the ability of the HBFP-PEG system to uptake water has a large influence on the dynamic reorganization of the system, including structural and topological impacts.[40, 41, 89] Interestingly, the new LC-HBFP-PEG system absorbed significantly (*i.e.* 3 times) more water than did the binary system (Figure 3.8). A possible explanation for the large difference in water uptake can be attributed to the packing arrangement from the addition of the liquid crystalline comonomer.[93, 103] Lupinacci and coworkers revealed, through models, that the flexibility in the hexamethylene spacer group can allow the biphenyl segment to bend backwards toward the polymer chain, resulting in stacks of biphenyl groups.[93] An alternative explanation is provided by hydrogen bonding interactions, where the additional oxygen atoms from the LC comonomer allow for higher numbers of favorable interactions between water and the polymer matrix.[104] Similar characteristics were identified between all three polymer arrays, including a direct relationship between the wt % of PEG and H_2O uptake. It is important to note that the formulations composed of higher

than 30 wt % PEG content from the [3, 5] LC-HBFP system disintegrated during submersion and, therefore, full hydration could not be determined. Due to these results, the [3, 5] system was not investigated in further experiments.

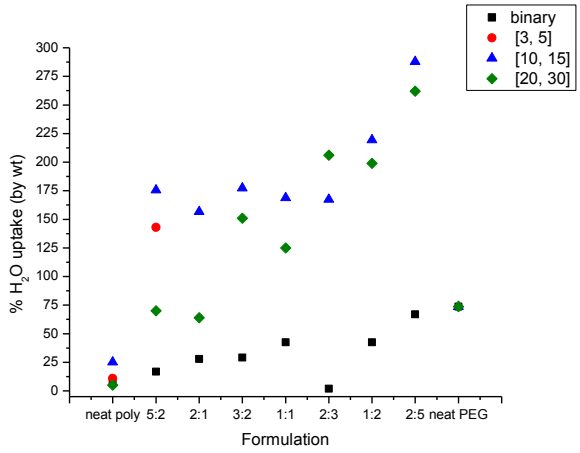

Figure 3.8. Wt % H_2O uptake of the three series of LC-HBFP-PEG coatings as a function of formulation with the binary system (black) as a reference.

Due to the increase in water uptake of the LC-HBFP-PEG system, 300 wt % water was added to each sample, previously cast and annealed in 40 μL aluminum DSC pans, for DSC studies so the films would be fully hydrated in the presence of excess free water. Anti-icing performance was assessed from the calorimetric properties of the seven LC-HBFP-PEG networks from the two different molecular weight polymers and control samples of neat LC-HBFP and PEG, totaling 17 samples. The networks were investigated from -50 to 20 °C, over three cycles, in both heating and cooling modes. Analysis was performed according to previous experiments, where the melting transition

temperature of water provided an upper limit of anti-icing behavior and was used to assess whether the films could depress the freezing point of water.[89] As in the binary system, two water melting transitions (T_m) were observed, corresponding to the bound water within the crosslinked network and the free water on the surface of the coating.[70, 89] Additionally, similar trends between the wt % PEG and the T_m of free water were also observed; as the wt % PEG increased, the T_m of free water decreased and approached the T_m observed in the presence of neat PEG (Table 3.1). Within the two different molecular weight polymers, as polymer size increased, the formulations with higher wt % PEG had lower T_m values. While bound water did not vary noticeably across the two polymers, the T_m did increase as wt % PEG increased. Interestingly, by increasing the wt % PEG in the [20, 30] system, a comparable T_m between the 2:5 formulation with neat PEG was achieved, indicating that the addition of the LC moiety had a greater positive effect on the freezing point depression of water in a larger molecular weight polymer.

Table 3.1. Average free water onset melting temperatures (T_m) for the array of [10, 15] and [20, 30] LC-HBFP-PEG systems and LC-HBFP and PEG control samples, each with 300 wt % water.

System	**Mass ratio LC-HBFP to PEG (wt %)**								
	LC-HBFP	*5:2*	*2:1*	*3:2*	*1:1*	*2:3*	*1:2*	*2:5*	*PEG*
	Avg. free H_2O T_m onset (°C)								
[10, 15]	-1.8 ± 0.1	-2.1 ± 0.1	-4.2 ± 0.0	-5.3 ± 0.2	-2.2 ± 0.1	-6.0 ± 0.1	-7.4 ± 0.1	-6.7 ± 0.3	-10.4 ± 1.3
[20, 30]	-1.7 ± 0.1	-2.0 ± 0.1	-3.4 ± 0.0	-4.3 ± 0.3	-5.9 ± 0.2	-6.6 ± 0.2	-8.1 ± 0.5	-9.9 ± 0.1	-10.4 ± 1.3

To assess gross wettability, water contact angle measurements were performed on dry and water-swollen films cast on glass (Table 3.2). Swollen films were submerged in deionized water for 24 h before measurements. Using a 3 μL sessile drop, measurements were taken for each film at three different locations on the film. In general, water contact angles for the dry coatings were higher than the binary system, which was attributed to the addition of the more hydrophobic biphenyl segments provided by the LC comonomer. Overall, as the wt % PEG increased, the water contact angle decreased for the dry and swollen films in the [10, 15] system, indicating a strong effect by the PEG. However, the [20, 30] system revealed more interesting results, showing a steady increase in water contact angle followed by a sudden decrease when there was more than 65 wt % PEG in the dry films (Figure 3.9).

Table 3.2. Summary of static water contact angle measurements of [10, 15] and [20, 30] LC-HBFP-PEG systems in dry and water swollen states. *Indicates contact angle was too small to be measured.

System		**Mass ratio LC-HBFP to PEG (wt %)**							
		LC-HBFP	*5:2*	*2:1*	*3:2*	*1:1*	*2:3*	*1:2*	*2:5*
		Static Water Contact Angle							
[10, 15]	*Dry*	104 ± 2°	101 ± 6°	91 ± 7°	85 ± 14°	84 ± 11°	83 ± 8°	78 ± 2°	61 ± 6°
	Swollen	102 ± 3°	92 ± 4°	59 ± 5°	28 ± 4°	*	*	*	*
[20, 30]	*Dry*	111 ± 2°	100 ± 1°	111 ± 4°	112 ± 5°	122 ± 3°	124 ± 11°	84 ± 8°	66 ± 10°
	Swollen	110 ± 1°	57 ± 1°	71 ± 1°	48 ± 5°	28 ± 1°	*	*	*

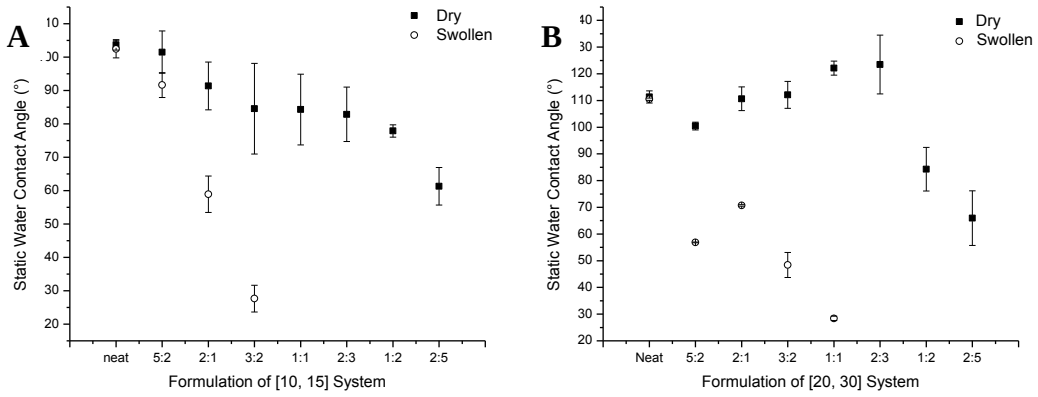

Figure 3.9. Average static water contact angles of the array of (A) [10, 15] LC-HBFP-PEG system and (B) [20, 30] LC-HBFP-PEG system in dry and swollen states.

Due to this unexpected behavior, additional contact angle measurements were performed on the dry [20, 30] system, where measurements were recorded every 5 s for a period of 3 min (Figure 3.10). In general, all formulations showed a decrease in contact angle, over time, and formulations with analogous wt % PEG showed similar trends overall. Additionally, the majority of formulations reached equilibria within the 3 min time period. Swollen films showed comparable trends to their corresponding dry system, where the water contact angle on the [10, 15] system decreased as the wt % PEG increased, and the [20, 30] system experienced an increase in contact angle before decreasing with respect to wt % PEG. Notably, contact angle was measurable for swollen films with up to 50 wt % PEG in the [20, 30] system and only up to 40 wt % PEG in the [10, 15] system. For the [10, 15] system, the reduction in water contact angle correlated with an increase in water uptake, until the system became saturated at ca. 3:2; the 3:2 and 1:1 formulations had comparable percentages of water uptake (*i.e.* 177%

and 169%, respectively). The [20, 30] system with higher than 50 wt % PEG did not have a measurable swollen contact angle and showed greater than 200 % water uptake.

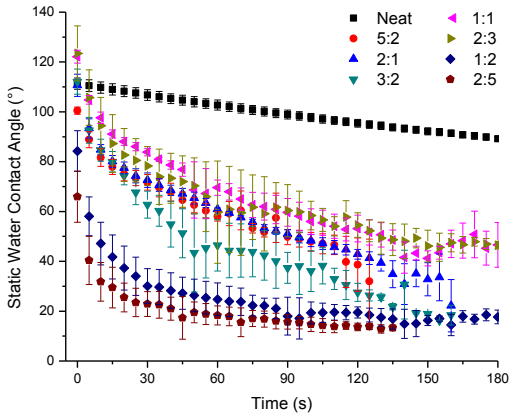

Figure 3.10. Average static water contact angles of the array of dry [20, 30] LC-HBFP-PEG system with respect to time.

Macroscopic phase segregation and film homogeneity was investigated by infrared microscopy on dry coatings to verify a proportionate distribution of LC character across the surface of the coatings and assess the macroscopic homogeneity. A total of twelve scans per film were performed to encompass an area of 300 μm x 200 μm. Although some signal saturation can be observed on the reflection mode scans, the chemical compositions of these films do not show macroscopic segregation of the components (Figure 3.11).

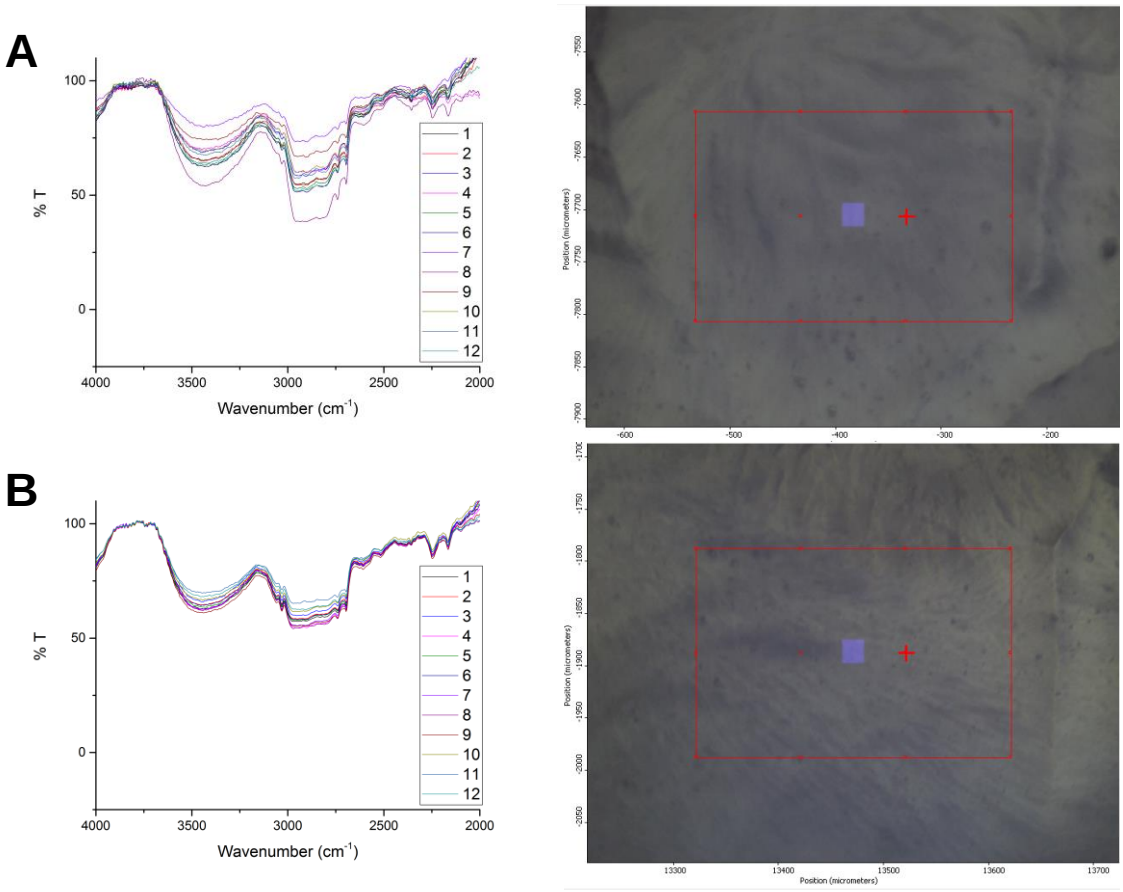

Figure 3.11. Infrared spectra (left) and corresponding microscopy images (right) of area scanned, outlined in red, of 1:1 LC-HBFP-PEG coating for (A) [10, 15] system and (B) [20, 30] system.

To understand morphology and topography, 3D optical microscopy was utilized as a non-contact surface metrology technique. Dry [20, 30] films cast onto glass microscope cover slips were placed on the sample stage and by using white light interferometry, a sample area of 300 μm x 250 μm was scanned using a 20x magnification objective. In general, microscopic features were evident across all samples with a visible decrease in ordered structures as the wt % PEG increased (Figure 3.12). In the neat LC-HBFP sample, sharp peaks with a height of approximately 400 nm

dominated the surface. These data suggest that a high degree of ordering, attributed by the liquid crystalline comonomer, was retained after polymerization, which agreed with POM images taken at 30 °C. Once crosslinked with PEG, these sharp, structured peaks were no longer obvious on the surface, but were replaced by smaller, rounded features, with an overall topography that was also visible in POM images. As we progressed

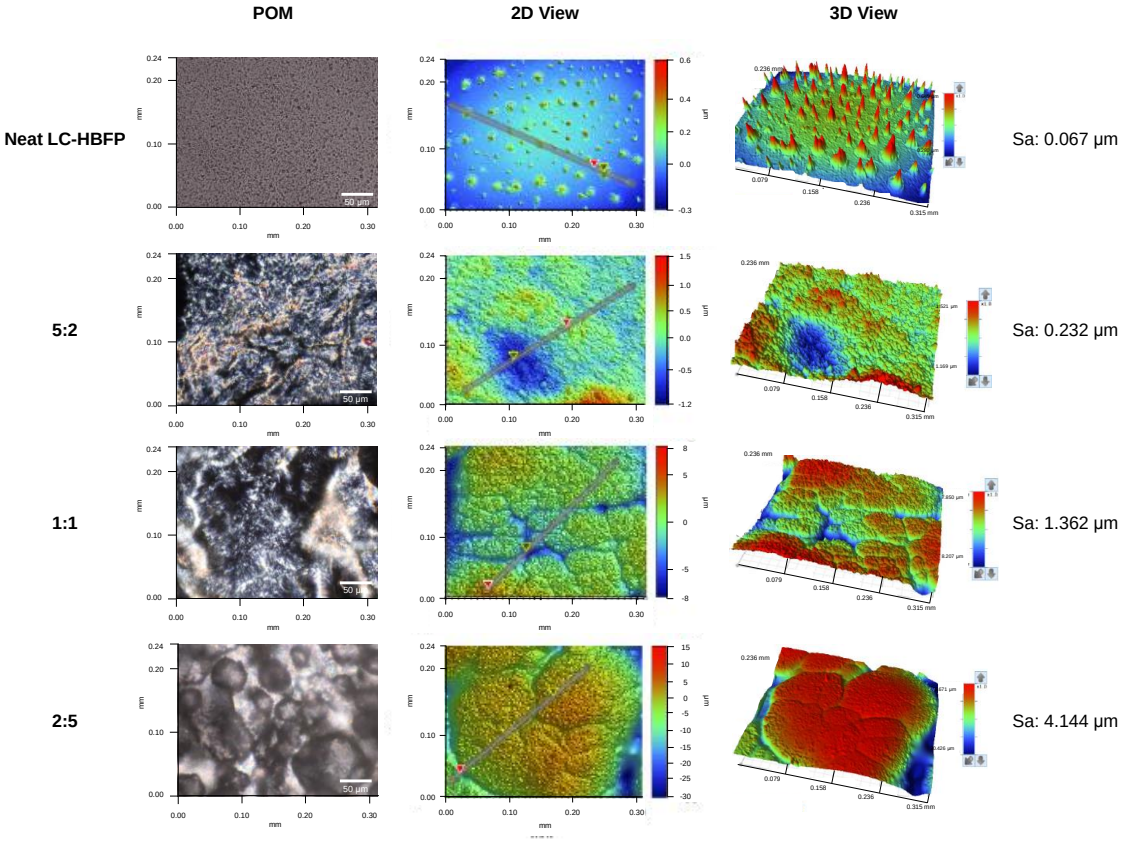

Figure 3.12. POM* and 3D optical microscopy images (2D and 3D views) of dry coatings from the [20, 30] LC-HBFP-PEG system with Sa roughness values. *The area imaged in POM does not correlate to the same area scanned in 3D optical microscopy.

across the array toward higher wt % PEG, these surface features continued to decrease in size, but subsequently, increased the surface area roughness (Sa). This trend in increasing surface roughness with increasing wt % PEG was also observed in previous investigations of the binary system, as well as the ternary system.[41, 43] Measurements of water-swollen coatings were also taken, but due to the increased water uptake causing large distortions in the coatings, accurate measurements were only obtained for the neat LC-HBFP and the 5:2 formulations (Figure 3.13). Both water-swollen coatings exhibited a higher surface area roughness as well as a loss of structured features compared to the dry coatings.

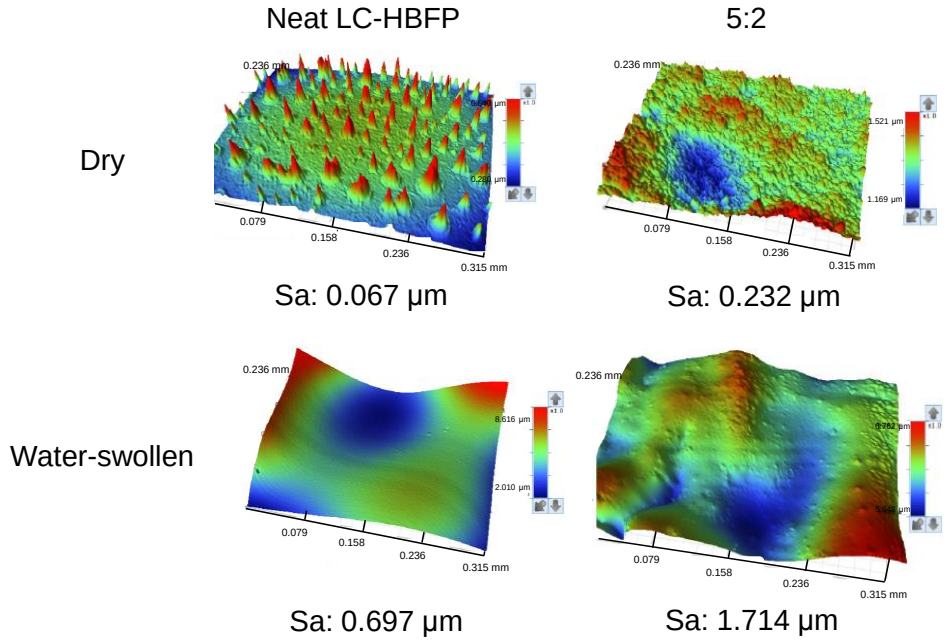

Figure 3.13. 3D optical microscopy images of [20, 30] LC-HBFP-PEG system (neat LC-HBFP and 5:2) dry and water-swollen coatings with surface area roughness (Sa) values.

3.4 Conclusions

In summary, we have demonstrated the successful incorporation of an LC moiety to enhance the ordering and dynamic character of amphiphilic crosslinked polymer networks. Through DSC studies, the new LC-HBFP-PEG system has shown improvement (-9.9 °C) over the binary system (-4.6 °C) to depress the freezing/melting temperature of water, by tuning the molecular weight and weight percentage of PEG. Additionally, the liquid crystalline comonomer has positively increased the water contact angle in dry and water-swollen states resulting in a more hydrophobic surface while maintaining an overall macroscopic homogeneous coating. Surprisingly, as the water contact angle increased, the water uptake % also increased. These results have been attributed to the added ordering parameter contributed by the LC comonomer, which was observed by polarized and 3D optical microscopy measurements. The ability for the polymer matrix to coincidently sequester and confine water molecules, while also being able to undergo dynamic reorganization and result in depression of water freezing point offers interesting potential for these materials as protective coatings in aeronautic, aquatic and other extreme environment applications.

3.5 Acknowledgements

We thank Joseph Fornefeld from Midwest Microlab LLC for elemental analysis, Dr. Anup Bandyopadhyay from Materials Science & Engineering for XRD, Peng Liu and Dr. Hung-Jue Sue in Materials Science & Engineering for use of their POM, the

Laboratory of Biological Mass Spectrometry, and Eric Rufe from Bruker for the 3D Optical Microscopy results.

CHAPTER IV

AMPHIPHILIC CROSSLINKED LIQUID CRYSTALLINE FLUOROPOLYMER-POLY(ETHYLENE GLYCOL) COATINGS FOR APPLICATION IN CHALLENGING CONDITIONS: COMPARATIVE STUDY BETWEEN DIFFERENT LIQUID CRYSTALLINE COMONOMERS AND POLYMER ARCHITECTURES

4.1 Overview

The use of liquid crystalline polymers (LCPs) for coating technologies has gained attention, due to their environmental chemical and weather resistance, wide thermal range and fracture toughness.[24-26, 36] In extreme environments, such as icing, marine fouling and continuous wetting conditions, where a robust, sustainable coating is a priority, long-term retention of properties is essential. Through the use of amphiphilic polymer coatings, several groups have demonstrated success in the field of anti-biofouling or reducing protein adhesion.[41, 43, 105-107] Recently, Hwang and coworkers synthesized and investigated the protein adsorption of random, amphiphilic copolymer films composed of polystyrene (PS), poly(ethylene glycol) methacrylate (PEGMA) and poly(hydroxyethyl) methacrylate (PHEMA), and demonstrated that polymers containing EGMA and HEMA exhibited enhanced anti-biofouling properties over those composed of PS.[106] Additionally, the PS-PEGMA materials had the lowest fluorescence intensities of adsorbed BSA, in comparison to the PS, PS-PHEMA and PS-PEGMA-PHEMA.[106] Segalman and coworkers functionalized an amphiphilic diblock copolymer of PS and poly(ethylene oxide) (PEO) with peptoids, and studied the attachment of zoospores and

adhesion strength of sporelings.[107] They concluded the coatings provided superior anti-fouling properties compared to a glass and a PDMS standard, and through modification of peptoid length, were able to obtain a higher percentage of sporeling removal.[107] Genzer *et al.* demonstrated effective minimization of protein fouling with their amphiphilic coatings formed from fluorinated PHEMA brushes.[105] Several groups have shown that the incorporation of liquid crystalline polymers results in an increase in general coating properties, such as flexibility, hardness and adhesion, over polymers that did not contain an LC moiety.[25, 37-39] It was hypothesized that by combining amphiphilic polymer coatings and liquid crystalline polymers, a dynamic, robust crosslinked coating with enhanced properties could be obtained for use in environmentally challenging conditions. Our laboratory recently incorporated a liquid crystalline (LC) comonomer, composed of a rigid biphenyl segment, into amphiphilic hyperbranched fluoropolymer (HBFP) crosslinked networks to yield dynamic coatings with topographical, morphological and compositional complexities.[108] Prior to LC integration, the HBFP-PEG binary system was shown to reduce fouling in marine environments and depress the freezing/melting point of water by *ca*. -5 °C, credited to the dynamic complexity, low surface energy and nanoscopic surface topography of water-swollen coatings.[40, 41, 89] The addition of the thermally-dynamic LC molecule resulted in a further depression of the freezing point of water (*ca*. -10 °C) over the binary system.[108] Additionally, there was an increase in water contact angle values in the dry and water-swollen states, as well as a three-fold increase in percent water uptake. Due to the success of the original LC(biphenyl)-HBFP-PEG system, it is important to understand the impact of different

LC comonomers and explore the effect of polymer topology on the performance of the coating, not only towards anti-icing applications, but also anti-biofouling and other wetting venues.

With this objective, two additional monomers, 6-phenoxyhexyl acrylate (LC(phenol)) and 6-((4'-cyano-[1,1'-biphenyl]4-yl)oxy)hexyl acrylate (LC(cyano)), were chosen for incorporation into the amphiphilic fluoropolymer, either with a linear (L) or hyperbranched (HB) architecture. The LC(cyano) monomer is well-known and has been extensively studied over the last several decades, toward a variety of applications;[109-117] however, investigation of LC monomers composed of a single aromatic ring, like the LC(phenol), has been explored less.[118-124] For comparison purposes, the original LC(biphenyl)-HBFP was used as a baseline system.

4.2 Experimental Section

4.2.1 Materials

Reagents and starting materials were purchased from Sigma-Aldrich, Acros and VWR and used as received unless otherwise noted. 2,3,4,5,6-Pentafluorostyrene (PFS) was purchased from Apollo Scientific (U.K.). Monomers were purified by passing through a neutral alumina column to remove the inhibitor prior to use.

4.2.2 Instrumentation

Nuclear magnetic resonance spectroscopy and mass spectrometry. Small molecules, monomers and polymers were characterized by ^{1}H and ^{13}C nuclear magnetic resonance (NMR) spectroscopies using a Varian Inova 300 spectrometer. Fluorinated

compounds were also characterized by ^{19}F NMR spectroscopy using a Varian Inova 300 spectrometer. Spectra were analyzed using the solvent signal as an internal reference. High resolution mass spectrometry (HRMS) for the small molecules was conducted on an Applied Biosystems PE SCIEX QSTAR.

Size exclusion chromatography. The polymer molecular weight and molecular weight distribution were determined by size exclusion chromatography (SEC) performed on a Waters 1515 HPLC pump (Waters Chomatography, Inc.) equipped with a 2414 differential refractometer (Waters, Inc.), a PD2020 dual-angle (15° and 90°) light scattering detector (Precision Detectors, Inc.) and a four-column series of PL gel columns (Polymer Laboratories, Inc.): 5 μm Guard (50 x 7.5 mm), 5 μm Mixed C (300 x 7.5 mm), 5 μm 10^4 Å (300 x 7.5 mm) and 5 μm 500 Å (300 x 7.5 mm). Polymer solutions were prepared at a known concentration (3-6 mg/mL) and an injection volume of 200 μL was used. The system was equilibrated at 40 °C in THF, which served as the polymer solvent and eluent (flow rate set to 1.00 mL min^{-1}). The differential refractometer was calibrated with Polymer Laboratories, Inc. polystyrene standards (300 to 467,000 Da). Data collection and analysis were performed using Breeze (version 3.30, Waters, Inc.) software.

Fourier-transform infrared spectroscopy. Infrared spectra were obtained on a Shimadzu IR Prestige attenuated total reflectance Fourier-transform infrared spectrometer (ATR-FTIR). Spectra were analyzed using IRsolution software.

Elemental Analysis. Elemental analysis of the polymers was performed at Midwest Microlab, LLC (Indianapolis, IN).

Thermal analysis. Differential scanning calorimetry (DSC) studies were performed on a Mettler Toledo DSC822 (Mettler Toledo, Inc.) with a heating rate of 5 °C/min and a cooling rate of 2 °C/min. Traces were analyzed using STAR^e Evaluation software (version 10.00d, Mettler Toledo, Inc.) and the T_m was taken at the onset threshold upon the average of the second and third heating scans. Thermogravimetric analysis was performed under Ar atmosphere using a Mettler-Toledo model TGA/DSC 1 STAR^e system, with a heating rate of 10 °C/min. Measurements were analyzed using STAR^e Evaluation software (version 10.00d, Mettler Toledo, Inc.).

Static surface contact angle. Water contact angles were measured as static contact angles using the sessile drop technique with an Attension Theta optical tensiometer (Biolin Scientific). Drops were fitted with a Young-Laplace formula to calculate the static contact angle in the Theta software (Biolin Scientific).

Water uptake studies. Water uptake studies were performed on prepared films that underwent two soakings in deionized water. The first was to remove excess residual PEG and was followed by drying under vacuum at 35 °C for 16 h. Dried films were weighed and then submerged in deionized water for 24 h. The wet films were removed and lightly patted with a Kimwipe to remove any free surface water and subsequently weighed.

X-ray diffraction. X-ray diffraction (XRD) patterns were obtained on a Bruker D8 Advanced Power X-ray diffractometer with Cu-K_α incident radiation (λ = 1.5418 Å). Scans were taken in increments of 0.05 between 2Θ of 3 and 40 at a scan speed of 1 s^{-1}. The heating and cooling rate was 0.08 °C/s.

Polarized optical microscopy. Polarized optical micrographs were collected using an Olympus BX60 optical microscope and cross polarizers at 10x or 20x magnification in conjunction with a Mettler FP80 Hot Stage. The heating rate was 5 °C/min and the cooling rate was 2 °C/min.

3D optical microscopy. 3D optical micrographs were collected using a Bruker Contour GT-K Optical Profiler at 20x magnification.

Solution stability studies. Solution stability studies were performed on prepared films previously annealed in 5-mL shell vials. Samples were submerged in 2 mL of an aqueous media (deionized water, brine or acidic water), capped and placed in a shaker at 37 °C for 24 h. Upon removal, samples were allowed to sit at room temperature for 30 mins before solvent was removed *via* syringe and needle. Samples that were submerged in brine or acidic water were also rinsed with deionized water (*ca.* ~1 mL). A Kimwipe was used to remove any free surface water and samples were subsequently weighed. Samples were allowed to dry in a vacuum oven at 30 °C for 20 h and weighed. The acidic water was a buffer solution prepared from acetic acid and sodium acetate with a pH of 5 – 6 to represent acid rain.

4.2.3 Synthesis

6-(1,1'-biphenyl]-4-yloxy)hexan-1-ol (1). To a flame dried 100 mL Schlenk flask equipped with a magnetic stir bar, potassium carbonate (12.2 g, 88.1 mmol) and a trace amount of potassium iodide (198 mg, 1.22 mmol) were dried under reduced pressure for 1.5 h. A solution of 4-phenylphenol (5.06 g, 29.4 mmol) in dry DMF (41.0 mL) was added and allowed to stir at room temperature for 1 h. A solution of 6-chloro-

1-hexanol (4.00 mL, 29.4 mmol) was added dropwise and the reaction was placed in a preheated oil bath (70 °C) for 16 h. Unreacted solid was filtered off and the remaining solution was washed against deionized water, sodium bicarbonate solution and brine. The organic phase was dried over sodium sulfate, filtered and concentrated *in vacuo* to afford an off-white powder. The crude product was purified by recrystallization using a 1:1 hexanes:ethyl acetate solution to afford the mesogen as a translucent solid in 72% yield (5.69 g). T_m = 80 and 97 °C. TGA in Ar: 278 - 361 °C, 99% mass loss; 0.7% mass remaining at 500 °C. ^{1}H NMR (300 MHz, $CDCl_3$, ppm): δ 7.54 (m, 4H, ***meta-H*** to –O-CH_2-R and ***2'-H*** to Ar-O-CH_2-R), 7.42 (m, 2H, ***3'-H*** to Ar-O-CH_2-R), 7.30 (m, 1H, ***4'-H*** to Ar-O-CH_2-R), 6.97 (m, 2H, ***ortho-H*** to -O-CH_2-R), 4.01 (t, J = 6.5 Hz, 2H, Ar-O-C***H₂***-R), 3.68 (t, J = 6.0 Hz, 2H, R-C***H₂***-OH), 1.83 (quintet, J = 6.8 Hz, 2H, Ar-O-CH_2-C***H₂***-R), 1.69-1.39 (m, 6H, R-C***H₂***-C***H₂***-C***H₂***-CH_2-OH) and 1.34 (s, 1H, R-O***H***). ^{13}C NMR (75 MHz, $CDCl_3$, ppm): δ 158.7, 140.9, 133.6, 128.7, 128.1, 126.7, 126.6, 114.8, 67.9, 62.9, 32.7, 29.3, 26.0 and 25.6. GC/MS m/z calculated for $C_{18}H_{22}O_2$ [M+TMS] 342.36 Da, found 342.10 Da. FTIR (ATR): 3310, 3080 - 3010, 2180 - 1665, 1605, 1520, 1475, 1400, 1245, 1190, 1120, 1070, 1035, 995, 915, 835, 755, 715, 685 cm^{-1}.

6-([1,1'-biphenyl]-4-yloxy)hexyl acrylate (2). To a flame dried 200 mL Schlenk flask equipped with a magnetic stir bar and suspended in an ice bath, a solution of **1** (4.00 g, 14.8 mmol) and triethylamine (2.50 mL, 17.8 mmol) in dry THF (82.0 mL) was added. A solution of acryloyl chloride (1.80 mL, 22.2 mmol) in dry THF (6.00 mL) was added dropwise and the reaction was allowed to stir at 0 °C for 2 h and then at room

temperature for an additional 12 h. The reaction mixture was concentrated, dissolved in chloroform and washed against deionized water, sodium bicarbonate solution and brine. The organic phase was dried over sodium sulfate, filtered and concentrated *in vacuo* to afford a white solid in 86% yield (4.11 g). T_m = 41°C. TGA in Ar: 353 - 432 °C, 94% mass loss; 5% mass remaining at 500 °C. ^{1}H NMR (300 MHz, $CDCl_3$, ppm): δ 7.53 (m, 4H, ***meta-H*** to -O-CH_2-R and ***2'-H*** to Ar-O-CH_2-R), 7.41 (m, 2H, ***3'-H*** to Ar-O-CH_2-R), 7.32 (m, 1H, ***4'-H*** to Ar-O-CH_2-R), 6.98 (m, 2H, ***ortho-H*** to -O-CH_2-R), 6.40 (d, *J* = 17 Hz, 1H, ***H***(H)C=CH-R (*trans*)), 6.12 (dd, *J* = 17 Hz and 10 Hz, 1H, H_2C=C***H***-R), 5.82 (d, *J* = 10 Hz, 1H, H(***H***)C=CH-R (*cis*)), 4.18 (t, *J* = 6.0 Hz, 2H, R-C***H$_2$***-O(O)C-R'), 4.00 (t, *J* = 6.5 Hz- 2H, Ar-O-C***H$_2$***-R) and 1.89 - 1.41 (m, 8H, R-C***H$_2$***-C***H$_2$***-C***H$_2$***-C***H$_2$***-CH_2-O(O)C-R'). ^{13}C NMR (75 MHz, $CDCl_3$, ppm): δ 166.3, 158.6, 140.9, 133.6, 130.6, 128.7, 128.6, 128.1, 126.7, 126.6, 114.8, 67.9, 64.6, 29.2, 28.6 and 25.8. GC/MS m/z calculated for $C_{21}H_{24}O_3$ [M] 324.17 Da, found 324.11 Da. FTIR (ATR): 3105 – 3005, 2190 – 1845, 1710, 1605, 1520, 1485, 1405, 1295, 1195, 995, 825, 760, 695 cm^{-1}.

6-phenoxyhexan-1-ol (3). To a flame dried 200 mL Schlenk flask equipped with a magnetic stir bar, potassium carbonate (44.1 g, 319 mmol) and a trace amount of potassium iodide (743 mg, 4.43 mmol) were dried under reduced pressure for 2 hours. A solution of phenol (10.1 g, 106 mmol) in dry DMF (74.0 mL) was added and allowed to stir at room temperature for 1.5 hours. A solution of 6-chloro-1-hexanol (10.0 mL, 75.0 mmol) was added dropwise and the reaction was placed in a preheated oil bath (70 °C) for 16 hours. Unreacted solid was filtered off and the remaining solution was washed against deionized water, sodium bicarbonate solution and brine. The organic

phase was dried over sodium sulfate, filtered and concentrated *in vacuo* to afford an offwhite powder. Further purification by silica gel flash chromatography using a gradient of hexanes to ethyl acetate as eluent afforded **3** as a translucent solid in 72% yield (10.5 g). T_m = 21 °C. TGA in Ar: 191 – 261 °C, 53% mass loss, 261 – 348 °C, 24% mass loss, 348 – 362 °C, 15% mass loss; 6% mass remaining at 500 °C. ^{1}H NMR (300 MHz, $CDCl_3$, ppm): δ 7.22 (m, 2H, ***meta-H*** to –O-CH_2-R), 6.88 (m, 3H, ***ortho-H*** and ***para-H*** to –O-CH_2-R), 3.93 (t, *J* = 6.6 Hz, 2H, Ar-O-C***H₂***-R), 3.63 (t, *J* = 6.5 Hz, 2H, R-C***H₂***-OH), 2.31 (s, 1H, R-O***H***), 1.77 (quintet, *J* = 6.8 Hz, 2H, Ar-O-CH_2-C***H₂***-R), 1.58 (quintet, *J* = 6.8 Hz, 2H, R-C***H₂***-CH_2-OH) and 1.53 – 1.35 (m, 4H, R-C***H₂***-C***H₂***-CH_2-CH_2-OH). ^{13}C NMR (75 MHz, $CDCl_3$, ppm): δ 159.1, 129.5, 120.6, 114.5, 67.8, 62.8, 62.9, 32.7, 29.3, 26.7 and 25.6. ESIHRMS m/z calculated for $C_{12}H_{18}O_2$ $[M+H]^+$ 195.27 Da, found 195.1450. FTIR (ATR): 3310, 3080 – 3010, 2940, 2860, 1600, 1585, 1495, 1475, 1440, 1420, 1395, 1375, 1295, 1245, 1170, 1155, 1120, 1105, 1075, 1060, 1030, 1005, 990, 960, 915, 885, 835, 810, 750, 695, 610 cm^{-1}.

6-phenoxyhexyl acrylate (4). To a flame dried 200 mL Schlenk flask equipped with a magnetic stir bar and suspended in an ice bath, a solution of **3** (5.01 g, 25.7 mmol) and triethylamine (4.40 mL, 30.9 mmol) in dry THF (102 mL) was added. A solution of acryloyl chloride (3.20 mL, 38.6 mmol) in dry THF (8.00 mL) was added dropwise and the reaction was allowed to stir at 0 °C for 1 hour and then at room temperature for an additional 12 hours. The reaction mixture was concentrated, dissolved in chloroform and washed against deionized water, sodium bicarbonate solution and brine. The organic phase was dried over sodium sulfate, filtered and concentrated *in vacuo* to afford

a yellow liquid in 58% yield (3.70 g). T_g = 13 °C. TGA in Ar: 204 – 294 °C, 62% mass loss, 294 – 375 °C, 6% mass loss, 375 – 428 °C, 29% mass loss; 2% mass remaining at 500 °C. ^{1}H NMR (300 MHz, $CDCl_3$, ppm): δ 7.27 (m, 2H, ***meta-H*** to –O-CH_2-R), 6.90 (m, 3H, ***ortho-H*** and ***para-H*** to –O-CH_2-R), 6.41 (d, *J* = 17 Hz, 1H, ***H***(H)C=CH-R (*trans*)), 6.13 (dd, *J* = 17 Hz and 10 Hz, 1H, H_2C=C***H***-R), 5.82 (d, *J* = 10 Hz, 1H, H(***H***)C=CH-R (*cis*)), 4.17 (t, *J* = 6.6 Hz, 2H, R-C***H₂***-O(O)C-R'), 3.96 (t, *J* = 6.3 Hz, 2H, Ar-O-C***H₂***-R), 1.85 – 1.67 (m, 4H, RO-CH_2-C***H₂***-CH_2-CH_2-C***H₂***-CH_2-OH) and 1.57 – 1.39 (m, 4H, RO-CH_2-CH_2-C***H₂***-C***H₂***-CH_2-CH_2-OH). ^{13}C NMR (75 MHz, $CDCl_3$, ppm): δ 166.2, 159.0, 130.4, 129.3, 128.5, 120.4, 114.4, 67.5, 64.5, 29.1, 28.5 and 25.7. ESIHRMS m/z calculated for $C_{15}H_{20}O_3$ $[M+Li]^+$ 255.32 Da, found 256.3113. FTIR (ATR): 3105 - 3035, 2940, 2860, 1720, 1635, 1620, 1600, 1585, 1495, 1470, 1405, 1295, 1270, 1240, 1185, 1055, 1035, 985, 885, 810, 755, 690, 665 cm^{-1}.

4'-((6-hydroxyhexyl)oxy)-[1,1'-biphenyl]-4-carbonitrile (5). To a flame dried 200 mL Schlenk flask equipped with a magnetic stir bar, potassium carbonate (21.2 g, 154 mmol) and a trace amount of potassium iodide (358 mg, 2.13 mmol) were dried under reduced pressure for 2 hours. A solution of 4-cyano-4'-hydroxybiphenyl (10.0 g, 51.2 mmol) in dry DMF (74.0 mL) was added and allowed to stir at room temperature for 1.5 hours. A solution of 6-chloro-1-hexanol (7.00 mL, 51.2 mmol) was added dropwise and the reaction was placed in a preheated oil bath (70 °C) for 16 hours. Unreacted solid was filtered off and the remaining solution was washed against deionized water, sodium bicarbonate solution and brine. The organic phase was dried over sodium sulfate, filtered and concentrated *in vacuo* to afford an offwhite powder.

The crude product was purified by recrystallization using a 1:1 hexanes:ethyl acetate solution to afford the **5** as a translucent solid in 83% yield (12.5 g). T_m = 88 and 110 °C. TGA in Ar: 324 – 409 °C, 95% mass loss; 5% mass remaining at 500 °C. ^{1}H NMR (300 MHz, $CDCl_3$, ppm): δ 7.67 (m, 4H, ***meta-H*** to –O-CH_2-R and ***2'-H*** to Ar-O-CH_2-R), 7.53 (m, 2H, ***3'-H*** to Ar-O-CH_2-R), 6.99 (m, 2H, ***ortho-H*** to -O-CH_2-R), 4.02 (t, *J* = 6.5 Hz, 2H, Ar-O-C***H$_2$***-R), 3.68 (t, *J* = 6.5 Hz, 2H, R-C***H$_2$***-OH), 1.84 (quintet, *J* = 7.0 Hz, 2H, Ar-O-CH_2-C***H$_2$***-R), 1.63 (quintet, *J* = 6.8 Hz, 2H, R-C***H$_2$***-CH_2-OH), 1.56 – 1.42 (m, 4H, R-C***H$_2$***-C***H$_2$***-CH_2-CH_2-OH) and 1.25 (s, 1H, R-O***H***). ^{13}C NMR (75 MHz, $CDCl_3$, ppm): δ 159.7, 145.3, 133.0, 128.4, 128.3, 127.1, 119.2, 115.1, 110.0, 68.0, 62.9, 32.7, 29.2, 25.9 and 25.6. ESIHRMS m/z calculated for $C_{19}H_{21}O_2N$ $[M+H]^+$ 295.39 Da, found 295.1070. FTIR (ATR): 3325, 2980 – 2790, 2225, 1600, 1580, 1525, 1490, 1470, 1425, 1390, 1315, 1290, 1270, 1250, 1215, 1180, 1135. 1115, 1060, 1025, 1005, 980, 910, 850, 825, 805, 775, 760, 730, 715, 685 cm^{-1}.

6-((4'-cyano-[1,1'-biphenyl]4-yl)oxy)hexyl acrylate (6). To a flame dried 200 mL Schlenk flask equipped with a magnetic stir bar and suspended in an ice bath, a solution of **5** (5.00 g, 16.9 mmol) and triethylamine (3.00 mL, 20.3 mmol) in dry THF (103 mL) was added. A solution of acryloyl chloride (2.10 mL, 25.4 mmol) in dry THF (7.00 mL) was added dropwise and the reaction was allowed to stir at 0 °C for 1 hour and then at room temperature for an additional 12 hours. The reaction mixture was concentrated, dissolved in chloroform and washed against deionized water, sodium bicarbonate solution and brine. The organic phase was dried over sodium sulfate, filtered and concentrated *in vacuo* to afford a pale yellow solid in 84% yield (4.95 g). T_m

= 60°C. TGA in Ar: 367 – 449 °C, 88% mass loss; 10% mass remaining at 500 °C. ^{1}H NMR (300 MHz, $CDCl_3$, ppm): δ 7.66 (m, 4H, ***meta-H*** to –O-CH_2-R and ***2'-H*** to Ar-O-CH_2-R), 7.53 (m, 2H, m, 2H, ***3'-H*** to Ar-O-CH_2-R), 6.99 (m, 2H, ***ortho-H*** to -O-CH_2-R), 6.41 (d, *J* = 17 Hz, 1H, ***H***(H)C=CH-R (*trans*)), 6.13 (dd, *J* = 17 Hz and 10 Hz, 1H, H_2C=C***H***-R), 5.82 (d, *J* = 10 Hz, 1H, H(***H***)C=CH-R (*cis*)), 4.18 (t, *J* = 6.8 Hz, 2H, R-C***H₂***-O(O)C-R'), 4.01 (t, *J* = 6.3 Hz, 2H, Ar-O-C***H₂***-R), 1.88 – 1.68 (m, 4H, RO-CH_2-C***H₂***-CH_2-CH_2-C***H₂***-CH_2-OH) and 1.52 – 1.42 (m, 4H, RO-CH_2-CH_2-C***H₂***-C***H₂***-CH_2-CH_2-OH). ^{13}C NMR (75 MHz, $CDCl_3$, ppm): δ 166.3, 159.7, 145.2, 132.5, 131.3, 130.5, 128.5, 128.3, 127.0, 119.1, 115.0, 110.0, 77.2, 67.9, 64.5, 29.1, 28.5 and 25.7. ESIHRMS m/z calculated for $C_{22}H_{23}O_3N$ $[M+H]^+$ 349.42 Da, found 350.1840 Da. FTIR (ATR): 2960 – 2865, 2225, 1715, 1635, 1600, 1520, 1495, 1475, 1400, 1380, 1290, 1245, 1195, 1180, 1115, 1075, 1040, 1025, 1005, 995, 975, 890, 850, 820, 730, 670, 660, 630 cm^{-1}.

4-[Oxy(tri(ethylene glycol))bromoisopropionyl] -2,3,5,6-tetrafluorostyrene (7). Compound **7** was prepared according to a previously reported method.[89] Briefly, to a 1000 mL two-neck round bottom flask equipped with a magnetic stir bar and addition funnel suspended in an ice bath, a solution of 4-[oxy(tri(ethylene glycol))]-2,3,5,6-tetrafluorostyrene (10.0 g, 30.8 mmol), triethylamine (16.0 mL, 111 mmol) in THF (235 mL) was added. A solution of 2-bromopropionyl bromide (3.90 mL, 37.0 mmol) in THF (20.0 mL) was added dropwise. The solution was allowed to warm to room temperature and stir under N_2 for 14 h. The reaction was concentrated, and crude product was washed three times against brine. The organic phase was dried over sodium sulfate,

filtered, and concentrated *in vacuo* to afford a pale yellow oil. Further purification by silica gel flash chromatography using a gradient of hexanes:ethyl acetate as eluent afforded 7 as a clear, pale yellow oil in 59% yield (8.40 g). TGA in Ar: 248 - 327 °C, 20% mass loss, 327 – 430 °C, 58% mass loss; 19% mass remaining at 500 °C. ^{1}H NMR (300 MHz, $CDCl_3$, ppm): δ 6.61 (dd, *J* = 18 Hz and 12 Hz, 1H, H_2C=C***H***-R), 6.02 (d, *J* = 18 Hz, 1H, ***H***(H)C=CH-R (*trans*)), 5.62 (d, *J* = 12 Hz, 1H, H(***H***)C=CH-R (*cis*)), 4.39 (q, *J* = 6.9 Hz, 1H, R-C(***H***)(Br)CH_3), 4.37 (t, *J* = 4.8 Hz, 2H, TFS-O-C***H*****$_2$**-CH_2-OR), 4.31 (t, *J* = 4.8 Hz, 2H, R-O-CH_2-C***H*****$_2$**-O(O)C-R'), 3.83 (t, *J* = 4.8 Hz, 2H, TFS-O-CH_2-C***H*****$_2$**-OR), 3.75-3.60 (m, 6H, R-O-C***H*****$_2$**-C***H*****$_2$**-O-C***H*****$_2$**-CH_2-O(O)C-R') and 1.81 (d, *J* = 6.9 Hz, 3H, R-C(H)(Br)C***H*****$_3$**). ^{13}C NMR (75 MHz, $CDCl_3$, ppm): δ 170.9, 146.6, 143.3, 142.8, 139.3, 136.3, 122.2, 122.0, 110.8, 74.1, 70.8, 70.6, 70.1, 68.8, 64.6, 55.6 and 30.5. ^{19}F NMR (282 MHz, $CDCl_3$, ppm): δ -145 (m, 2F, ***ortho-F*** to -CH=CH_2) and -158 (m, 2F, ***meta-F*** to -CH=CH_2). ESIHRMS m/z calculated for $C_{17}H_{19}O_5F_4Br$ $[M+H]^+$ 459.02 Da, found 459.0430. FTIR (ATR): 3070 - 2750, 1740, 1640, 1485, 1450, 1405, 1335, 1225, 1120, 1080, 965, 935, 855, 760, 675 cm^{-1}.

4-[Oxy(tri(ethylene glycol))azidoisopropionyl] -2,3,5,6-tetrafluorostyrene (8). To a flame dried 10 mL Schlenk flask equipped with a magnetic stir bar, sodium azide (212 mg, 3.27 mmol) was added and dried under reduced pressure for 10 min. A solution of **7** (1.02 g, 2.18 mmol) in dry DMF (2.50 mL) was added and the solution was allowed to stir at room temperature for 48 h. The reaction was concentrated, dissolved in DCM and washed two times against deionized water and two times with brine. The organic phase was dried over sodium sulfate, filtered and concentrated *in vacuo* to afford

a dark yellow oil in 74% yield (675 mg). TGA in Ar: 161 - 310 °C, 14% mass loss, 310 – 405 °C, 45% mass loss; 34% mass remaining at 500 °C. ^{1}H NMR (300 MHz, $CDCl_3$, ppm): δ 6.62 (dd, *J* = 18 Hz and 12 Hz, 1H, H_2C=C***H***-R), 6.03 (d, *J* = 18 Hz, 1H, ***H***(H)C=CH-R (*trans*)), 5.64 (d, *J* = 12 Hz, 1H, H(***H***)C=CH-R (*cis*)), 4.36 (t, *J* = 4.5 Hz, 2H, TFS-O-C***H*****$_2$**-CH_2-OR), 4.32 (t, *J* = 4.8 Hz, 2H, R-O-CH_2-C***H*****$_2$**-O(O)C-R'), 3.97 (q, *J* = 6.9 Hz, 1H, R-C(***H***)(N_3)CH_3), 3.82 (t, *J* = 4.5 Hz, 2H, TFS-O-CH_2-C***H*****$_2$**-OR), 3.75-3.61 (m, 6H, R-O-C***H*****$_2$**-C***H*****$_2$**-O-C***H*****$_2$**-CH_2-O(O)C-R') and 1.47 (d, *J* = 6.9 Hz, 3H, R-C(H)(N_3)C***H*****$_3$**). ^{13}C NMR (75 MHz, $CDCl_3$, ppm): δ 170.9, 146.6, 143.3, 142.8, 139.3, 136.3, 122.2, 122.0, 110.8, 74.1, 70.8, 70.6, 70.1, 68.8, 64.6, 57.2 and 16.8. ^{19}F NMR (282 MHz, $CDCl_3$, ppm): δ -145 (m, 2F, ***ortho-F*** to –CH=CH_2) and -158 (m, 2F, ***meta-F*** to -CH=CH_2). ESIHRMS m/z calculated for $C_{17}H_{19}O_5F_4N_3$ $[M+H]^+$ 422.34 Da, found 422.1238 Da. FTIR (ATR): 3050 – 2755, 2110, 1745, 1645, 1500, 1485, 1450, 1425, 1405, 1380, 1350, 1250, 1190, 1115, 1075, 1030, 965, 935, 855 cm^{-1}.

Prop-2-yn-1-yl 2-(dodecylthiocarbonothioyl thio)-2-methylpropanoic acid (9). To a flame dried 10 mL Schlenk flask equipped with a magnetic stir bar, 2-(dodecylthiocarbonothioylthio)-2-methylpropionic acid (1.00 g, 2.74 mmol) and 4-(dimethylamino)pyridine (69.0 mg, 0.55 mmol) were added and dried under reduced pressure for 30 mins. A solution of *N,N'* – dicyclohexylcarbodiimide (0.68 g, 3.29 mmol) in dry DCM (8.50 mL) was added. A solution of propargyl alcohol (0.56 mL, 9.60 mmol) in dry DCM (8.50 mL) was added dropwise and the reaction was allowed to stir overnight at room temperature. The solid was filtered off and the organic phase was washed three times against a sodium bisulfate solution and a sodium bicarbonate

solution. The organic phase was dried over sodium sulfate, filtered and concentrated *in vacuo* to afford a dark yellow solid in 58% yield (641 mg). T_m = 11 and 20 °C. TGA in Ar: 196 - 254 °C, 31% mass loss, 254 – 331 °C, 55% mass loss; 8% mass remaining at 500 °C. ^{1}H NMR (300 MHz, $CDCl_3$, ppm): δ 4.70 (d, *J* = 2.4 Hz, 2H, HC≡C***H₂***-OR), 3.27 (t, *J* = 7.5 Hz, 2H, R-S(S)S-C***H₂***-R'), 2.46 (t, *J* = 2.4 Hz, 1H, ***H***C≡CH_2-OR), 1.71 (s, 6H, R-O(O)C-C(C***H₃***)(C***H₃***)-S(S)S-R'), 1.69 – 1.60 (m, 2H, R-S(S)S-CH_2-C***H₂***-R'), 1.34 – 1.22 (m, 18H, R-S(S)S-CH_2-CH_2-C***H₂***-C***H₂***-C***H₂***-C***H₂***-C***H₂***-C***H₂***-C***H₂***-C***H₂***-C***H₂***-CH_3) and 0.88 (t, *J* = 6.9 Hz, 3H, R-C***H₃***). ^{13}C NMR (75 MHz, $CDCl_3$, ppm): δ 221.1, 172.3, 77.3, 75.1, 55.6, 53.3, 37.0, 31.9, 29.6, 29.5, 29.4, 29.3, 29.1, 28.9, 27.8, 25.2, 22.7 and 14.1. ESIHRMS m/z calculated for $C_{20}H_{34}O_2S_3$ $[M+H]^+$ 403.17 Da, found 403.1797 Da. FTIR (ATR): 3300, 3030 - 2765, 2125, 1740, 1465, 1385, 1365, 1245, 1150, 1120, 1065, 1010, 990, 815, 745, 715, 670, 630 cm^{-1}.

Macro 'click' chain transfer monomer (10). To a flame dried 10 mL Schlenk flask equipped with a magnetic stir bar, a solution of **8** (565 mg, 1.34 mmol), **9** (479 mg, 1.19 mmol) and *N,N,N'N'',N''*-pentamethyldiethylenetriamine (50.0 mg, 0.29 mmol) in dry DMF (8.00 mL) was added. A solution of Cu(I)Br (58.0 mg, 0.41 mmol) dissolved in dry DMF (0.50 mL) was added and the reaction was allowed to stir for 30 h at room temperature. Copper was removed by elution through an aluminum oxide plug and the product was obtained after drying *in vacuo* to afford a dark brown oil in 94% yield (924 mg). T_g = 34 °C. TGA in Ar: 229 - 280 °C, 18% mass loss, 280 – 394 °C, 62% mass loss; 16% mass remaining at 500 °C. ^{1}H NMR (300 MHz, $CDCl_3$, ppm): δ 7.77 (s, 1H, R-C(H)(CH_3)-N_3C_2***H***-R'), 6.62 (dd, *J* = 18 Hz and 12 Hz, 1H, H_2C=C***H***-R), 6.02 (d, *J* =

18 Hz, 1H, ***H***(H)C=CH-R (*trans*)), 5.66 (d, *J* = 12 Hz, 1H, H(***H***)C=CH-R (*cis*)), 5.48 (q, *J* = 7.5 Hz, 1H, R-C(***H***)(CH_3)-N_3C_2H-R'), 5.26 (d, *J* = 5.4 Hz, 2H, R-N_3C_2H-C***H₂***-O(O)C-R'), 4.37 (t, *J* = 4.5 Hz, 2H, TFS-O-C***H₂***-CH_2-OR), 4.32 (t, *J* = 4.8 Hz, 2H, R-O-CH_2-C***H₂***-O(O)C—C(H)(CH_3)-N_3C_2H-R'), 3.82 (t, *J* = 4.5 Hz, 2H, TFS-O-CH_2-C***H₂***-OR), 3.72 – 3.58 (m, 6H, R-O-C***H₂***-C***H₂***-O-C***H₂***-CH_2-O(O)C—C(H)(CH_3)-N_3C_2H-R'), 3.22, (t, *J* = 7.5 Hz, 2H, R-S(S)S-C***H₂***-R'), 1.84 (d, *J* = 7.5 Hz, 3H, R-C(H)(C***H₃***)-N_3C_2H-R') 1.70 – 1.56 (m, 8H, R-O(O)C-C(C***H₃***)(C***H₃***)-S(S)S-CH_2-C***H₂***-R'), 1.31 – 1.23 (m, 18H, R-S(S)S-CH_2-CH_2-C***H₂***-C***H₂***-C***H₂***-C***H₂***-C***H₂***-C***H₂***-C***H₂***-C***H₂***-CH_3) and 0.87 (t, *J* = 6.6 Hz, 3H, R-C***H₃***). ^{13}C (75 MHz, $CDCl_3$, ppm): δ 221.1, 172.9, 169.1, 146.6, 143.3, 142.8, 142.6, 139.3, 136.3, 123.4, 122.2, 122.0, 110.8, 74.2, 70.9, 70.6, 70.3, 68.7, 65.2, 59.1, 58.2, 55.9, 37.0, 31.9, 29.6, 29.5, 29.4, 29.3, 29.1, 28.9, 27.8, 25.2, 22.7, 18.3 and 14.1. ^{19}F NMR (282 MHz, $CDCl_3$, ppm): δ 145 (m, 2F, ***ortho-F*** to –CH=CH_2) and -158 (m, 2F ***meta-F*** to -CH=CH_2). ESIHRMS m/z calculated for $C_{36}H_{63}O_7F_4N_3S_3$ $[M+H]^+$ 825.02 Da, found 825.3180 Da. FTIR (ATR): 3050 - 2700, 1740, 1680, 1485, 1385, 1250, 1150, 1120, 1075, 965, 940, 865, 815, 720, 655 cm^{-1}.

Liquid crystalline hyperbranched fluoropolymer (LC(biphenyl)$_{20}$-HBFP$_{30}$), (11). To a flame dried 10 mL Schlenk flask equipped with a magnetic stir bar, a solution of **2** (885 mg, 2.74 mmol), **7** (1.26 g, 2.74 mmol), **10** (74.0 mg, 0.09 mmol) and azobisisobutyronitrile (3.00 mg, 0.02 mmol) in dry DMF (8.00 mL) was added. The solution was deoxygenated *via* freeze-pump-thaw cycles (x3) then placed in a preheated oil bath (70 °C) and allowed to react for 27 h. The polymerization was quenched by opening the flask to air and submerging the flask in liquid nitrogen. Polymer was

obtained after two precipitations in cold diethyl ether to afford a yellow viscous oil in 38% yield (721 mg). M_n^{GPC} = 19 kDa, M_w/M_n.= 1.44. T_g = 85 °C. TGA in Ar: 283 - 359 °C, 31% mass loss, 359 - 446 °C, 43% mass loss; 22% mass remaining at 500 °C. ^{1}H NMR (300 MHz, $CDCl_3$, ppm): δ 7.58 – 7.29 (br, m, ***meta-H*** to –O-CH_2-R and ***2'-H***, ***3'-H*** and ***4'-H*** to Ar-O-CH_2-R), 7.00 – 6.85 (br, m, ***ortho-H*** to –O-CH_2-R), 4.47 – 4.14 (br, m, Ar-R-C***H₂***-O(O)C-R' and TFS-O-C***H₂***-CH_2-O-CH_2-CH_2-O-CH_2-C***H₂***-O(O)C-R'), 4.03 - 3.88 (br, m, Ar-O-C***H₂***-R), 3.85 - 3.55 (br, m, TFS-O-CH_2-C***H₂***-O-C***H₂***-C***H₂***-O-C***H₂***-CH_2-O(O)C-R'), 2.85 – 2.62 (br, m, C***H₂***-C***H***(R)- backbone), 2.10 – 1.05 (br, m, R-C***H₂***-C***H₂***-C***H₂***-C***H₂***-CH_2-O(O)C-R' and C-C***H₃***). ^{13}C NMR (75 MHz, $CDCl_3$, ppm): δ 170.2, 160.0, 158.2, 146.7, 142.5, 140.7, 139.1, 136.0, 133.5, 128.7, 128.0, 126.7, 114.7, 74.3, 70.7, 69.9, 68.7, 68.1, 67.8, 65.0, 64.4, 40.0, 34.7, 30.3, 29.1, 28.3, 25.7, 21.6, 16.9 and 14.3. ^{19}F NMR (282 MHz, $CDCl_3$, ppm): δ -143 (br, m, ***ortho-F*** (TFS)) and -157 (br, m, ***meta-F*** (TFS)). Elem. Anal. Calcd. for $C_{862}H_{1028}S_3N_3F_{124}Br_{30}$: C, 53.09; H, 5.31; S, 0.49; N, 0.22; F, 12.08; Br, 12.29%. Found: C, 55.17; H, 4.94; S, 0.78; N, 0.21; F, 11.12; Br, 7.63%. FTIR (ATR): 3030 – 2800, 1730, 1650, 1610, 1490, 1460, 1365, 1245, 1120, 960, 830, 765, 695 cm^{-1}.

Liquid crystalline linear fluoropolymer (LC(biphenyl)$_{20}$-LFP$_{30}$), (12). To a flame dried 10 mL Schlenk flask equipped with a magnetic stir bar, a solution of **2** (894 mg, 2.74 mmol), **7** (1.26 g, 2.74 mmol), 2-(dodecylthiocarbonothioylthio)-2-methylpropionic acid (33.0 mg, 0.09 mmol) and azobisisobutyronitrile (3.00 mg, 0.02 mmol) in dry DMF (9.00 mL) was added. The solution was deoxygenated *via* freeze-pump-thaw cycles (x3) then placed in a preheated oil bath (70 °C) and allowed to react

for 21 hours. The polymerization was quenched by opening the flask to air and submerging the flask in liquid nitrogen. Polymer was obtained after two precipitations in cold diethyl ether to afford a yellow viscous oil in 50% yield (1.04 g). M_n^{GPC} = 23 kDa, M_w/M_n.= 1.17. T_g = -27 °C. TGA in Ar: 288 – 331 °C, 26% mass loss, 331 – 444 °C, 53% mass loss; 19% mass remaining at 500 °C. ^{1}H NMR (300 MHz, $CDCl_3$, ppm): δ 7.58 – 7.27 (br, m, ***meta-H*** to –O-CH_2-R and ***2'-H***, ***3'-H*** and ***4'-H*** to Ar-O-CH_2-R), 6.99 – 6.84 (br, m, ***ortho-H*** to –O-CH_2-R), 4.47 – 4.15 (br, m, Ar-R-C***H₂***-O(O)C-R' and TFS-O-C***H₂***-CH_2-O-CH_2-CH_2-O-CH_2-C***H₂***-O(O)C-R'), 4.03 - 3.86 (br, m, Ar-O-C***H₂***-R), 3.81 - 3.55 (br, m, TFS-O-CH_2-C***H₂***-O-C***H₂***-C***H₂***-O-C***H₂***-CH_2-O(O)C-R'), 2.85 – 2.62 (br, m, C***H₂***-C***H***(R)- backbone), 2.10 – 1.17 (br, m, R-C***H₂***-C***H₂***-C***H₂***-C***H₂***-CH_2-O(O)C-R' and C-C***H₃***). ^{13}C NMR (75 MHz, $CDCl_3$, ppm): δ 170.2, 159.9, 158.6, 147.0, 142.4, 140.7, 139.1, 136.1, 133.4, 128.7, 128.0, 126.6, 114.7, 77.2, 74.2, 70.6, 69.9, 68.7, 68.1, 68.0, 67.8, 65.0, 64.4, 40.0, 30.3, 29.1, 28.4, 25.6, 21.6, and 16.9. ^{19}F NMR (282 MHz, $CDCl_3$, ppm): δ -143 (br, m, ***ortho-F*** (TFS)) and -157 (br, m, ***meta-F*** (TFS)).Elem. Anal. Calcd. for $C_{1094}H_{1249}S_3F_{120}Br_{30}$: C, 57.16; H, 5.48; S, 0.42; F, 9.92; Br, 10.43%. Found: C, 57.31; H, 5.58; S, 0.49; F, 9.59; Br, 7.64%. FTIR (ATR): 3100 – 2795, 1730, 1650, 1610, 1490, 1450, 1330, 1245, 1155, 1065, 960, 835, 765, 720, 695 cm^{-1}.

Liquid crystalline (phenol) hyperbranched fluoropolymer (LC(phenol)$_{20}$-HBFP$_{30}$), (13). To a flame dried 10 mL Schlenk flask equipped with a magnetic stir bar, a solution of **4** (681 mg, 2.74 mmol), **7** (1.26 g, 2.74 mmol), **10** (75.3 mg, 0.09 mmol) and azobisisobutyronitrile (3.30 mg, 0.02 mmol) in dry DMF (8.00 mL) was added. The

solution was deoxygenated *via* freeze-pump-thaw cycles (x3) then placed in a preheated oil bath (70 °C) and allowed to react for 26 hours. The polymerization was quenched by opening the flask to air and submerging the flask in liquid nitrogen. Polymer was obtained after two precipitations in cold diethyl ether to afford a yellow viscous oil in 45% yield (855 mg). M_n^{GPC} = 39 kDa, M_w/M_n.= 1.35. T_g = -42 °C. TGA in Ar: 285 – 332 °C , 30% mass loss, 332 – 441 °C, 47% mass loss; 21% mass remaining at 500 °C. ^{1}H NMR (300 MHz, $CDCl_3$, ppm): δ 7.33 – 7.20 (br, m, ***meta-H*** to –O-CH_2-R), 6.95 – 6.82 (br, m, ***ortho-H*** and ***para-H*** to –O-CH_2-R), 4.49 – 4.13 (br, m, Ar-R-C***H₂***-O(O)C-R' and TFS-O-C***H₂***-CH_2-O-CH_2-CH_2-O-CH_2-C***H₂***-O(O)C-R'), 4.03 - 3.54 (br, m, Ar-O-C***H₂***-R and TFS-O-CH_2-C***H₂***-O-C***H₂***-C***H₂***-O-C***H₂***-CH_2-O(O)C-R'), 2.85 – 2.62 (br, m, C***H₂***-C***H***(R)- backbone), 2.10 – 1.04 (br, m, R-C***H₂***-C***H₂***-C***H₂***-C***H₂***-CH_2-O(O)C-R' and C-C***H₃***). ^{13}C NMR (75 MHz, $CDCl_3$, ppm): δ 170.1, 159.9, 159.0, 146.8, 143.0, 139.4, 136.2, 129.4, 120.5, 114.4, 74.3, 70.7, 70.0, 68.8, 68.1, 67.6, 65.0, 64.4, 39.9, 29.1, 28.3, 25.7, 21.6 and 16.9. ^{19}F NMR (282 MHz, $CDCl_3$, ppm): δ -143 (br, m, ***ortho-F*** (TFS)) and -157 (br, m, ***meta-F*** (TFS)). Elem. Anal. Calcd. for $C_{1852}H_{2330}S_{12}N_{12}F_{184}Br_{42}$: C, 57.08; H, 6.03; S, 0.99; N, 0.43; F, 8.97; Br, 8.61%. Found: C, 52.46; H, 5.31; S, 0.75; N, 0.31; F, 9.67; Br, 8.62%. FTIR (ATR): 3095 – 2765, 1730, 1650, 1600, 1490, 1450, 1330, 1240, 1125, 1030, 955, 880, 860, 755, 690 cm^{-1}.

Liquid crystalline (phenol) linear fluoropolymer (LC(phenol)$_{20}$-LFP$_{30}$), (14). To a flame dried 10 mL Schlenk flask equipped with a magnetic stir bar, a solution of **4** (459 mg, 1.83 mmol), **7** (852 mg, 1.83 mmol), 2-(dodecylthiocarbonothioylthio)-2-methylpropionic acid (22.2 mg, 0.06 mmol) and azobisisobutyronitrile (2.20 mg, 0.01

mmol) in dry DMF (7.00 mL) was added. The solution was deoxygenated *via* freeze-pump-thaw cycles (x3) then placed in a preheated oil bath (70 °C) and allowed to react for 23 hours. The polymerization was quenched by opening the flask to air and submerging the flask in liquid nitrogen. Polymer was obtained after two precipitations in cold diethyl ether to afford a yellow viscous oil in 34% yield (404 mg). M_n^{GPC} = 30 kDa, M_w/M_n.= 1.12. T_g = -38 °C. TGA in Ar: 259 – 322 °C, 2% mass loss, 322 – 439 °C, 46% mass loss; 29% mass remaining at 500 °C. ^{1}H NMR (300 MHz, $CDCl_3$, ppm): δ 7.30 – 7.20 (br, m, ***meta-H*** to –O-CH_2-R), 6.95 – 6.82 (br, m, ***ortho-H*** and ***para-H*** to –O-CH_2-R), 4.49 – 4.14 (br, m, Ar-R-C***H₂***-O(O)C-R' and TFS-O-C***H₂***-CH_2-O-CH_2-CH_2-O-CH_2-C***H₂***-O(O)C-R'), 4.01 – 3.85 (br, m, Ar-O-C***H₂***-R), 3.84 - 3.54 (br, m, TFS-O-CH_2-C***H₂***-O-C***H₂***-C***H₂***-O-C***H₂***-CH_2-O(O)C-R'), 2.85 – 2.62 (br, m, C***H₂***-C***H***(R)-backbone), 2.18 – 1.09 (br, m, R-C***H₂***-C***H₂***-C***H₂***-C***H₂***-CH_2-O(O)C-R' and C-C***H₃***). ^{13}C NMR (75 MHz, $CDCl_3$, ppm): δ 170.2, 159.9, 159.0, 146.8, 142.5, 139.0, 136.0, 129.4, 120.5, 114.4, 74.3, 70.6, 69.9, 68.8, 68.1, 67.6, 65.0, 64.4, 40.0, 32.4, 29.1, 28.2, 25.6, 21.6 and 16.7. ^{19}F NMR (282 MHz, $CDCl_3$, ppm): δ -143 (br, m, ***ortho-F*** (TFS)) and -157 (br, m, ***meta-F*** (TFS)). Elem. Anal. Calcd. for $C_{842}H_{1022}S_3F_{120}Br_{30}$: C, 52.26; H, 5.32; S, 0.50; F, 11.78; Br, 12.39%. Found: C, 52.15; H, 5.35; S, 0.54; F, 11.69; Br, 12.35%. FTIR (ATR): 3050 – 2795, 1730, 1650, 1600, 1490, 1450, 1330, 1245, 1120, 1035, 960, 880, 860, 755, 690 cm^{-1}.

Liquid crystalline (cyano) hyperbranched fluoropolymer (LC(cyano)$_{20}$-HBFP$_{30}$), (15). To a flame dried 25 mL Schlenk flask equipped with a magnetic stir bar, a solution of **6** (958 mg, 2.74 mmol), **7** (1.26 g, 2.74 mmol), **10** (76.5 mg, 0.09 mmol)

and azobisisobutyronitrile (3.50 mg, 0.02 mmol) in dry DMF (10.0 mL) was added. The solution was deoxygenated *via* freeze-pump-thaw cycles (x3) then placed in a preheated oil bath (70 °C) and allowed to react for 24 hours. The polymerization was quenched by opening the flask to air and submerging the flask in liquid nitrogen. Polymer was obtained after two precipitations in cold diethyl ether to afford a yellow viscous oil in 46% yield (968 mg). M_n^{GPC} = 41 kDa, M_w/M_n.= 1.50. T_g = -2 °C. TGA in Ar: 337 – 424 °C, 64% mass loss; 31% mass remaining at 500 °C. ^{1}H NMR (300 MHz, $CDCl_3$, ppm): δ 7.77 – 7.40 (br, m, ***meta-H*** to –O-CH_2-R and ***2'-H*** and ***3'-H*** to Ar-O-CH_2-R), 7.04 – 6.84 (br, m, ***ortho-H*** to –O-CH_2-R), 4.40 – 4.14 (br, m, Ar-R-C***H$_2$***-O(O)C-R' and TFS-O-C***H$_2$***-CH_2-O-CH_2-CH_2-O-CH_2-C***H$_2$***-O(O)C-R'), 4.08 - 3.87 (br, m, Ar-O-C***H$_2$***-R), 3.84 - 3.50 (br, m, TFS-O-CH_2-C***H$_2$***-O-C***H$_2$***-C***H$_2$***-O-C***H$_2$***-CH_2-O(O)C-R'), 2.85 – 2.62 (br, m, C***H$_2$***-C***H***(R)- backbone), 2.40 – 1.13 (br, m, R-C***H$_2$***-C***H$_2$***-C***H$_2$***-C***H$_2$***-CH_2-O(O)C-R' and C-C***H$_3$***). ^{13}C NMR (75 MHz, $CDCl_3$, ppm): δ 174.0, 159.7, 146.8, 145.0, 142.4, 139.1, 136.0, 132.5, 131.2, 128.3, 127.0, 119.1, 115.0, 110.1, 77.2, 74.2, 72.6, 70.7, 70.2, 69.8, 67.9, 64.7, 61.5, 41.5, 29.1, 28.3, 25.7 and 23.9. ^{19}F NMR (282 MHz, $CDCl_3$, ppm): δ -144 (br, m, ***ortho-F*** (TFS)) and -157 (br, m, ***meta-F*** (TFS)). Elem. Anal. Calcd. for $C_{2035}H_{2240}S_{12}N_{57}F_{196}Br_{45}$: C, 59.40; H, 5.49; S, 0.94; N, 1.94; F, 9.05; Br, 8.74%. Found: C, 60.39; H, 5.53; S, 0.71; N, 1.85; F, 9.45%. FTIR (ATR): 3020 – 2795, 2225, 1730, 1650, 1600, 1490, 1450, 1395, 1360, 1290, 1245, 1180, 1115, 1065, 960, 885, 820, 660 cm^{-1}.

Liquid crystalline (cyano) linear fluoropolymer (LC(cyano)$_{20}$-LFP$_{30}$), (16). To a flame dried 10 mL Schlenk flask equipped with a magnetic stir bar, a solution of **6**

(642 mg, 1.83 mmol), **7** (840 mg, 1.83 mmol), 2-(dodecylthiocarbonothioylthio)-2-methylpropionic acid (22.2 mg, 0.06 mmol) and azobisisobutyronitrile (2.30 mg, 0.01 mmol) in dry DMF (7.00 mL) was added. The solution was deoxygenated *via* freeze-pump-thaw cycles (x3) then placed in a preheated oil bath (70 °C) and allowed to react for 22 hours. The polymerization was quenched by opening the flask to air and submerging the flask in liquid nitrogen. Polymer was obtained after two precipitations in cold diethyl ether to afford a yellow viscous oil in 54% yield (728 mg). M_n^{GPC} = 28 kDa, M_w/M_n.= 1.18. T_g = -21 °C, T_m = 45 °C. TGA in Ar: 279 – 339 °C, 31% mass loss, 339 – 437 °C, 35% mass loss; 30% mass remaining at 500 °C. ^{1}H NMR (300 MHz, $CDCl_3$, ppm): δ 7.73 – 7.42 (br, m, ***meta-H*** to –O-CH_2-R and ***2'-H*** and ***3'-H*** to Ar-O-CH_2-R), 7.01 – 6.87 (br, m, ***ortho-H*** to –O-CH_2-R), 4.46 – 4.13 (br, m, Ar-R-C***H₂***-O(O)C-R' and TFS-O-C***H₂***-CH_2-O-CH_2-CH_2-O-CH_2-C***H₂***-O(O)C-R'), 4.05 - 3.87 (br, m, Ar-O-C***H₂***-R), 3.83 - 3.54 (br, m, TFS-O-CH_2-C***H₂***-O-C***H₂***-C***H₂***-O-C***H₂***-CH_2-O(O)C-R'), 2.85 – 2.62 (br, m, C***H₂***-C***H***(R)- backbone), 2.15 – 1.14 (br, m, R-C***H₂***-C***H₂***-C***H₂***-C***H₂***-CH_2-O(O)C-R' and C-C***H₃***). ^{13}C NMR (75 MHz, $CDCl_3$, ppm): δ 170.2, 160.0, 159.6, 147.0, 145.1, 142.5, 139.2, 136.0, 132.5, 131.2, 128.3, 127.0, 125.5, 119.0, 115.0, 110.1, 77.2, 74.2, 70.7, 70.0, 68.7, 68.1, 67.9, 64.9, 64.4, 39.9, 30.3, 29.4, 29.1, 28.3, 25.7, 21.6 and 16.9. ^{19}F NMR (282 MHz, $CDCl_3$, ppm): δ -144 (br, m, ***ortho-F*** (TFS)) and -157 (br, m, ***meta-F*** (TFS)). Elem. Anal. Calcd. for $C_{1033}H_{1130}S_3N_{23}F_{120}Br_{30}$: C, 56.40; H, 5.18; S, 0.44; N, 1.46; F, 10.36; Br, 10.90%. Found: C, 56.42; H, 5.28; S, 0.56; N, 1.38; F, 10.21; Br, 10.42%. FTIR (ATR): 3025 – 2795, 2225, 1730, 1650, 1600, 1490, 1450, 1365, 1290, 1245, 1115, 1070, 1030, 960, 855, 820, 660 cm^{-1}.

General procedure for the preparation of LC-FP-PEG crosslinked networks. To a scintillation vial, bis(3-aminopropyl) terminated PEG (20.0 mg, 0.013 mmol) and THF (0.50 mL) were added and stirred until homogeneous (~10 min). To the solution, **11** (20.0 mg, 0.001 mmol) and *N,N*-diisopropylethylamine (DIPEA) (9.50 μL) were added and allowed to stir for 30 min. The solution was drop cast onto circular glass microscope cover slips or 40 μL aluminum DSC pans. A period of about 1 h allowed for the excess solvent to evaporate and afford a pre-gel that was cured at 110 °C for 45 min under N_2 atmosphere. T_g = 5 °C. T_m = 27 and 36 °C. TGA in Ar: 252 - 350 °C, 20% mass loss, 350 – 433 °C, 43% mass loss; 33% mass remaining at 500 °C. FTIR (ATR): 3690 – 3225, 1730, 1650, 1610, 1490, 1450, 1350, 1245, 1095, 955, 835, 765, 695 cm^{-1}. Subsequent films were prepared in the same manner by varying the wt % PEG , calculated as w/w % of the total mass to afford a total of eight formulations within the series. The same procedure was followed for the preparation of films from **12 - 16** to afford five additional series with a total of 24 formulations.

4.3 Results and Discussion

The LC monomers were synthesized and characterized by previously-reported methods.[82, 125, 126] Briefly, the LC monomers were obtained through a two-step reaction, starting with the synthesis of the mesogenic unit *via* nucleophilic substitution with 6-chloro-1-hexanol in the presence of excess potassium carbonate. The subsequent step involved the esterification of the remaining alcohol by reaction with acryloyl chloride to afford the desired LC monomer. All polymers were synthesized through reversible

addition-fragmentation chain-transfer (RAFT) copolymerization of the LC monomer and inimer using either the macro ‘click’ chain-transfer monomer (CTM) for hyperbranched versions, or 2-(dodecylthiocarbonothioylthio)-2-methylpropionic acid for linear analogs (Scheme 4.1).

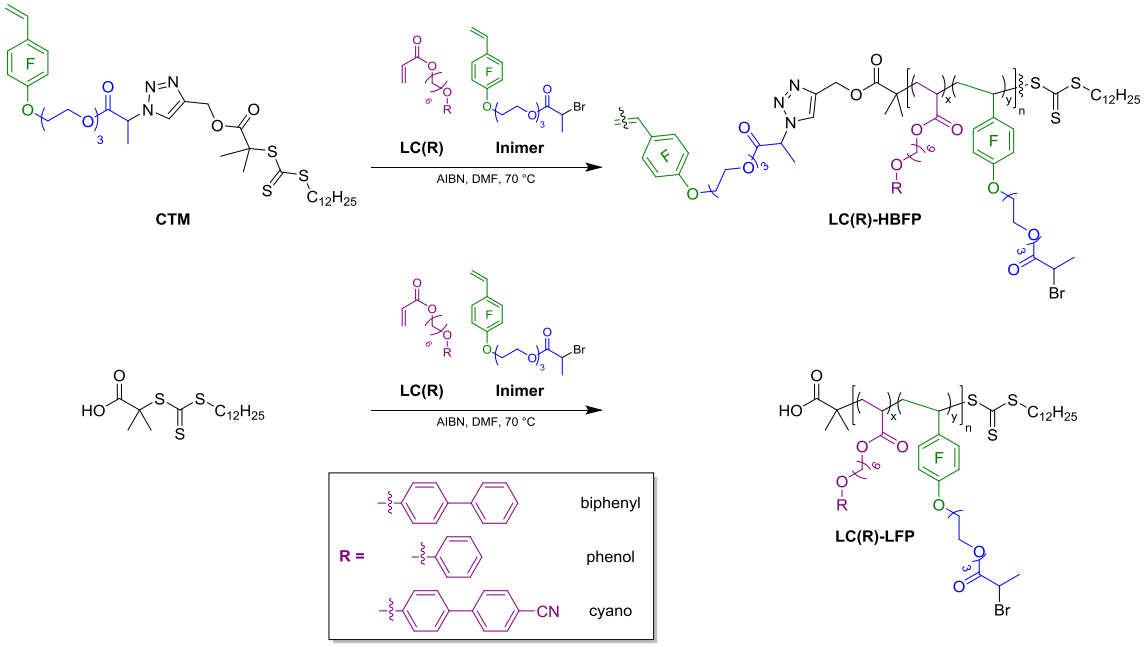

Scheme 4.1. Synthesis of LC(R)-HBFP and LC(R)-LFP polymers, where R signifies the type liquid crystalline monomer and the molar ratio x:y corresponds to 40:60.

The liquid crystalline character of the mesogenic units and corresponding monomers was investigated through the combination of differential scanning calorimetry (DSC), x-ray diffraction (XRD) and polarized optical microscopy (POM). Similar to the LC(biphenyl) mesogenic unit and monomer, LC(cyano) exhibited two melting transitions observed by DSC, 88 and 110 °C, for the mesogenic unit and one melting

transition at 60 °C for its corresponding acrylate monomer. Analogous transitions were also displayed in XRD (Figure 4.1) and POM.

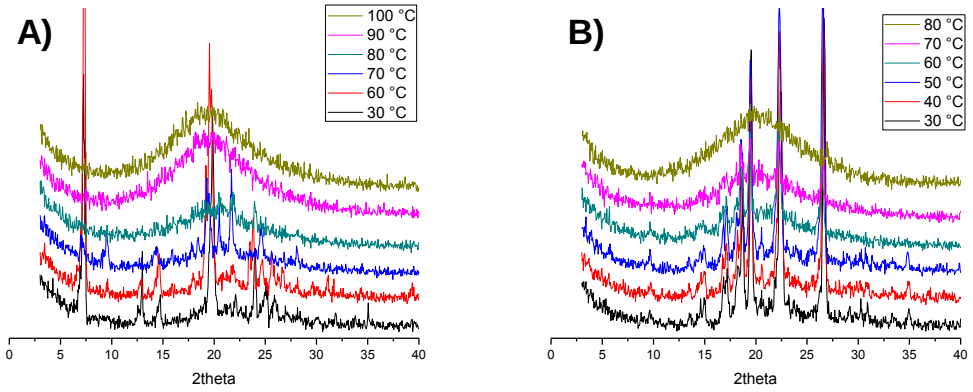

Figure 4.1. X-ray diffractograms of (A) LC(cyano) mesogen and (B) LC(cyano) monomer at different temperatures during heating.

Interestingly, POM images of the mesogenic unit showed fan-like shapes during the heating and cooling cycles, whereas the monomer only showed these structures upon cooling (Figure 4.2). Additionally, the original crystalline phase was not observed on cooling back to 30 °C, suggesting a longer time-span of the liquid crystalline phase. Due to the low transition temperatures of the LC(phenol) mesogenic unit and corresponding monomer, and the lower temperature limitations of the heating stage used in POM and XRD, the phase transitions were not captured. However DSC measurements showed a single melting transition for the mesogenic unit at 21 °C and a glass transition of 13 °C for the acrylate monomer.

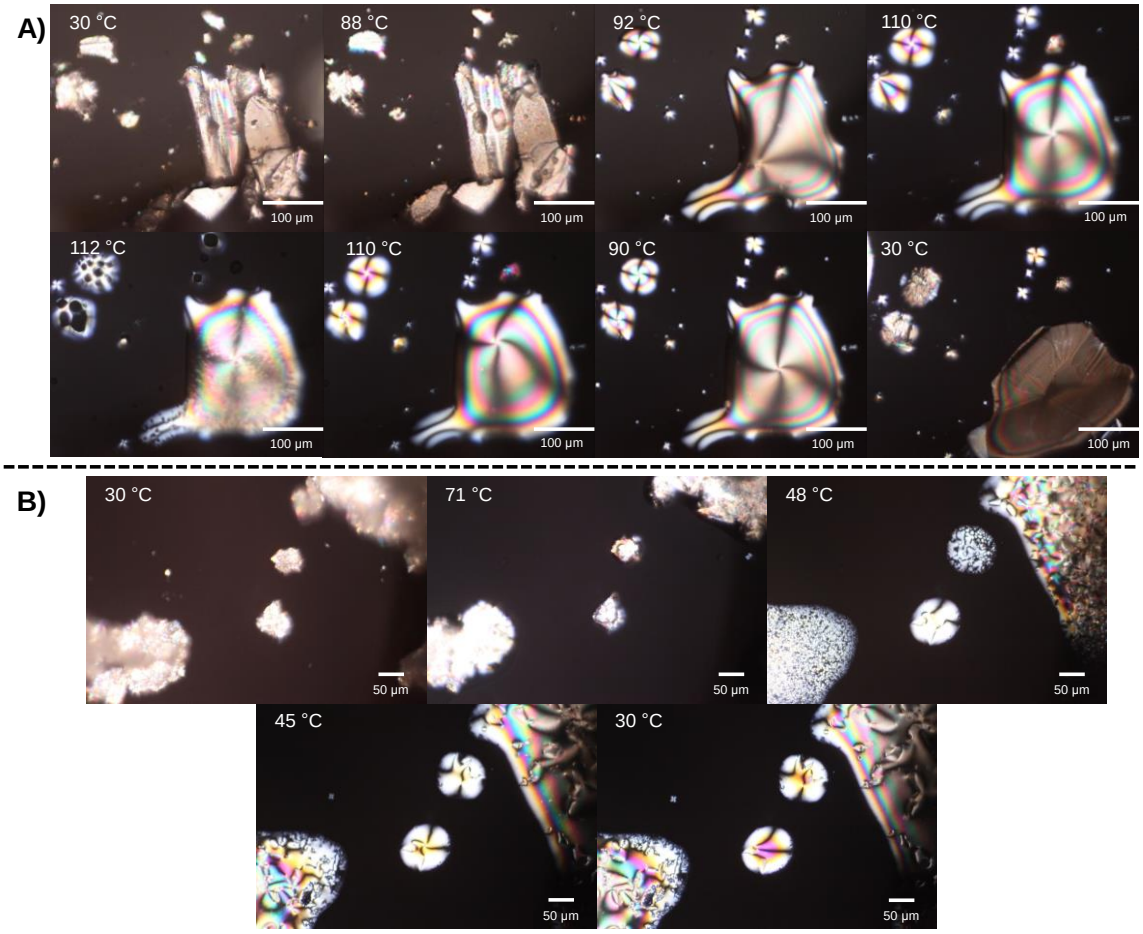

Figure 4.2. Polarized optical microscopy images of (A) LC(cyano) mesogen and (B) LC(cyano) monomer at various temperatures during heating (top) and cooling (bottom).

Amphiphilic networks were generated using a previously described method[40, 89] through nucleophilic substitution between the amino chain ends of bis(3-aminopropyl) terminated PEG (M_n = 1500 Da) and the bromoacetyl functionalities of the LC fluorocopolymers (LC-FP), either LC(R)-HBFP or LC(R)-LFP, upon casting from a tetrahydrofuran (THF) solution onto glass microscope cover slips or into 40 µL aluminum DSC pans, followed by a thermal cure at 110 °C for 45 min under inert atmosphere (Scheme 4.2). The stoichiometries of the LC-FP and PEG were varied to

produce an array (neat LC-FP, 5:2, 1:1, 2:5, LC-FP:PEG mass ratios) of coatings for each of the six systems, giving a total of twenty-four variations that allowed for evaluation of the compositional and topological effects on surface, thermal and wettability properties.

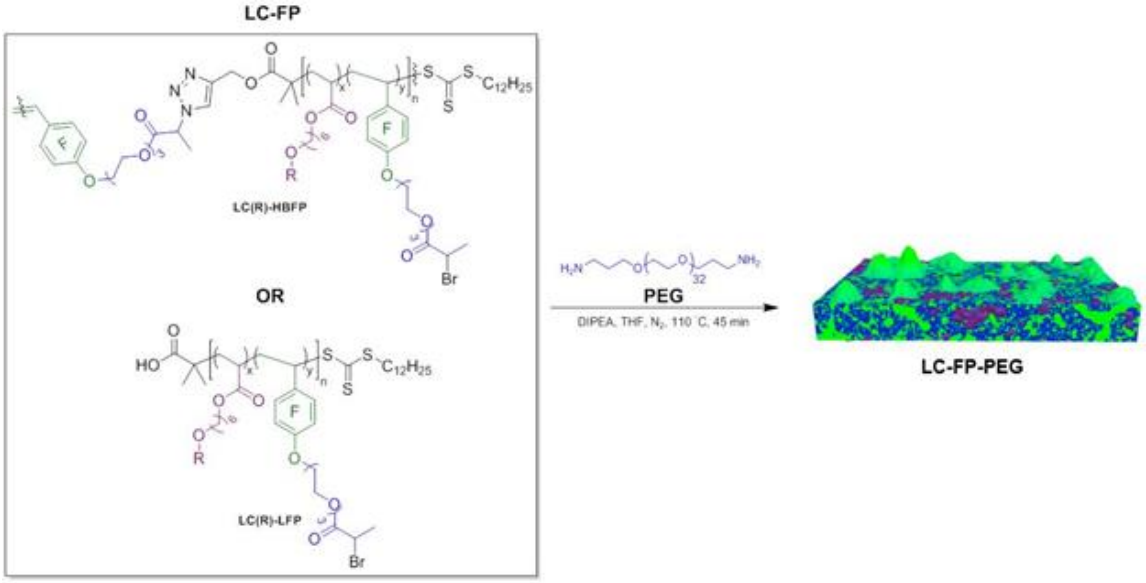

Scheme 4.2. Preparation of LC-FP-PEG crosslinked networks from PEG and either the LC(R)-HBFP or LC(R)-LFP polymers.

Water uptake experiments revealed similar results to the LC(biphenyl)-HBFP system including an increase in water wt % uptake as PEG wt % increased. While LC(biphenyl)-HBFP and LC(phenol)-HBFP exhibited similar water absorption capabilities compared to their linear versions, LC(cyano)-HBFP and LC(cyano)-LFP displayed no commonalities once crosslinked with PEG (Figure 4.3). Interesting, the

coatings formed from hyperbranched FPs displayed lower water uptake compared to all of the linear LC-FP systems and even the binary system.[89]

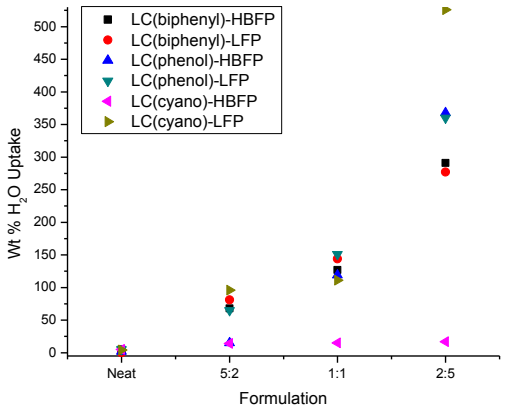

Figure 4.3. Water uptake (wt %) of the LC-HBFP-PEG and LC-LFP-PEG coatings as a function of formulation with the original LC(biphenyl)-HBFP (black) as a reference.

Due to the varying water uptake of each LC-FP system, the wt % of water added to each sample for DSC studies, within an array, ranged from 50 – 550%, to ensure the films would be fully hydrated in the presence of excess free water. Anti-icing performance was assessed from the calorimetric properties of three formulations from each of the five new LC-FP-PEG networks (the data for the biphenyl HBFP system were reported previously[108]) and control samples of neat LC-FP and PEG, totaling twenty-one samples. All networks were investigated from -50 °C to 20 °C, over three cycles, in both heating and cooling modes and the melting transition temperature of water was used to assess whether the films could depress the freezing point of water.[89] Two water

melting transitions (T_m) were observed for each coating, corresponding to the bound water within the crosslinked network and the free water on the surface of the coating.[70, 89] All LC-FP-PEG networks showed a decrease in free water T_m as wt % PEG increased (Figure 4.4). Networks containing less than 50 wt % PEG had a lower free water T_m than the LC(biphenyl)-HBFP system. However, within the 2:5 formulation, only the LC(cyano)-HBFP and LC(biphenyl)-LFP systems displayed a lower free water T_m than the LC(biphenyl)-HBFP system. In general, hyperbranched versions showed lower free water T_m values than their linear analogs, with the exception of LC(biphenyl)-LFP (Table 4.1). It is important to note that all the 2:5 formulations and the 1:1 of LC(biphenyl)-LFP achieved comparable free water T_m values to neat PEG, -10.4 ± 1.4 °C. For bound water, with the exception of the LC(cyano) system, all other networks showed an increase in T_m with wt % PEG. No overall trend in T_m with respect to wt % PEG was observed for the LC(cyano) networks, due to variability of each formulation. The decrease in free water T_m with increasing PEG is explained by an increasing PEG concentration for interaction with the surface water, whereas the increase in bound water T_m with increasing PEG is due to the water becoming less confined and increasingly bulk-like.

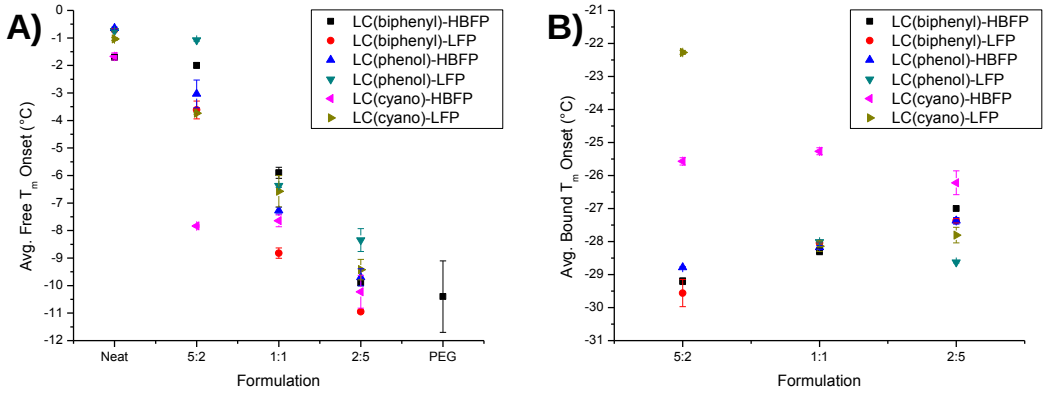

Figure 4.4. Average (A) free water and (B) bound water onset melting temperature (T_m) for the LC-LFP-PEG and LC-HBFP-PEG coatings, in terms of formulation.

Table 4.1. Average onset melting temperatures (T_m) for the arrays of LC-HBFP-PEG and LC-LFP-PEG coatings, each with 50 – 550 wt % water, with LC(biphenyl)-HBFP* as a reference.

System		**Mass ratio LC-FP to PEG (wt %)**							
		Neat polymer		*5:2*		*1:1*		*2:5*	
		Avg. H_2O T_m onset (°C)							
		Bound	*Free*	*Bound*	*Free*	*Bound*	*Free*	*Bound*	*Free*
LC (biphenyl)	*HBFP**	-1.7 ± 0.1		-29.2 ± 0.1	-2.0 ± 0.1	-28.3 ± 0.1	-5.9 ± 0.2	-27.0 ± 0.0	-9.9 ± 0.1
	LFP	-0.7 ± 0.0		-29.6 ± 0.4	-3.6 ± 0.3	-28.0 ± 0.0	-8.8 ± 0.2	-27.4 ± 0.1	-11.0 ± 0.1
LC (phenol)	*HBFP*	-0.6 ± 0.0		-28.8 ± 0.0	-3.0 ± 0.5	-28.2 ± 0.1	-7.3 ± 0.1	-27.4 ± 0.1	-9.7 ± 0.3
	LFP	-0.7 ± 0.0		-1.1 ± 0.0		-28.0 ± 0.0	-6.4 ± 0.1	-28.6 ± 0.0	-8.3 ± 0.4
LC (cyano)	*HBFP*	-1.7 ± 0.1		-25.6 ± 0.1	-7.8 ± 0.0	-25.3 ± 0.1	-7.6 ± 0.2	-26.2 ± 0.4	-10.2 ± 0.6
	LFP	-1.0 ± 0.1		-22.3 ± 0.1	-3.7 ± 0.0	-28.1 ± 0.2	-6.6 ± 0.6	-27.8 ± 0.2	-9.4 ± 0.4

Gross wettability was assessed through water contact angle measurements performed on dry and water-swollen films cast on glass. In general, across the five neat LC-FP samples, comparable water contact angles were observed for dry and water-swollen films (Table 4.2). However, differences became apparent once crosslinked with PEG, where linear analogs had larger dry and water-swollen contact angles than the hyperbranched versions at higher wt % PEG (> 50%). Majority of networks showed a decrease in water contact angle from dry to water-swollen and as wt % PEG increased.

Table 4.2. Average static water contact angles of the LC-LFP-PEG and LC-HBFP-PEG systems in dry and water-swollen states.

System		**Mass ratio LC-FP to PEG (wt %)**							
		Neat polymer		*5:2*		*1:1*		*2:5*	
		Static Water Contact Angle							
		Dry	*Swollen*	*Dry*	*Swollen*	*Dry*	*Swollen*	*Dry*	*Swollen*
LC (biphenyl)	*HBFP*	111 ± 2°	110 ± 0°	100 ± 1°	57 ± 0°	122 ± 3°	28 ± 1°	66 ± 10°	*
	LFP	111 ± 2°	104 ± 1°	109 ± 2°	96 ± 3°	101 ± 4°	64 ± 4°	90 ± 9°	111 ± 26°
LC (phenol)	*HBFP*	113 ± 1°	108 ± 6°	111 ± 7°	89 ± 8°	106 ± 4°	101 ± 6°	94 ± 10°	64 ± 13°
	LFP	113 ± 3°	105 ± 6°	105 ± 3°	57 ± 9°	82 ± 3°	86 ± 7°	98 ± 2°	76 ± 8°
LC (cyano)	*HBFP*	102 ± 2°	102 ± 2°	104 ± 3°	42 ± 13°	88 ± 7°	44 ± 9°	22 ± 2°	19 ± 4°
	LFP	108 ± 4°	109 ± 4°	94 ± 4°	103 ± 6°	88 ± 5°	77 ± 14°	94 ± 4°	84 ± 4°

Additional contact angle measurements were performed on dry coatings, where measurements were recorded every 5 s for a period of 3 min (Figure 4.5). Overall, formulations showed a decrease in contact angle, over time. From an exponential decay fit, the rate of change in contact angle was calculated, which showed a faster rate for the hyperbranched LC-FPs compared to the linear LC-FPs, with the exception of the

LC(biphenyl) (Table 4.3). While there was no correlation between the calculated rate and the contact angle values (dry or water-swollen), faster rates did correspond to lower free water T_m values observed in DSC measurements.

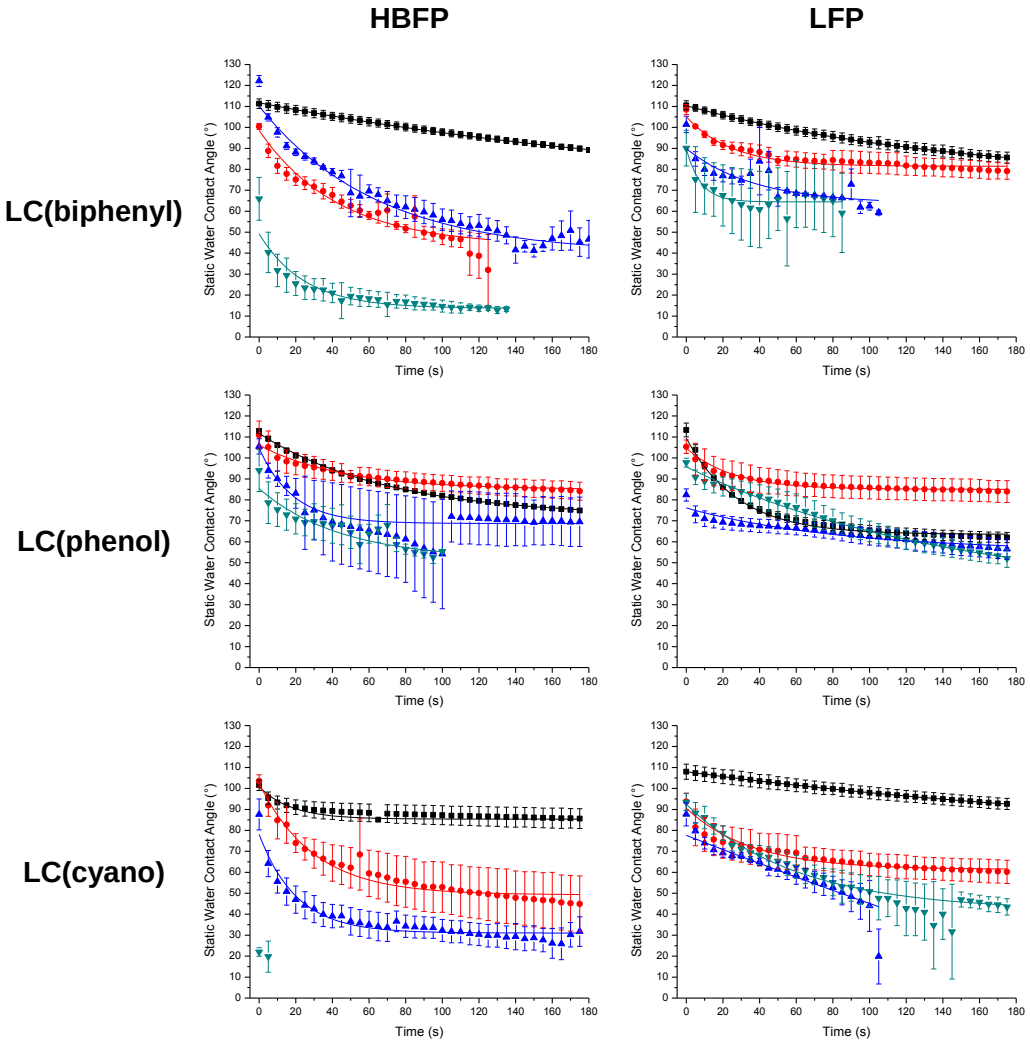

Figure 4.5. Average static water contact angles (with respect to time) of dry coatings for neat LC-FP (black), 5:2 (red), 1:1 (blue) and 2:5 (cyan), of each LC-FP-PEG system. Data was fit to an exponential decay function.

Table 4.3. Rate of change in contact angle for the arrays of LC-HBFP-PEG and LC-LFP-PEG coatings calculated from an exponential decay function. *Indicates rate could not be calculated.

System		Mass ratio LC-FP to PEG (wt %)				
		Neat polymer	*5:2*	*1:1*	*2:5*	*Average*
		Rate of Change in Contact Angle				
LC(biphenyl)	*HBFP*	0.004	0.023	0.016	0.041	0.021
	LFP	0.007	0.041	0.027	0.126	0.050
LC(phenol)	*HBFP*	0.014	0.022	0.054	0.022	0.028
	LFP	0.035	0.039	0.012	0.007	0.023
LC(cyano)	*HBFP*	0.057	0.034	0.049	*	0.047
	LFP	0.004	0.028	0.001	0.017	0.012

Macroscopic phase segregation and morphology was investigated by polarized optical microscopy (POM) and 3D optical microscopy. The POM images for each formulation of the hyperbranched networks were quite different from those of the linear analogs. One obvious difference was the lack of birefringence in the linear systems (Figure 4.6), suggesting the linear nature of the polymer impacted the alignment of the LC component within the crosslinked network. Topographies within each formulation were similar, where circular features were evident for the 5:2 and 1:1 samples, and elongated, ridge-like features were observed for the 2:5 formulations. The neat hyperbranched FPs showed ordered structures and as the wt % PEG increased, the

systems became more disordered, where birefringence was spread throughout the sample area (Figure 4.7 and 4.8).

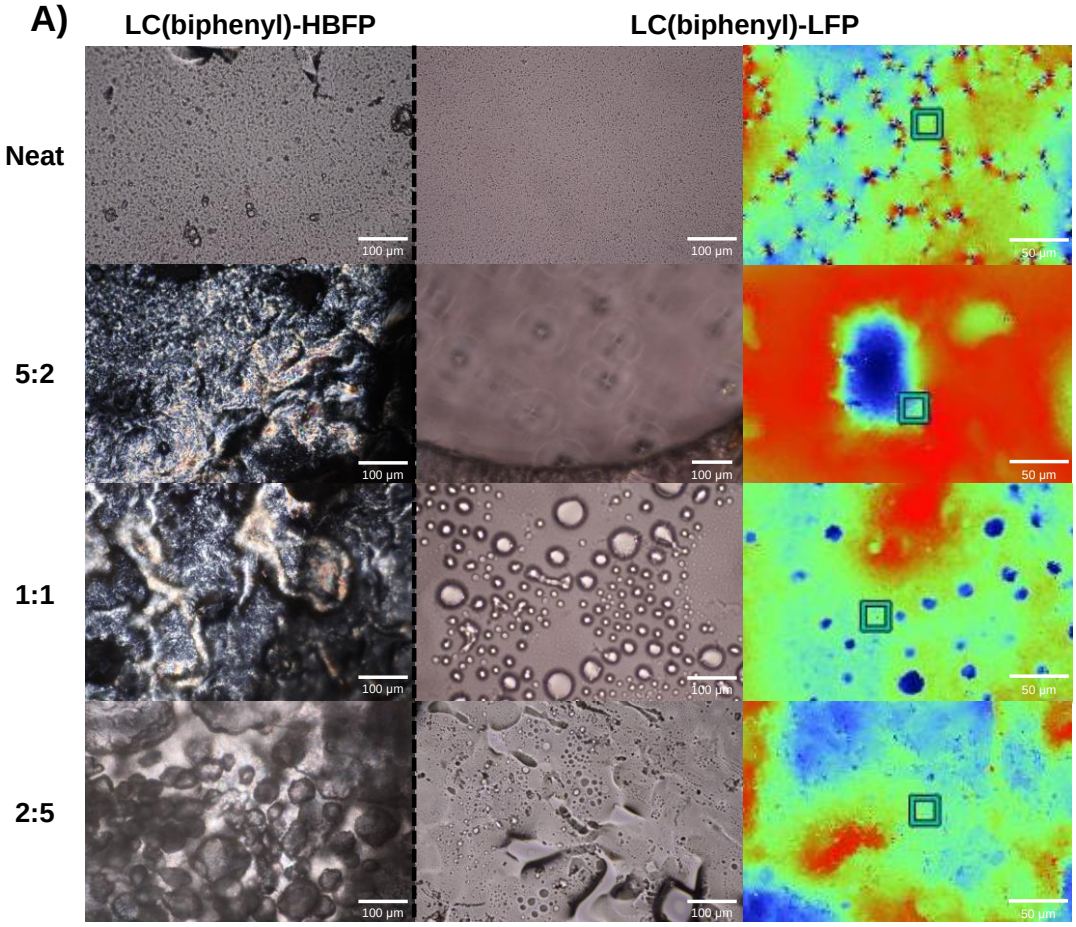

Figure 4.6. POM images of dry coatings for the LC(biphenyl)-HBFP crosslinked networks (left) and POM* and 3D optical microscopy images (2D view) for the LC(biphenyl)-LFP crosslinked networks. *The area imaged in POM does not correlate to the same area scanned in 3D optical microscopy.

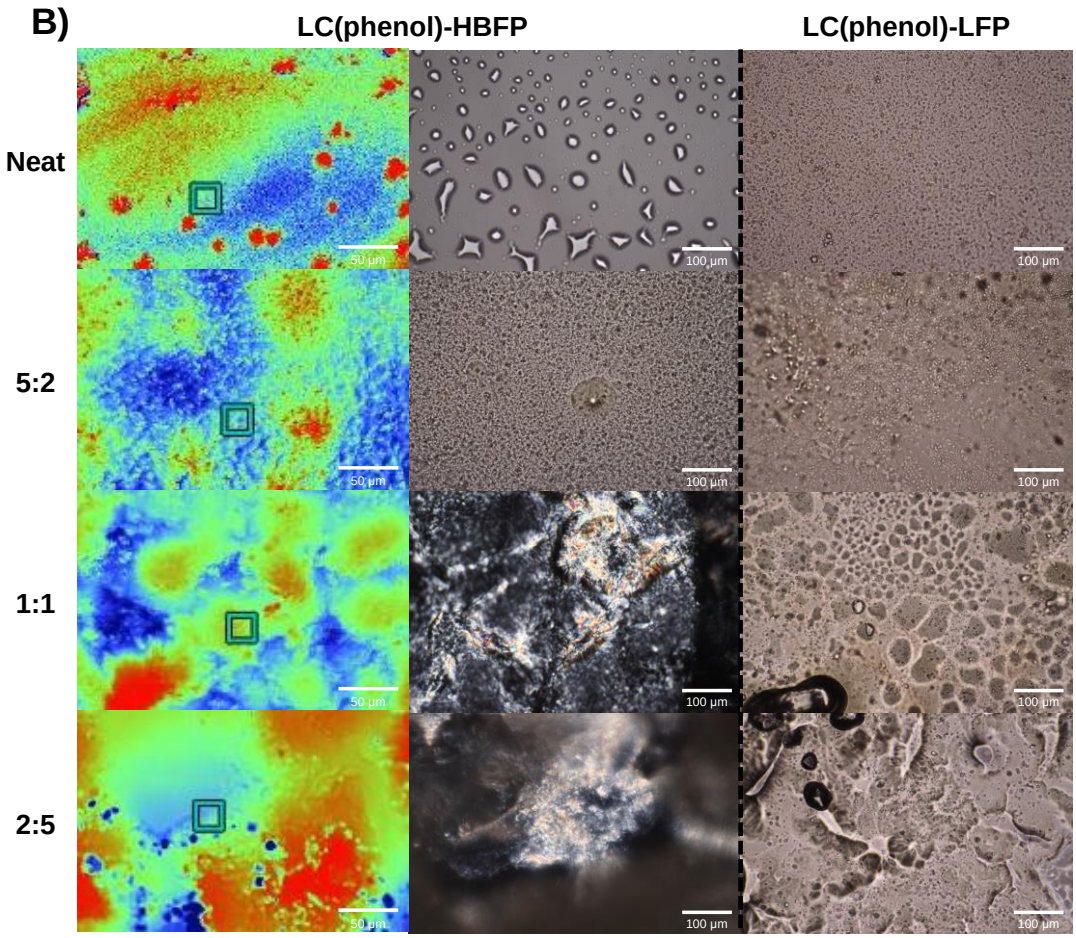

Figure 4.7. POM* and 3D optical microscopy images (2D view) images of dry coatings for the LC(phenol)-HBFP crosslinked networks and POM images for the LC(phenol)-LFP crosslinked networks (right). *The area imaged in POM does not correlate to the same area scanned in 3D optical microscopy.

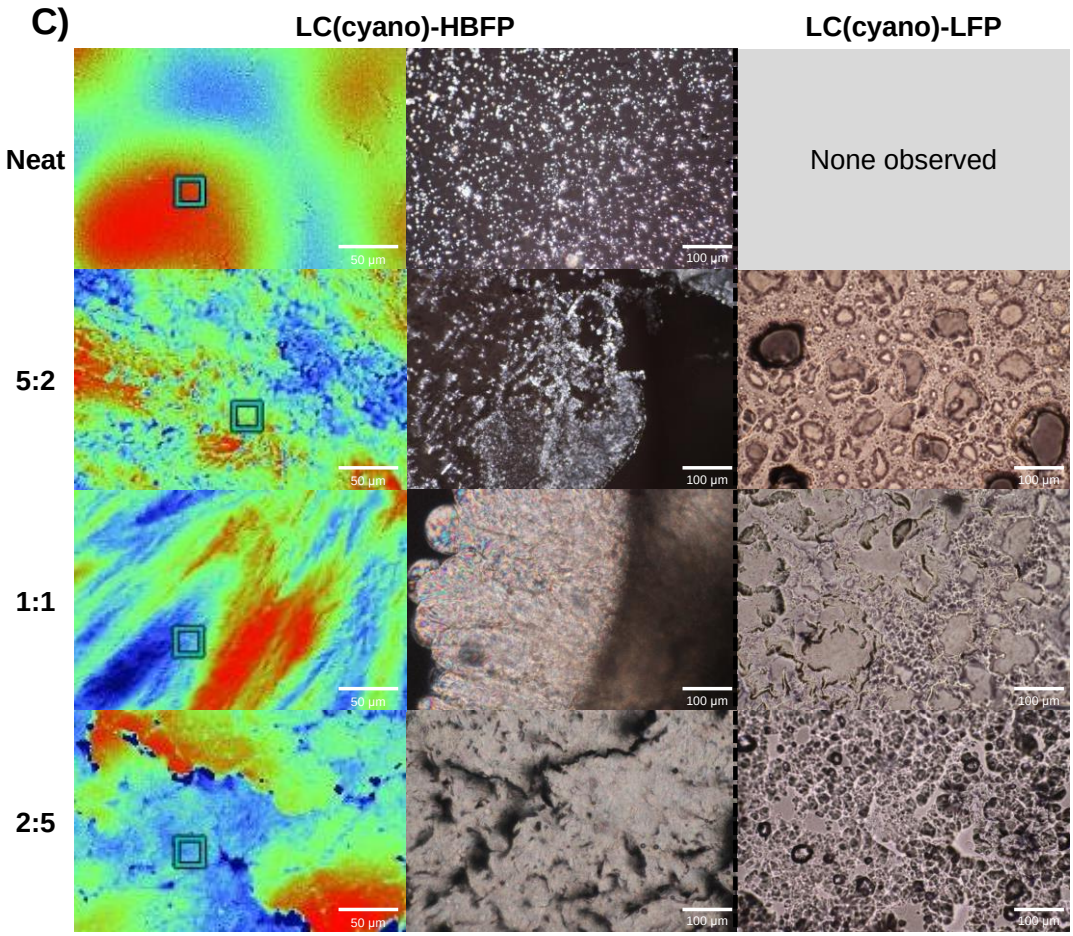

Figure 4.8. POM* and 3D optical microscopy images (2D view) images of dry coatings for the LC(cyano)-HBFP crosslinked networks and POM images for the LC(cyano)-LFP crosslinked networks (right). *The area imaged in POM does not correlate to the same area scanned in 3D optical microscopy.

While there were slight topographical differences between each LC-FP hyperbranched system, there was an overall macroscopic heterogeneity within each formulation. Coupled with DSC results, the analogous topographies of the coatings prepared from the linear and hyperbranched systems provided a possible explanation for the small differences in free water T_m. 3D optical microscopy was performed on the

LC(biphenyl)-LFP, for topological comparison to LC(biphenyl)-HBFP, and only the hyperbranched versions of LC(phenol) and LC(cyano) were investigated due to a lack of birefringence in the linear analogs. Overall, POM and 3D optical microscopy showed similar topographical features, corroborating these findings. Additionally, the hyperbranched systems showed an increase in roughness (R_a) as the wt % PEG increased, whereas the LC(biphenyl)-LFP 5:2 and 1:1 formulations had comparable roughness values (Figure 4.9).

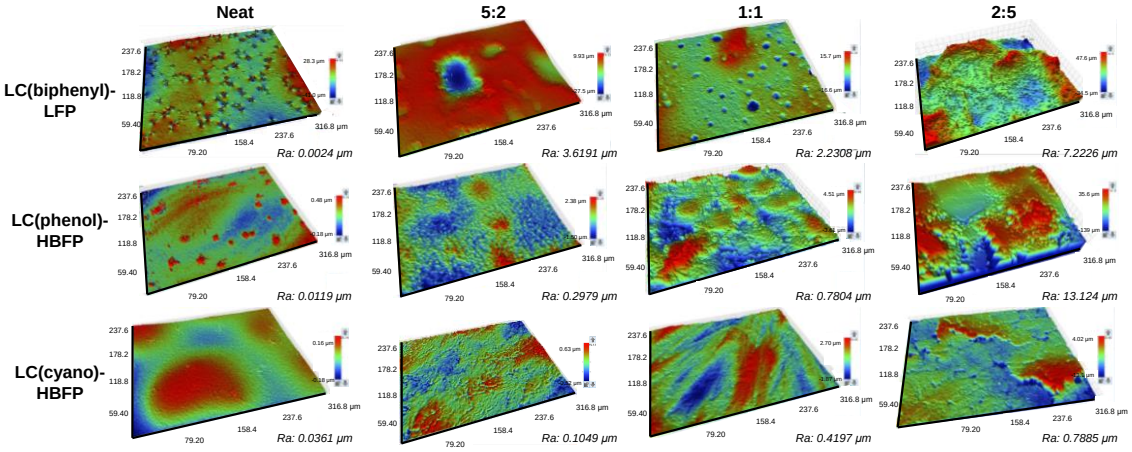

Figure 4.9. 3D optical microscopy images of LC(biphenyl)-LFP-PEG, LC(phenol)-HBFP-PEG and LC(cyano)-HBFP-PEG coatings with roughness (R_a) values.

Since the incorporation of an LC moiety resulted in an increased water contact angle in dry and water-swollen coatings, as well as a further depression of the freezing/melting point of water, it was important to test the viability of the coating in different aqueous environments to investigate its application in a variety of venues.

Therefore, solution stability studies were performed on the three LC-FP-PEG hyperbranched systems since they visually retained LC character, as observed by POM. In these studies, films were directly drop-cast and annealed in 5 mL shell vials, where samples were immersed by either deionized water, brine or an acidic (pH 5.4) buffer solution. Within each polymer network, four formulations were investigated, in triplicate, for each aqueous solution, totaling 108 samples, over 1 week. Most of the formulations in each polymer system reached equilibrium at 3 days, regardless of the solution (Figure 4.10). Other commonalities included the neat and 5:2 formulations retained more than 50% of their initial mass, an increase in wt % PEG resulted in greater mass loss and the majority of the 2:5 formulations disintegrated within the time period of this test. A possible explanation for the increased mass loss and disintegration of PEG-rich formulations is the excess of unreacted diamine-functionalized PEG or PEG that had only reacted at one chain terminus. This may result in an increase in the water solubility of the polymer and/or lack of crosslinks, which would cause instability of the network. Among the hyperbranched networks, the LC(phenol)-HBFP system retained more mass across the four formulations in the presence of each solution. Looking at individual solutions, the brine resulted in a reduced mass loss for the three polymer networks, suggesting these crosslinked networks would be most stable in a salt water environment. PEG has been known to undergo a salting-out effect, in high salt concentrations, which results in an increased solvent surface tension, decreased solubility, stronger hydrophobic interactions and a reduced size in solution.[127-130] This

effect may cause the networks to be more resistant to solubilization by the surrounding solution, providing an explanation for their stability in brine.

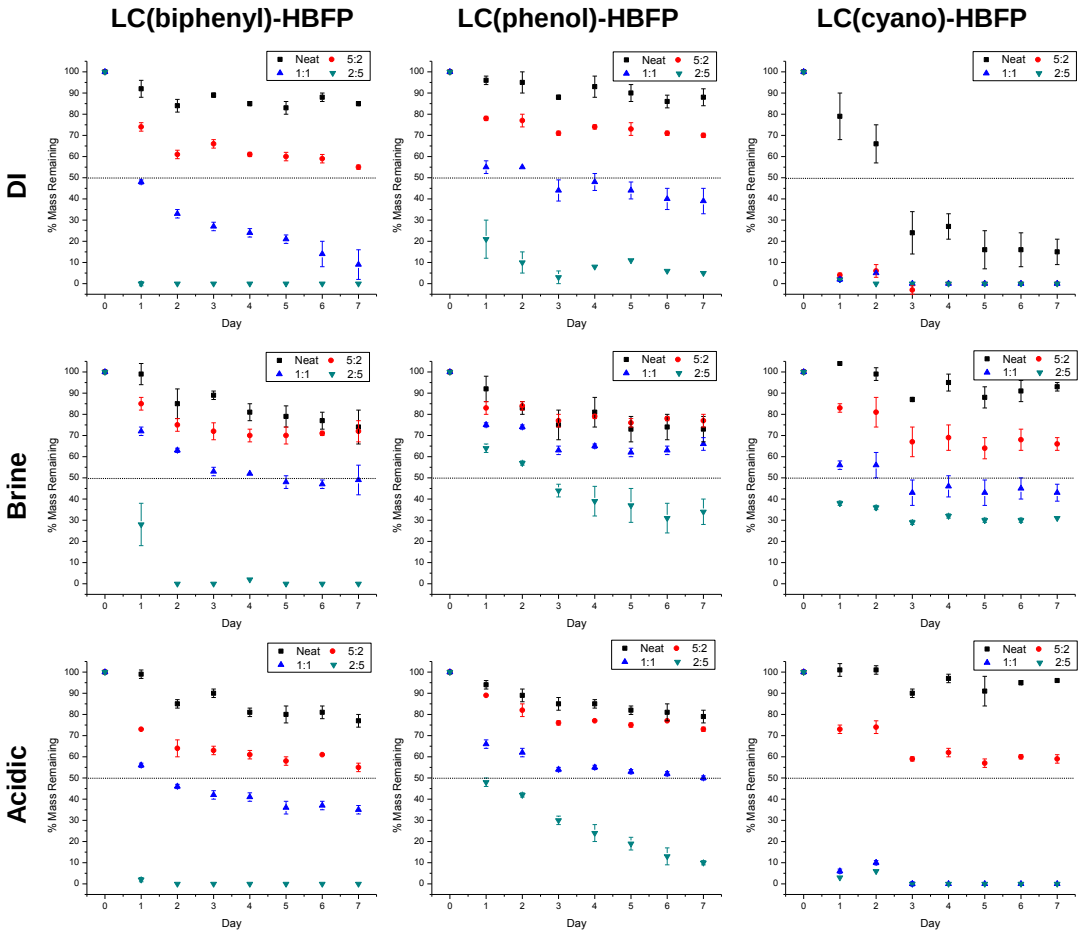

Figure 4.10. Solution stability studies in deionized water (DI), brine and acidic water for the LC(biphenyl)-HBFP, LC(phenol)-HBFP and LC(cyano)-HBFP crosslinked networks showing percentage of mass remaining over 1-week.

4.4 Conclusions

In summary, we have demonstrated that the incorporation of phenol-, cyano- or biphenyl LC moieties into either linear or hyperbranched amphiphilic fluoropolymers and their crosslinked networks with PEG leads to interesting compositional and topological influences on the properties of the materials and on water in contact with the materials. Overall, coatings formed from hyperbranched FPs visually retained LC character in the dry state, as seen in POM. In contrast, the linear analogs did not. In evaluation of the ability of these materials to serve as anti-icing coatings, it was observed that both the phenol- and cyano-containing LC comonomers result in further depression of the freezing/melting temperature of water compared to the original LC(biphenyl)-HBFP-PEG system, which is within the range of neat PEG. However, the greatest influence on the water melting transition temperature was the percentage of PEG incorporated into the composition. The percentage of water taken up into the systems also increased within the PEG wt %. The topology of the fluoropolymer had little impact on water uptake, except in the case of the LC(cyano) mesogen-containing materials, where the hyperbranched version exhibited the lowest water uptake (<50 wt%) and the linear analog gave the highest (>500 wt% water uptake). The dynamic restructuring within the materials during water uptake was observed as reductions in the water contact angle for water swollen *vs*. dry state coatings. Evaluation of water contact angle vs. time indicated that a faster rate of change directly correlated to a lower free water T_m value, measured by DSC, and the LC(biphenyl)-linear fluoropolymer system underwent the most rapid change. From solution stability studies, the hyperbranched

crosslinked networks demonstrated superior stability in a salt-saturated media *vs*. deionized or acidic aqueous solutions, suggesting their promise as protective coatings in marine or biological environments. Taken together, the findings from these studies indicate that crosslinked networks that contain a complex mixture of liquid crystalline, hydrophilic, hydrophobic, linear and hyperbranched components exhibit diverse behaviors that may be of value in extreme environments, as may be encountered in coatings used in nautical, aeronautical or medical applications, among others.

4.5 Acknowledgements

We thank Joseph Fornefeld from Midwest Microlab LLC for elemental analysis, Dr. Anup Bandyopadhyay from Materials Science & Engineering for XRD, Peng Liu and Dr. Hung-Jue Sue in Materials Science & Engineering for use of their POM, the Laboratory of Biological Mass Spectrometry, and Eric Rufe and Tom Stout from Bruker for the 3D Optical Microscopy results.

CHAPTER V

CONCLUSIONS

This body of work has focused on the design, development and investigation of dynamic, amphiphilic crosslinked hyperbranched fluoropolymer coatings for application in extreme environments; notably, as anti-icing coatings in the aviation and defense industries. Promising anti-icing performance was observed with the incorporation of a liquid crystalline moiety into the hyperbranched fluoropolymers, promoting the expansion of the original HBFP$^{(III)}$-PEG system into additional technologies beyond anti-biofouling to encompass the wide field of protective coatings. Additionally, the multi-responsive dynamic character of these coatings has provided a foundation for the production of new systems that can be tailored for a specific environment and application.

The original binary HBFP$^{(III)}$-PEG was explored for its potential to inhibit the formation of ice by taking advantage of the compositional, topographical and morphological complexities that had been previously established from prior anti-biofouling investigations. DSC studies provided an accurate means to study the anti-icing character of the coatings and revealed two well-defined melting transitions, one corresponding to bound water and the other to free water. Through the variation of hydrophobic:hydrophilic component ratios, the materials demonstrated that by tuning one melting transition, the other would alter in a predictable manner. Additionally, by adjusting the drop-casting solvent, greater effects on the organization of water molecules

were observed. In addition to DSC, the combination of multiple techniques including FTIR, water contact angle and DMA provided an understanding of common behaviors within the system such as confinement of water molecules by the polymer matrix and sequestration of the hydrophilic PEG resulting in a dynamic surface reorganization upon full hydration. Due to these unique characteristics, the concept of anti-icing systems was extended to include complex, heterogeneous amphiphilic materials.

Since anti-icing character was clearly demonstrated in the binary $HBFP^{(III)}$-PEG system, it was important to expand the system in an attempt to further enhance its ability to prevent the organization of water molecules. Chapter III incorporated a dynamic mesogenic unit, found in liquid crystalline polymers, to provide favorable anti-icing properties to the hyperbranched fluoropolymers. During the development of this project, numerous attempts were made to find an appropriate, feasible route for incorporating the mesogenic unit. Due to the limitations of ATRP and the need for a model reaction to guide the inclusion of the liquid crystalline functionality, a novel chain-transfer monomer (CTM) was synthesized. With this unique CTM in hand, liquid crystalline hyperbranched fluoropolymers were successfully synthesized *via* RAFT in a variety of molecular weights, which subsequently led to the generation of a series of crosslinked coatings. As predicted, integration of the liquid crystalline comonomer resulted in a further depression of water's melting temperature by a surprising, 5 °C improvement over the original $HBFP^{(III)}$-PEG binary system. Additionally, the enhanced hydrophobic character of the mesogenic unit led to increased contact angles in the dry and water-swollen states and interestingly an increased absorption of water. The ordering

parameter lended by the LC comonomer was observed in polarized optical microscopy (POM) and 3D optical microscopy, which showed in a proportionate distribution of LC character across the film while maintaining a macroscopic homogeneous surface.

With the successful incorporation of LC character into the amphiphilic hyperbranched crosslinked coatings by establishment of synthetic methodology, and the achievement of lower melting transition temperatures for water, the fundamentals of the material and behavior of the system were further explored in Chapter IV. Through variation of LC comonomer and polymer topology, five additional polymers were synthesized with either linear or hyperbranched architectures. DSC experiments demonstrated that by varying the LC comonomer, a further depression of water's freezing/melting temperature was achievable. Water uptake studies and contact angle showed an increased water absorption while maintaining increased contact angles in dry and water-swollen states. From POM images, only the hyperbranched systems visually retained LC character, and 3D optical microscopy revealed similar topographical features of coatings formed from all hyperbranched systems as observed in the original LC-HBFP-PEG system. Finally, solution stability studies demonstrated the stability of the coatings in salt water conditions in addition to cold weather environments observed from DSC experiments, broadening the application of these materials for use in aeronautic, aquatic and other challenging, continuous wetting environments.

In all, this dissertation facilitates the evolution of anti-icing materials and protective coatings. This body of work demonstrated an alternative application in anti-icing for the well-established anti-biofouling HBFP$^{(III)}$-PEG binary coatings alluding to a

wide range of possibilities for these previously-synthesized, complex materials. Additionally, the knowledge gained from the inclusion of a dynamic, temperature-responsive liquid crystalline moiety will aid in optimization and enhancement of the next generation of coatings. While the fundamental investigations of crosslinked liquid crystalline hyperbranched fluoropolymers, including synthetic methodology, led to promising results for anti-icing applications, further investigations and optimization can be performed.

Currently, the largest concerns for the generation of these coatings are the application method and high-temperature annealing requirement. Drop-casting is not a feasible method for applying this material to large surface areas (*e.g.* airplane wings or ship decks/hulls) and thus requiring a spray-casting procedure. However, the type of casting method alters the surface features of the coating, and therefore, these materials will need to undergo further analysis to understand how anti-icing performance may be affected. Related to casting method, the use of an organic solvent will need to be either eliminated or substituted with an environmentally-benign solvent. Additionally, different temperatures should be investigated to determine if crosslinked networks can be achieved at a lower temperature, preferably near room temperature, to avoid energy-intensive high-temperature thermal annealing.

A future generation of coatings will need to involve cost-effective materials that are amenable to scale-up. The liquid crystalline hyperbranched fluoropolymers described in this dissertation are not facile or cost-effective for commercial production. While the unique chain-transfer monomer allows for a hyperbranched network *via*

RAFT polymerization, it requires multiple steps to be synthesized and the use of an expensive pentafluorostyrene monomer. Fortunately, the production of the LC monomer only requires two steps, is cost-effective and can be obtained within high yield. Future generations of amphiphilic, crosslinked liquid crystalline hyperbranched networks will need to incorporate a low cost hydrophobic substituent capable of generating morphologically, topographically and compositionally complex materials once crosslinked with a hydrophilic moiety. Overall, this dissertation provides fundamental knowledge on structure-function relationships, water-polymer interactions and contributes to the advancement of liquid crystalline polymers and anti-icing materials. The combination of complex properties such as water sequestration and confinement, dynamic reorganization upon full hydration and thermally-responsive dynamic character will impact how future protective coatings are designed, characterized and tested.

REFERENCES

1. *AC 00-6A - Aviation Weather For Pilots and Flight Operations Personnel*. Federal Aviation Administration, National Oceanic and Atmospheric Administration, asa publications, U.S. Government Printing Office: Washington, D.C., **1975**; pp 91-104.

2. Petty, K. R.; Floyd, C. D. J., *A statistical review of aviation airframe icing accidents in the U.S.* National Transportation Safety Board: Washington, DC, **2004**; pp 1-6.

3. Taylor, R. P.; Hughes, K.; Godley, S., *Runway excursions: Part 1 - A worldwide review of commercial jet aircraft runway excursions*. Australian Transport Safety Bureau: Canberra City, Australian Capital Territory, **2009**; p 114.

4. *Deicing: Dollars and sense*. http://www.nbaa.org/ops/safety/icing/20110110-deicing-dollars-and-sense.php (accessed 2012).

5. Swanson, B. *Winter, snow, ice*. http://usatoday30.usatoday.com/weather/resources/askjack/wasnow.htm (accessed 2012).

6. *Standardized International Aircraft Ground Deice Program (SIAGDP)*. Federal Aviation Administration, U.S. Government Printing Office: Washington, D.C., **2010**; pp 1-36.

7. Kent, R. A.; Andersen, D.; Caux, P.-Y.; Teed, S., Canadian water quality guidelines for glycols–An ecotoxicological review of glycols and associated aircraft anti-icing and deicing fluids. *Environ. Toxicol.* **1999,** *14* (5), 481-522.

8. Jeck, R. K., *A history and interpretation of aircraft icing intensity definitions and FAA rules for operating in icing conditions*. U.S. Department of Transportation, Federal Aviation Administration, Office of Aviation Research: Washington, D.C., **2001**; pp 1-26.

9. Antonini, C.; Innocenti, M.; Horn, T.; Marengo, M.; Amirfazli, A., Understanding the effect of superhydrophobic coatings on energy reduction in anti-icing systems. *Cold Reg. Sci. Technol.* **2011,** *67* (1–2), 58-67.

10. Cao, L.; Jones, A. K.; Sikka, V. K.; Wu, J.; Gao, D., Anti-icing superhydrophobic coatings. *Langmuir* **2009,** *25* (21), 12444-12448.

11. Erbil, H. Y.; Demirel, A. L.; Avcı, Y.; Mert, O., Transformation of a simple plastic into a superhydrophobic surface. *Science* **2003,** *299* (5611), 1377-1380.

12. Farhadi, S.; Farzaneh, M.; Kulinich, S. A., Anti-icing performance of superhydrophobic surfaces. *Appl. Surf. Sci.* **2011,** *257* (14), 6264-6269.

13. Kulinich, S. A.; Farzaneh, M., Ice adhesion on super-hydrophobic surfaces. *Appl. Surf. Sci.* **2009,** *255* (18), 8153-8157.

14. Kulinich, S. A.; Farzaneh, M., How wetting hysteresis influences ice adhesion strength on superhydrophobic surfaces. *Langmuir* **2009,** *25* (16), 8854-8856.

15. Kulinich, S. A.; Farzaneh, M., On ice-releasing properties of rough hydrophobic coatings. *Cold Reg. Sci. Technol.* **2011,** *65* (1), 60-64.

16. Mateo, J. N.; Kulkarni, S. S.; Das, L.; Bandyopadhyay, S.; Tepper, G. C.; Wynne, K. J.; Bandyopadhyay, S., Wetting behavior of polymer coated nanoporous anodic alumina films: Transition from super-hydrophilicity to super-hydrophobicity. *Nanotechnology* **2011,** *22* (3), 035703-035713.

17. Meuler, A. J.; Smith, J. D.; Varanasi, K. K.; Mabry, J. M.; McKinley, G. H.; Cohen, R. E., Relationships between water wettability and ice adhesion. *ACS Appl. Mater. Interfaces* **2010,** *2* (11), 3100-3110.

18. Ruan, M.; Li, W.; Wang, B.; Deng, B.; Ma, F.; Yu, Z., Preparation and anti-icing behavior of superhydrophobic surfaces on aluminum alloy substrates. *Langmuir* **2013,** *29* (27), 8482-8491.

19. Tourkine, P.; Le Merrer, M.; Quéré, D., Delayed freezing on water repellent materials. *Langmuir* **2009,** *25* (13), 7214-7216.

20. Xie, Q.; Xu, J.; Feng, L.; Jiang, L.; Tang, W.; Luo, X.; Han, C. C., Facile creation of a super-amphiphobic coating surface with bionic microstructure. *Adv. Mater. (Weinheim, Ger.)* **2004,** *16* (4), 302-305.

21. Yang, H.; Cheng, Y.; Xiao, F., Thermal stable superhydrophobic polyphenylsilsesquioxane/nanosilica composite coatings. *Appl. Surf. Sci.* **2011,** *258* (4), 1572-1580.

22. Yang, J.; Li, W., Preparation of superhydrophobic surfaces on Al substrates and the anti-icing behavior. *J. Alloys Compd.* **2013,** *576* (0), 215-219.

23. Yuan, Z.; Wang, X.; Bin, J.; Liu, Q.; Jiang, H.; Zhao, D.; Wu, R.; Cheng, H., Anti-icing properties of superhydrophobic poly (vinyl chloride) coatings. *Adv. Mat. Res.* **2013,** *634-638*, 2969-2972.

24. Carfagna, C.; Giamberini, M.; Amendola, E., Can liquid crystalline polymers find application in the field of protective coatings? *Anti-Corros. Method M.* **1999,** *46* (2), 95-99.

25. Guerriero, G.; Alderliesten, R.; Dingemans, T.; Benedictus, R., Thermotropic liquid crystalline polymers as protective coatings for aerospace. *Prog. Org. Coat.* **2011,** *70* (4), 245-251.

26. Rowan, S.; Mather, P., Supramolecular interactions in the formation of thermotropic liquid crystalline polymers. In *Liquid Crystalline Functional Assemblies and Their Supramolecular Structures*, Kato, T., Ed. Springer Berlin Heidelberg: Heidelberg, Germany, **2008**; Vol. 128, pp 119-149.

27. Yagci, Y. E.; Antonietti, M.; Börner, H. G., Synthesis of poly(tartar amides) as bio-inspired antifreeze additives. *Macromol. Rapid Commun.* **2006,** *27* (19), 1660-1664.

28. Walters, K. R., Jr.; Serianni, A. S.; Sformo, T.; Barnes, B. M.; Duman, J. G., A nonprotein thermal hysteresis-producing xylomannan antifreeze in the freeze-tolerant Alaskan beetle Upis ceramboides. *Proc. Natl. Acad. Sci. U. S. A.* **2009,** *106* (48), 20210-5.

29. Gibson, M. I., Slowing the growth of ice with synthetic macromolecules: beyond antifreeze(glyco) proteins. *Polym. Chem.* **2010,** *1* (8), 1141-1152.

30. Neinhuis, C.; Barthlott, W., Characterization and distribution of water-repellent, self-cleaning plant surfaces. *Ann. Bot-London* **1997,** *79* (6), 667-677.

31. Barthlott, W.; Neinhuis, C., Purity of the sacred lotus, or escape from contamination in biological surfaces. *Planta* **1997,** *202* (1), 1-8.

32. Gao, X.; Jiang, L., Biophysics: water-repellent legs of water striders. *Nature* **2004,** *432* (7013), 36.

33. Saito, H.; Takai, K.; Yamauchi, G., Water- and ice-repellent coatings. *Surf. Coat. Int.* **1997,** *4*, 168-171.

34. Yuan, Z.; Wang, X.; Bin, J.; Liu, Q.; Jiang, H.; Zhao, D.; Wu, R.; Chen, H., Anti-icing properties of superhydrophobic poly (vinyl chloride) coatings. *Advanced Materials Research* **2013,** *634-638*, 2969-2972.

35. Hirao, A.; Sugiyama, K.; Yokoyama, H., Precise synthesis and surface structures of architectural per- and semifluorinated polymers with well-defined structures. *Prog. Polym. Sci.* **2007,** *32* (12), 1393-1438.

36. Gahde, J.; Mix, R.; Goering, H.; Schulz, G.; Funke, W.; Hermann, U., Increase in coating wet adhesion stability by highly-ordered polymers. *J. Adhes. Sci. Technol.* **1997,** *11* (6), 861-875.

37. Athawale, V. D.; Bailkeri, R. S.; Athawale, M., Comb-like liquid crystalline polymers for coating applications. *Prog. Org. Coat.* **2001,** *42* (3–4), 132-141.

38. Yoshida, K.; Kakuchi, T., UV curable coatings with mesogenic side groups. *Prog. Org. Coat.* **2005,** *52* (3), 165-172.

39. van der Wielen, M. W. J.; Cohen Stuart, M. A.; Fleer, G. J.; Nieuwhof, R. P.; Marcelis, A. T. M.; Sudhölter, E. J. R., A paint removal concept with side-chain liquid crystalline polymers as primer material. *Prog. Org. Coat.* **2001,** *41* (1–3), 157-165.

40. Bartels, J. W.; Cheng, C.; Powell, K. T.; Xu, J.; Wooley, K. L., Hyperbranched fluoropolymers and their hybridization into complex amphiphilic crosslinked copolymer networks. *Macromol. Chem. Phys.* **2007,** *208* (15), 1676-1687.

41. Imbesi, P. M.; Finlay, J. A.; Aldred, N.; Eller, M. J.; Felder, S. E.; Pollack, K. A.; Lonnecker, A. T.; Raymond, J. E.; Mackay, M. E.; Schweikert, E. A.; Clare, A. S.; Callow, J. A.; Callow, M. E.; Wooley, K. L., Targeted surface nanocomplexity: two-dimensional control over the composition, physical properties and anti-biofouling performance of hyperbranched fluoropolymer-poly(ethylene glycol) amphiphilic crosslinked networks. *Polym. Chem.* **2012,** *3* (11), 3121-3131.

42. Gudipati, C. S.; Finlay, J. A.; Callow, J. A.; Callow, M. E.; Wooley, K. L., The antifouling and fouling-release perfomance of hyperbranched fluoropolymer (HBFP)−poly(ethylene glycol) (PEG) composite coatings evaluated by adsorption of biomacromolecules and the green fouling alga ulva. *Langmuir* **2005,** *21* (7), 3044-3053.

43. Pollack, K. A.; Imbesi, P. M.; Raymond, J. E.; Wooley, K. L., Hyperbranched fluoropolymer-polydimethylsiloxane-poly(ethylene glycol) cross-linked terpolymer networks designed for marine and biomedical applications: Heterogeneous nontoxic antibiofouling surfaces. *ACS Appl. Mater. Interfaces* **2014,** *6* (21), 19265-19274.

44. Imbesi, P. M.; Gohad, N. V.; Eller, M. J.; Orihuela, B.; Rittschof, D.; Schweikert, E. A.; Mount, A. S.; Wooley, K. L., Noradrenaline-functionalized hyperbranched fluoropolymer–poly(ethylene glycol) cross-linked networks as dual-mode, anti-biofouling coatings. *ACS Nano* **2012,** *6* (2), 1503-1512.

45. Powell, K. T.; Cheng, C.; Wooley, K. L., Complex amphiphilic hyperbranched fluoropolymers by atom transfer radical self-condensing vinyl (co)polymerization. *Macromolecules* **2007,** *40* (13), 4509-4515.

46. Wang, X.-J.; Zhou, Q.-F., *Liquid crystalline polymers*. World Scientific Publishing Co. Pte. Ltd.: Hackensack, NJ, 2004; p 374.

47. McCulloch, I.; Heeney, M.; Bailey, C.; Genevicius, K.; MacDonald, I.; Shkunov, M.; Sparrowe, D.; Tierney, S.; Wagner, R.; Zhang, W.; Chabinyc, M. L.; Kline, R. J.; McGehee, M. D.; Toney, M. F., Liquid-crystalline semiconducting polymers with high charge-carrier mobility. *Nat. Mater.* **2006,** *5* (4), 328-333.

48. Funahashi, M., Development of liquid-crystalline semiconductors with high carrier mobilities and their application to thin-film transistors. *Polym. J* **2009,** *41* (6), 459-469.

49. Vita, F.; Sparnacci, K.; Panzarasa, G.; Placentino, I. F.; Marino, S.; Scaramuzza, N.; Portale, G.; Di Cola, E.; Ferrero, C.; Torgova, S. I.; Galli, G.; Laus, M.; Francescangeli, O., Evidence of cybotactic order in the nematic phase of a main-chain liquid crystal polymer with bent-core repeat unit. *ACS Macro Lett* **2014,** *3* (1), 91-95.

50. Tetzner, K.; Duffy, W.; Bock, K., Performance spread reduction in organic field-effect transistors using semiconducting liquid-crystal polymers. *Appl. Phys. Lett.* **2013,** *103* (9), 093304-1-4.

51. Li, F.; Chen, W.; Yuan, K.; Chen, Y., Photovoltaic performance enhancement in P3HT/ZnO hybrid bulk-heterojunction solar cells induced by semiconducting liquid crystal ligands. *Org. Electron.* **2012,** *13* (11), 2757-2762.

52. Lehmann, M.; Jahr, M.; Gutmann, J., Star-shaped oligobenzoates with a naphthalene chromophore as potential semiconducting liquid crystal materials? *J. Mater. Chem.* **2008,** *18* (25), 2995-3003.

53. Werzer, O.; Boucher, N.; de Silva, J. P.; Gbabode, G.; Geerts, Y. H.; Konovalov, O.; Moser, A.; Novak, J.; Resel, R.; Sferrazza, M., Interface induced crystal structures of dioctyl-terthiophene thin films. *Langmuir* **2012,** *28* (22), 8530-8536.

54. Weinkauf, D. H.; Paul, D. R., Gas transport properties of thermotropic liquid-crystalline copolyesters. I. The effects of orientation and annealing. *J. Polym. Sci., Part B: Polym. Phys.* **1992,** *30* (8), 817-835.

55. Park, J. Y.; Paul, D. R.; Haider, I.; Jaffe, M., Effect of thermal annealing on the gas permeability of HIQ-40 films. *J. Polym. Sci., Part B: Polym. Phys.* **1996,** *34* (10), 1741-1745.

56. Ramathal, H.; Lawal, A., Barrier properties of a thermotropic liquid-crystalline polymer. *J. Appl. Polym. Sci.* **2003,** *89* (9), 2457-2463.

57. Athawale, V. D.; Bailkeri, R. S., Synthesis, characterization and coating applications of liquid crystalline acrylic copolymers. *Liq. Cryst.* **2000,** *27* (8), 1021-1027.

58. Yoshida, K.; Anyashiki, T.; Kakuchi, T., Synthesis and flexibility–hardness of polymer coatings based on melamine with mesogenic groups. *Prog. Org. Coat.* **2005,** *52* (3), 227-237.

59. Merrill, H. M.; Feltes, J. W., Transmission icing: A physical risk with a physical hedge. In *IEEE PES General Meeting*, Merrill Energy LLC: Montreal, **2006**; pp 1-7.

60. Hunter, S. R.; Daniel, A., *The commercial development of water repellent coatings for high voltage transmission lines: Technical Report*. U.S. Dept. of Energy: Oak Ridge, TN, **2013**; pp 1-5.

61. Etemaddar, M. Atmospheric icing *WindTech International* [Online], 2012. http://www.windtech-international.com/articles/atmospheric-icing (accessed 2013).

62. Parent, O.; Ilinca, A., Anti-icing and de-icing techniques for wind turbines: Critical review. *Cold Reg. Sci. Technol.* **2011,** *65* (1), 88-96.

63. Klose, G.; Eisenblaetter, S.; Galle, J.; Islamov, A.; Dietrich, U., Hydration and structural properties of a homologous series of nonionic alkyl oligo(ethylene oxide) surfactants. *Langmuir* **1995,** *11* (8), 2889-2892.

64. Heuberger, M.; Drobek, T.; Spencer, N. D., Interaction forces and morphology of a protein-resistant poly(ethylene glycol) layer. *Biophys. J.* **2005,** *88* (1), 495-504.

65. Chen, S.; Li, L.; Zhao, C.; Zheng, J., Surface hydration: Principles and applications toward low-fouling/nonfouling biomaterials. *Polymer* **2010,** *51* (23), 5283-5293.

66. Harder, P.; Grunze, M.; Dahint, R.; Whitesides, G. M.; Laibinis, P. E., Molecular conformation in oligo(ethylene glycol)-terminated self-assembled monolayers on gold and silver surfaces determines their ability to resist protein adsorption. *J. Phys. Chem. B* **1998,** *102* (2), 426-436.

67. Schollbach, M.; Zhang, F.; Roosen-Runge, F.; Skoda, M. W. A.; Jacobs, R. M. J.; Schreiber, F., Gold nanoparticles decorated with oligo(ethylene glycol) thiols: Surface charges and interactions with proteins in solution. *J. Colloid Interface Sci.* **2014,** *426* (0), 31-38.

68. Ohashi, R.; Bartels, J. W.; Xu, J.; Wooley, K. L.; Schaefer, J., Solid-state NMR investigations of the unusual effects resulting from the nanoconfinement of water within amphiphilic crosslinked polymer networks. *Adv. Funct. Mater.* **2009,** *19* (21), 3404-3410.

69. Xu, J.; Bohnsack, D. A.; Mackay, M. E.; Wooley, K. L., Unusual mechanical performance of amphiphilic crosslinked polymer networks. *J. Am. Chem. Soc.* **2007,** *129* (3), 506-507.

70. Chan, K.; Hirotsu, T.; Hatakeyama, T., DSC studies on bound water in polypropylene films plasma-grafted with 2-hydroxyethyl acrylate and acrylic acid or methacrylic acid. *Eur. Polym. J.* **1992,** *28* (9), 1021-1025.

71. Black, S. B.; Chang, Y.; Bae, C.; Hickner, M. A., FTIR characterization of water–polymer interactions in superacid polymers. *J. Phys. Chem. B* **2013,** *117* (50), 16266-16274.

72. Smedley, S. B.; Chang, Y.; Bae, C.; Hickner, M. A., Measuring water hydrogen bonding distributions in proton exchange membranes using linear Fourier Transform Infrared spectroscopy. *Solid State Ionics* **2015,** *275* (0), 66-70.

73. Gallot, B., Comb-like and block liquid crystalline polymers for biological applications. *Prog. Polym. Sci.* **1996,** *21* (6), 1035-1088.

74. Imrie, C. T.; Ingram, M. D.; McHattie, G. S., Ion transport in glassy side-group liquid crystalline polymer electrolytes. *Adv. Mater. (Weinheim, Ger.)* **1999,** *11* (10), 832-834.

75. Rousseau, I. A.; Mather, P. T., Shape memory effect exhibited by smectic-C liquid crystalline elastomers. *J. Am. Chem. Soc.* **2003,** *125* (50), 15300-15301.

76. Yamada, M.; Kondo, M.; Mamiya, J.-i.; Yu, Y.; Kinoshita, M.; Barrett, C. J.; Ikeda, T., Photomobile polymer materials: Towards light-driven plastic motors. *Angew. Chem. Int. Ed. Engl.* **2008,** *47* (27), 4986-4988.

77. Ohm, C.; Brehmer, M.; Zentel, R., Liquid crystalline elastomers as actuators and sensors. *Adv. Mater. (Weinheim, Ger.)* **2010,** *22* (31), 3366-3387.

78. Cho, C. M.; Wang, X.; Li, J. J.; He, C.; Xu, J., Synthesis and self-assembly of halogen-bond donor–spacer–hydrogen-bond donor molecules: polymeric liquid crystals induced by combination of intermolecular halogen- and hydrogen-bonding interactions. *Liq. Cryst.* **2013,** *40* (2), 185-196.

79. Li, J.; Ou, X.; Sims, S.; Li, W.; Wu, L., Hybrid liquid crystal polymers from the self-assembly of poly(vinylpyridine) and polyoxometalates via multiple non-covalent bonds. *RSC Advances* **2014,** *4* (100), 56998-57008.

80. Minami, S.; Ashizawa, R.; Kondo, M.; Kawatsuki, N., Photoinduced orientation of hydrogen bonding liquid crystalline polymers / pyridine derivatives composite films. *Mol. Cryst. Liq. Cryst.* **2015,** *617* (1), 40-49.

81. Kato, T.; Hirota, N.; Fujishima, A.; Frechet, J. M. J., Supramolecular hydrogen-bonded liquid-crystalline polymer complexes. design of side-chain polymers and a host-guest system by noncovalent interaction. *J. Polym. Sci. A Polym. Chem.* **1996,** *34*, 57-62.

82. Kawakami, T.; Kato, T., Use of intermolecular hydrogen bonding between imidazolyl moieties and carboxylic acids for the supramolecular self-association of liquid-crystalline side-chain polymers and networks. *Macromolecules* **1998,** *31* (14), 4475-4479.

83. Thünemann, A. F.; Kubowicz, S.; Burger, C.; Watson, M. D.; Tchebotareva, N.; Müllen, K., α-helical-within-discotic columnar structures of a complex between poly(ethylene oxide)-block-poly(l-lysine) and a hexa-peri-hexabenzocoronene. *J. Am. Chem. Soc.* **2003,** *125* (2), 352-356.

84. Lin, H.-C.; Hendrianto, J., Synthesis and characterization of H-bonded side-chain and crosslinking LC polymers containing donor/acceptor homopolymers and copolymers. *Polymer* **2005,** *46* (26), 12146-12157.

85. Li, X.; Fang, L.; Hou, L.; Zhu, L.; Zhang, Y.; Zhang, B.; Zhang, H., Photoresponsive side-chain liquid crystalline polymers with amide group-substituted azobenzene mesogens: Effects of hydrogen bonding, flexible spacers, and terminal tails. *Soft Matter* **2012,** *8* (20), 5532-5542.

86. Hassan, S.; Anandakathir, R.; Sobkowicz, M. J.; Budhlall, B. M., Tuning oxygen permeability in azobenzene-containing side-chain liquid crystalline polymers. *Polym. Chem.* **2016,** *7* (7), 1452-1460.

87. Finkelmann, H.; Happ, M.; Portugal, M.; Ringsdorf, H., Liquid crystalline polymers with biphenyl-moieties as mesogenic group. *Macromol. Chem. Phys.* **1978,** *179* (10), 2541-2544.

88. Kato, T.; Kihara, H.; Ujiie, S.; Uryu, T.; Fréchet, J. M. J., Structures and properties of supramolecular liquid-crystalline side-chain polymers built through intermolecular hydrogen bonds. *Macromolecules* **1996,** *29* (27), 8734-8739.

89. Zigmond, J. S.; Pollack, K. A.; Smedley, S.; Raymond, J. E.; Link, L. A.; Pavía-Sanders, A.; Hickner, M. A.; Wooley, K. L., Investigation of intricate, amphiphilic crosslinked hyperbranched fluoropolymers as anti-icing coatings for extreme environments. *J. Polym. Sci. A Polym. Chem.* **2016,** *54* (2), 238-244.

90. Bresci, B.; Frosini, V.; Lupinacci, D.; Magagnini, P. L., Order in polymers with biphenylyl residues in the side-groups. *Macromol. Rapid Commun.* **1980,** *1* (3), 183-186.

91. Lupinacci, D.; Bresci, B.; Paci, M., Synthesis and characterization of copolymers containing biphenylyl rings linked to the main chain through spacers of various lengths. *Eur. Polym. J.* **1984,** *20* (1), 73-76.

92. Rottink, J. B. H.; Nijenhuis, K.; Addink, R.; Mijs, W. J., Dynamic mechanical properties of some liquid crystalline polyacrylates. *Polym. Bull. (Berlin) 31* (4), 487-494.

93. Lupinacci, D.; Winter, W. T., Three-dimensional crystalline order in an atactic comblike polymer. *J. Polym. Sci. Polym. Phys. Ed.* **1982,** *20* (6), 1013-1018.

94. Kim, S. I.; Ree, M.; Shin, T. J.; Jung, J. C., Synthesis of new aromatic polyimides with various side chains containing a biphenyl mesogen unit and their abilities to control liquid-crystal alignments on the rubbed surface. *J. Polym. Sci. A Polym. Chem.* **1999,** *37* (15), 2909-2921.

95. Bonnans-Plaisance, C.; Corvazier, L.; Skoulios, A., Functional polythiiranes: 5. Side chain liquid crystalline polythiiranes. *Polymer* **1997,** *38* (15), 3843-3854.

96. Brunet, D.; Mercier, R.; Gallot, B., Liquid crystalline comb-like polyimides with biphenyl-based side groups. *Liq. Cryst.* **2000,** *27* (4), 483-489.

97. Irie, Y.; Naka, K., Syntheses of biphenyl-terminated polyhedral oligomeric octasilicate-core dendrimers and their single-component optical transparent free-standing thermoplastic films. *J. Polym. Sci. A Polym. Chem.* **2015,** *53* (12), 1437-1443.

98. Jaglowski, A. J.; Singler, R. E.; Atkins, E. D. T., Liquid crystalline behavior of poly[((6-(4-phenylphenoxy)hexyl)oxy)(trifluoroethoxy)phosphazene]. *Macromolecules* **1995,** *28* (5), 1668-1672.

99. Park, S.-Y.; Zhang, T.; Interrante, L. V.; Farmer, B. L., Structures of side chain liquid crystalline poly(silylenemethylene)s. *Macromolecules* **2002,** *35* (7), 2776-2783.

100. Liu, X.; Xiang, H.; Yang, J.; Gu, Y., Preparation and properties of novel polyimides with side chains containing biphenyl units. *J. Appl. Polym. Sci.* **2003,** *90* (12), 3291-3298.

101. Wang, X.; Wang, H.; Luo, L.; Huang, J.; Gao, J.; Liu, X., Dependence of pretilt angle on orientation and conformation of side chain with different chemical structure in polyimide film surface. *RSC Advances* **2012,** *2* (25), 9463-9472.

102. Zhang, T.; Park, S.-Y.; Farmer, B. L.; Interrante, L. V., Synthesis of comb-type polycarbosilanes via nucleophilic substitution reactions on the main-chain silicon atoms. *J. Polym. Sci. A Polym. Chem.* **2003,** *41* (7), 984-997.

103. Ceccarelli, G.; Frosini, V.; Magagnini, P. L.; Newman, B. A., Chain configuration and molecular order in poly(p-biphenyl acrylate). *J. Polym. Science Polym. Lett. Ed.* **1975,** *13* (2), 101-108.

104. Ferey, G., Nanoporous materials: A selective magnetic sponge. *Nat. Mater.* **2003,** *2* (3), 136-137.

105. Goli, K. K.; Rojas, O. J.; Genzer, J., Formation and antifouling properties of amphiphilic coatings on polypropylene fibers. *Biomacromolecules* **2012,** *13* (11), 3769-3779.

106. Kim, S.-M.; Kim, A. Y.; Park, H.; Chun, H. H.; Lee, I.; Cho, Y.; Hwang, D.-H., Amphiphilic random copolymers consisting of styrene, EGMA, and HEMA for anti-biofouling coatings. *Mol. Cryst. Liq. Cryst.* **2015,** *622* (1), 151-157.

107. van Zoelen, W.; Buss, H. G.; Ellebracht, N. C.; Lynd, N. A.; Fischer, D. A.; Finlay, J.; Hill, S.; Callow, M. E.; Callow, J. A.; Kramer, E. J.; Zuckermann, R. N.; Segalman, R. A., Sequence of hydrophobic and hydrophilic residues in amphiphilic polymer coatings affects surface structure and marine antifouling/fouling release properties. *ACS Macro Lett* **2014,** *3* (4), 364-368.

108. Zigmond, J. S.; Pavía-Sanders, A.; Russell, J. D.; Wooley, K. L., Dynamic Anti-Icing Coatings: Complex, amphiphilic hyperbranched fluoropolymer poly(ethylene glycol) cross-linked networks with an integrated liquid crystalline comonomer. *Chem. Mater*. **2016**.

109. Albrecht, O.; Cumming, W.; Kreuder, W.; Laschewsky, A.; Ringsdorf, H., Monolayers of rod-shaped and disc-shaped liquid crystalline compounds at the air-water interface. *Colloid Polym. Sci.* **1986,** *264* (8), 659-667.

110. Mastrangelo, J. C.; Chen, S. H., New thermotropic chiral nematic polymers. 3. Copolymers containing a cyanobiphenyl group and (S)-(-)-1-phenylethanol or (S)-(-)-1-phenylethylamine. *Macromolecules* **1993,** *26* (22), 6132-6134.

111. Jerome, B.; Commandeur, J.; De Jeu, W. H., Backbone effects on the anchoring of side-chain polymer liquid crystals. *Liq. Cryst.* **1997,** *22* (6), 685-692.

112. Yonetake, K.; Masuko, T.; Morishita, T.; Suzuki, K.; Ueda, M.; Nagahata, R., Poly(propyleneimine) dendrimers peripherally modified with mesogens. *Macromolecules* **1999,** *32* (20), 6578-6586.

113. Hikmet, R. A. M.; Poels, H. L. P., An investigation of patterning anisotropic gels for switchable recordings. *Liq. Cryst.* **2000,** *27* (1), 17-25.

114. Çakır, T.; Önen, A.; Serhatlı, I. E., Graft copolymerization of methyl methacrylate with an N-substituted maleimide–liquid-crystalline copolymer by atom transfer radical polymerization. *J. Appl. Polym. Sci.* **2008,** *107* (4), 2074-2081.

115. Park, S.-Y.; Kavitha, T.; Kamal, T.; Khan, W.; Shin, T.; Seong, B., Self-assembly of dPS-liquid crystalline diblock copolymer in a nematic liquid crystal solvent. *Macromolecules* **2012,** *45* (15), 6168-6175.

116. Wu, G.; Jiang, Y.; Xu, D.; Tang, H.; Liang, X.; Li, G., Thermoresponsive inverse opal films fabricated with liquid-crystal elastomers and nematic liquid crystals. *Langmuir* **2011,** *27* (4), 1505-1509.

117. Xing, H.; Li, J.; Shi, Y.; Guo, J.; Wei, J., Thermally driven photonic actuator based on silica opal photonic crystal with liquid crystal elastomer. *ACS Appl. Mater. Interfaces* **2016,** *8* (14), 9440-9445.

118. Bao, X.; Dix, L. R., Synthesis and evaluation of novel side chain liquid crystal polymers with a single aromatic unit. *Mol. Cryst. Liq. Crys. A* **1997,** *304* (1), 41-46.

119. Caillier, L.; Taffin de Givenchy, E.; Geribaldi, S.; Guittard, F., Liquid crystal polymers for non-reconstructing fluorinated surfaces. *J. Mater. Chem.* **2008,** *18* (44), 5382-5389.

120. Darmanin, T.; Taffin de Givenchy, E.; Guittard, F., Superhydrophobic surfaces of electrodeposited polypyrroles bearing fluorinated liquid crystalline segments. *Macromolecules* **2010,** *43* (22), 9365-9370.

121. Dembinski, R.; Espinet, P.; Lentijo, S.; Markowicz, M. W.; Martín-Alvarez, J. M.; Rheingold, A. L.; Schmidt, D. J.; Sniady, A., Fluorophobic effect in metallomesogens – The synthesis and mesomorphism of Ag, Au, Cu, Fe, Pd, and Pt fluorous isocyanide complexes. *Eur. J. Inorg. Chem.* **2008,** *2008* (10), 1565-1572.

122. Kölbel, M.; Beyersdorff, T.; Cheng, X. H.; Tschierske, C.; Kain, J.; Diele, S., Design of liquid crystalline block molecules with nonconventional mesophase morphologies: Calamitic bolaamphiphiles with lateral alkyl chains. *J. Am. Chem. Soc.* **2001,** *123* (28), 6809-6818.

123. Li, X.; Andruzzi, L.; Chiellini, E.; Galli, G.; Ober, C. K.; Hexemer, A.; Kramer, E. J.; Fischer, D. A., Semifluorinated aromatic side-group polystyrene-based block copolymers: Bulk structure and surface orientation studies. *Macromolecules* **2002,** *35* (21), 8078-8087.

124. Martinelli, E.; Paoli, F.; Gallot, B.; Galli, G., Mesophase structure of low-wetting liquid crystalline polyacrylates with new perfluoroalkyl benzoate side groups. *J. Polym. Sci. A Polym. Chem.* **2010,** *48* (18), 4128-4139.

125. Hayata, Y.; Nagano, S.; Takeoka, Y.; Seki, T., Photoinduced volume transition in liquid crystalline polymer gels swollen by a nematic solvent. *ACS Macro Lett* **2012,** *1* (11), 1357-1361.

126. Jeong, Y. S.; Akagi, K., Liquid crystalline PEDOT derivatives exhibiting reversible anisotropic electrochromism and linearly and circularly polarized dichroism. *J. Mater. Chem.* **2011,** *21* (28), 10472-10481.

127. Bailey, F. E.; Callard, R. W., Some properties of poly(ethylene oxide)1 in aqueous solution. *J. Appl. Polym. Sci.* **1959,** *1* (1), 56-62.

128. Ananthapadmanabhan, K. P.; Goddard, E. D., Aqueous biphase formation in polyethylene oxide-inorganic salt systems. *Langmuir* **1987,** *3* (1), 25-31.

129. Hey, M. J.; Jackson, D. P.; Yan, H., The salting-out effect and phase separation in aqueous solutions of electrolytes and poly(ethylene glycol). *Polymer* **2005,** *46* (8), 2567-2572.

130. Zhang, Y.; Cremer, P. S., Interactions between macromolecules and ions: The Hofmeister series. *Curr. Opin. Chem. Biol.* **2006,** *10* (6), 658-663.

APPENDIX A

RESULTS FROM INVESTIGATIONS INTO OTHER HYPERBRANCHED FLUOROPOLYMER SYSTEMS AND FLUORINATED LIQUID CRYSTALLINE MONOMERS

A.1 HBFP$^{(III)}$-a Homopolymer

Table A.1. Average onset melting temperatures (T_m) for the array of HBFP$^{(III)}$-a-PEG coatings and HBFP$^{(III)}$ and PEG control samples, each with 200 wt % water.

Mass ratio HBFP$^{(III)}$-a to PEG (wt %)									
HBFP$^{(III)}$		5:2	2:1	3:2	1:1	2:3	1:2	2:5	PEG
Avg. H_2O T_m onset (°C)									
Bound	-0.6 ± 0.0	-3.6 ± 0.1	-3.6 ± 0.1	-3.3 ± 0.2	-28.1 ± 0.1	-27.8 ± 0.0	-29.0 ± 0.5	-27.8 ± 0.0	-10.4 ± 1.3
Free					-4.0 ± 0.7	-4.9 ± 0.2	-4.6 ± 0.1	-4.6 ± 0.0	

A.2 HBFP-PEG-PDMS Ternary System

Table A.2. Wt % H_2O uptake of HBFP-PEG-PDMS coatings.

H_2O uptake (wt %)		**Mass ratio PDMS to HBFP$^{(III)}$-b (wt %)**		
		25	*50*	*75*
Mass ratio PEG to HBFP$^{(III)}$-b (wt %)	*0*	2%	7%	13%
	25	101%	40%	117%
	50	79%	154%	99%
	75	166%	103%	93%

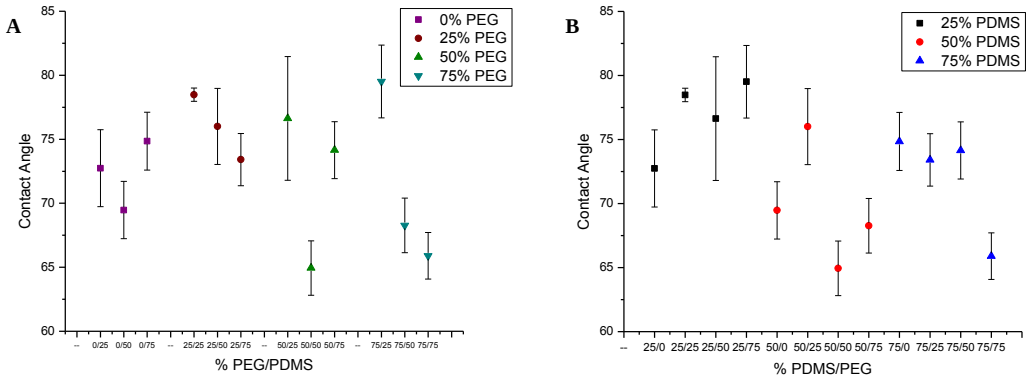

Figure A.1. Average static water contact angles of HBFP-PEG-PDMS dry coatings in relation to (A) wt % PEG/wt % PDMS and (B) wt % PDMS/wt % PEG.

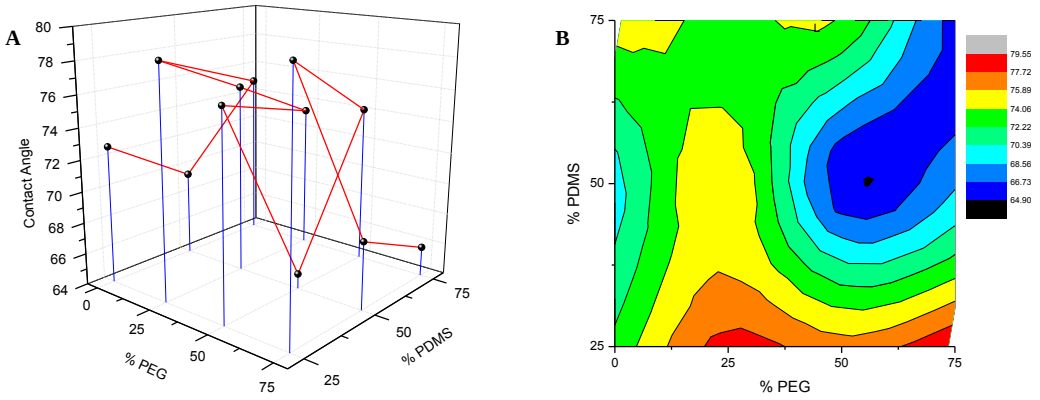

Figure A.2. Average static water contact angles of HBFP-PEG-PDMS dry coatings represented as (A) 3D scatter plot and (B) contour map.

Table A.3. Average free water onset melting temperatures (T_m) for the array of HBFP-PEG-PDMS ternary system, each with 200 wt % water.

Avg. free H_2O T_m onset (°C)		**Mass ratio PDMS to HBFP$^{(III)}$-b (wt %)**		
		25	*50*	*75*
Mass ratio PEG to HBFP$^{(III)}$-b (wt %)	*0*	-1.2 ± 0.0	-1.3 ± 0.0	-2.3 ± 0.2
	25	-2.5 ± 0.0	-2.1 ± 0.0	-2.6 ± 0.1
	50	-3.1 ± 0.3	-2.8 ± 0.1	-2.6 ± 0.1
	75	-4.0 ± 0.4	-3.7 ± 0.1	-3.2 ± 0.1

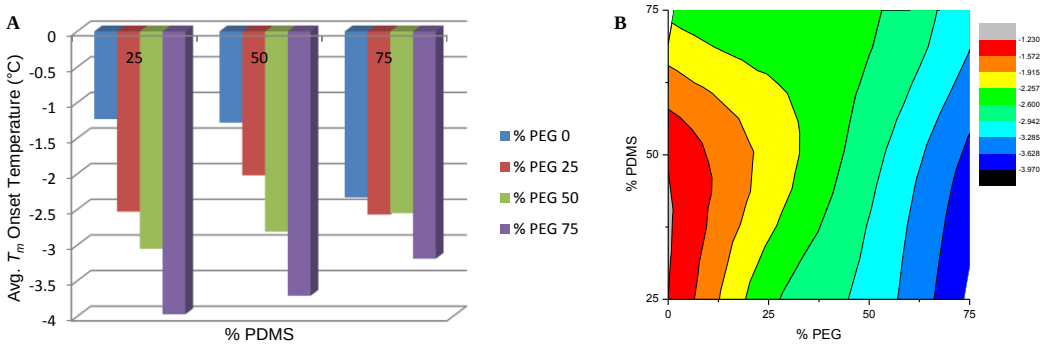

Figure A.3. Average free water onset melting temperatures (T_m) for the array of HBFP-PEG-PDMS ternary system, each with 200 wt % water, represented as (A) 3D bar graph and (B) contour map.

Table A.4. Average bound water onset melting temperatures (T_m) for the array of HBFP-PEG-PDMS ternary system, each with 200 wt % water. *Indicates no transition was observed.

Avg. bound H_2O T_m onset (°C)		**Mass ratio PDMS to HBFP$^{(III)}$-b (wt %)**		
		25	*50*	*75*
Mass ratio PEG to HBFP$^{(III)}$-b (wt %)	*0*	*	*	*
	25	-23.3 ± 0.0	-23.5 ± 0.1	-23.8 ± 0.1
	50	-23.9 ± 0.2	-23.8 ± 0.0	-23.5 ± 0.0
	75	-23.5 ± 0.3	-23.5 ± 0.0	-23.5 ± 0.0

A.3 Alternative Fluorinated Liquid Crystalline Monomers

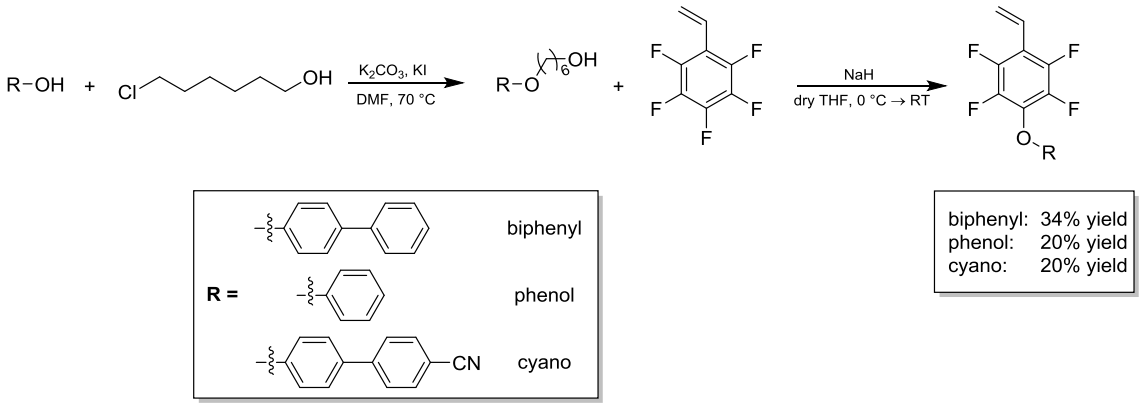

Scheme A.1. Synthesis of mesogenic units and fluorinated LC monomers with yields.